Theses and dissertations

1-1-2005

Simultaneous removal of metal ions and oxidation of linear alkylbenzene sulfonate by combined electrochemical and photocatalytic processes

Mitra Saidi
Ryerson University

SIMULTANEOUS REMOVAL OF METAL IONS AND OXIDATION OF LINEAR ALKYLBENZENE SULFONATE BY COMBINED ELECTROCHEMICAL AND PHOTOCATALYTIC PROCESSES

by

Mitra Saidi

(B.Sc., Amirkabir University, Iran, 1998)

A thesis

Presented to Ryerson University

In partial fulfillment of the

Requirements for the degree of

Master of Applied Science

In the program of

Chemical Engineering

Toronto, Ontario, Canada, 2005

©Mitra Saidi, 2005

UMI Number: EC53781

INFORMATION TO USERS

The quality of this reproduction is dependent upon the quality of the copy
submitted. Broken or indistinct print, colored or poor quality illustrations and
photographs, print bleed-through, substandard margins, and improper
alignment can adversely affect reproduction.

In the unlikely event that the author did not send a complete manuscript
and there are missing pages, these will be noted. Also, if unauthorized
copyright material had to be removed, a note will indicate the deletion.

UMI®

AUTHOR DECLARATION

I hereby declare that I am the sole author of this thesis.

I authorize Ryerson University to lend this thesis to other institutions or individuals for the purpose of scholarly research.

I further authorize Ryerson University to reproduce this thesis by photocopying or by other means, in total or in part, at the request of other institutions or individuals for the purpose of scholarly research.

BORROWER'S PAGE

Ryerson University requires the signature of all persons using or photocopying this thesis. Please sign below, and give address and date.

ABSTRACT

Simultaneous Removal of Metal Ions and Oxidation of Linear Alkylbenzene Sulfonate by Combined Electrochemical and Photocatalytic Processes

Mitra Saidi
MASc, Chemical Engineering Program
Ryerson University
Toronto, 2005

Simultaneous electrochemical removal of Zn^{+2} and Ni^{+2} ions and photooxidation of linear alkylbenzene sulfonate (LAS) over TiO_2 particles were investigated. To achieve this objective, first, the effect of different variables such as current density, pH and flow rate on sole electrochemical reduction of metal ions was studied. Both controlling pH in the range of 5.5-6 and increasing the liquid volumetric flux effectively improved the rate of Zn^{+2} ion reduction, but they did not have any significant effect on the rate of Ni^{+2} ion reduction. Under optimum operating conditions (pH=5.5-6, volumetric liquid flux=0.0172 m^3 m^2 s^{-1}, current density=0.166 mA cm^{-2}) and using total electrolyte volume of 6 L, zinc and nickel were reduced by 86% and 53%, respectively, over a 7-hour treatment period. Sole photocatalytic treatment of LAS and controlling pH between 5-5.5 resulted in 60% LAS degradation. However, temperature and flow rate did not have any considerable effect on the rate of oxidation. Finally, using the combined photolytic-electrolytic system enhanced the rate of LAS degradation compared to the photocatalytic system alone. LAS was degraded in the combined system by 76% compared to 60% in the sole photocatalytic system. However, using the combined system, zinc and nickel were reduced by 81% and 47%, respectively, which were slightly less than those obtained in the electrochemical system alone.

ACKNOWLEDGMENTS

Table of Contents

List of Figures

xi

List of Tables

NOMENCLATURE

Symbol	Description
A	Electrode area [m^2]
C	Concentration [$mol.m^{-3}$]
COD	Chemical oxygen demand [$mg.l^{-1}$]
D	Diffusion coefficient [$m^2.s^{-1}$]
E	Energy of photons [J]
E^o	Standard electrode potential [V]
E^e	Equilibrium potential [V]
e^-	An electron
F	Faraday's constant (96,485) [$A.s.mol^{-1}$]
G	Gibb's free energy [$J.mol^{-1}$]
h	Planck's constant (6.6256×10^{-34}) [$J.s^{-1}$]
h^+	hole
I	Current [A]
i	Current density [$A.m^{-2}$]
i_L	Limiting current density [$A.m^{-2}$]
K_a	Acid dissociation constant
K_b	Base dissociation constant
k	Reaction rate constant in a first-order kinetic expression [s^{-1}]
K_m	Average mass transfer coefficient for metal ions [$m.s^{-1}$]
L	Characteristic length [m]
M	Molecular weight

m	Number of moles of electroactive species [mol]
n	Number of electrons
N	Molar flux [mol.s^{-1}.m^{-2}]
O	Species that becomes reduced
Q	Volumetric flow rate [m^3.s^{-1}]
q	Electrical charge [C]
R	Universal gas constant (8.31457) [J.K^{-1}.mol^{-1}]; Resistance [ohm]
r	Reaction rate [mg.l^{-1}.s^{-1}]
T	Temperature [C]
t	Time [s]
u	Superficial velocity [m.s^{-1}]
V	Volume [m^3]
z	Electrical charge number

Greek Symbols

η	Overpotential [V]
ε	Current efficiency
μ	Viscosity [g.m^{-1}.s^{-1}]
τ	Residence time[s]
ν	Frequency of radiation [s^{-1}]
λ	Wavelength [nm]
ρ	Density [kg.m^{-3}]

Dimensionless Numbers

Re   Reynolds number: $\dfrac{u.L.\rho}{\mu}$

Subscripts

C, A   Cathode, Anode

HT   Holding tank

in   Inlet

o   Outlet

R   Reactor

Superscripts

s   Surface

b   Bulk

Abbreviations

AOP   Advanced oxidation process

COD   Chemical oxygen demand

LAS   Linear alkylbenzene sulfonate

ppm   Part per million

SHE   Standard hydrogen electrode

UV   Ultra Violet

CHAPTER 1
INTRODUCTION

Nowadays, one of the most important global issues is water due to its limited sources in the world. Industrial, agricultural, and urban developments have resulted in a great damage to human health and environment due to the high pollution rates. In the last century, investigations concerning the decontamination of drinking water and wastewater treatment have grown substantially.

In the present study, the treatment of wastewater from an electro-coating process containing both heavy metals and organic compounds was investigated. Electro-coating method is an "environmentally friendly" procedure in which an electrical current is used to deposit paint onto a part or an assembled product immersed in a bath of water-thinned paint. Due to the uniformity of the applied coating and excellent adhesion properties, electro-coating processes offer extremely high corrosion protection on both steel and aluminum substrates. However, a large volume of wastewater is generated during the electro-coating process from different stages containing various toxic heavy metals and organic compounds.

In this study, Zn and Ni were chosen as model heavy metals since they are used to protect automotive bodies from severely corrosive conditions. After pretreatment to clean and prepare substrates for painting, metallic substrates are sent to a phosphate conversion coating stage where a protective coating is applied. The rinse water from this unit contains those toxic heavy metals with typical concentrations of 20 ppm (Doan and Wu,

2002). The toxicity of heavy metals and the clinical symptoms of prolonged exposure to a heavy-metal-contaminated environment have been well defined (Waldron, 1980). For these reasons, the discharge of industrial wastewaters has been strictly regulated to reduce environmental impacts. The metal recovery from industrial wastewaters is very important from both environmental and economical points of view. Chemical precipitation is a conventional method for reducing the concentration of metal ions in industrial wastewaters. For some metals, such as zinc and nickel, this conventional method is efficient for complying the allowable limit for final discharge (Lanza and Bertazzoli, 2000; Juttner et al., 2000). The hydroxide precipitation method requires extensive use of various chemicals in different stages. The major drawback of this technique is the generation of a large amount of concentrated sludge, which is buried in landfills in most of the cases. In the near future, this method cannot be used any more due to the high cost of the further treatment of sludge prior to disposal, the loss of precious metals, and the increasing cost of land disposal and environmental impacts.

Metal ion concentrations can be reduced in aqueous solutions by means of electrochemical techniques via reduction reactions. Electrochemical removal of metal ions from rinse waters is of considerable interest since deposited metals are obtained in one stage without the necessity of sludge disposal. Electrochemical processes have low sludge production, low start-up and operating cost, and no chemical contamination in treated water. Electrochemical reactions are also carried out at low pressure and temperature and can be easily terminated by disconnecting the cell current. Diverse ranges of its applications and several commercial cell designs have been recently reviewed by Pletcher and Walsh (1990).

2

Additionally, wastewaters from electro-plating units contain some organics, which are used in various stages of the process. In the pretreatment stage, some organic compounds are applied for the cleaning purposes of various metallic surfaces. Surface-active agents or surfactants used widely as cleaning agents are the main component of the household and industrial detergents. Moreover, surfactants are added intentionally to nickel-plating bath to improve the quality of the plating surface (Huang, 1995). It has been known that a large percentage of refractory COD in municipal and industrial wastewaters is related to surfactants. It is well known that many of the surfactants widely used in various applications are not biodegradable or their biodegrdation is very slow (Hidaka and Kubota, 1986). Linear alkylbenzene sulfonate (LAS) or sodium dodecylbenzene sulphonate (DBS) is the most common anionic surfactant used in domestic and industrial detergents having a global production of over 2.4×10^6 tones per year (De Almedia et. al., 1994). It is synthetically produced by sulfonation of linear alkylbenzene with sulfur trioxide. In 1965, LAS was introduced as a biodegradable surfactant to substitute the non-biodegradable surfactant, alkyl aryl sulfonate (ABS) in detergents (Huang et al., 2000). LAS is more biodegradable than ABS since its alkyl portion is not branched. However, it has been known that high concentration of LAS in wastewaters does not respond to biological treatments (Zhang et al., 1999) and LAS is known to be recalcitrant at a high concentration of 3000 mg.l^{-1} (Patterson et al., 2002). Different methods have been employed for treatment of surfactants including biological treatment, chemical adsorption (flocculation and coagulation followed by settling) and advanced oxidation processes. In chemical adsorption processes undesirable sludge is produced, which needs further treatment. Biological treatments are very economical

3

compared to other methods; however, in the case of non-biodegradable compounds, these techniques cannot be used.

Advanced oxidation processes (AOPs) are promising methods for the treatment of the non-biodegradable. AOPs such as UV/TiO_2 (photocatalysis) are based on the production of highly reactive intermediates, mainly hydroxyl radicals, capable to oxidize almost all organic pollutants. AOPs have been widely employed as an alternative physical-chemical process for environmental remediation in the last two decades. With photocatalysis, the pollutants are degraded by irradiation of a metal oxide semiconductor such as titanium dioxide, acting as a photocatalyst, in the presence of the UV light. This method offers the advantage of destroying pollutants; in contrast to conventional techniques such as activated carbon or air stripping that only transfers contaminants from one phase to another.

For wastewaters containing both metal ions and organic compounds, an electrochemical cell alone can reduce concentration of metal ions but it is not capable of achieving complete degradation of organic compounds in the system. Furthermore, a photocatalytic cell alone can destroy organics effectively while it leaves metal ions in solution. The development of an effluent treatment technique, which could degrade organic pollutants and simultaneously remove metal ions from wastewaters, would be an important stage in industrial wastewater treatment. It is very important to note that in both techniques used in the present study no sludge is produced since both rely on oxidation-reduction reactions.

The objective of this study was:

- to investigate the feasibility of a combined electrochemical and photocatalytic system for the treatment of the simulated wastewater containing both metal ions and LAS

In order to achieve the above objective, the following steps were implemented.

- Photodegradation of LAS by means of UV/TiO_2 using a photolytic system alone
- Removal of Zn^{++} and Ni^{++} ions from simulated wastewater using a sole electrochemical process

CHAPTER 2
LITERATURE REVIEW

This chapter is divided in two main parts. The first part represents fundamental aspects of electrochemistry for metal ion removal. The second part deals with photocatalytic processes for the treatment of aqueous organic and inorganic compounds.

2.1 ELECTROCHEMICAL PROCESSES

Rapid advances in technology unfortunately have resulted in an increase in the amount and types of chemical compounds polluting the environment, especially water resources. The use of various toxic organic and inorganic compounds and their persistence in the aqueous environment have led to the need for the development of effective techniques to treat them. With new environmental regulations, industrial activities face stringent controls on industrial effluents. Table 1 lists current methods for the treatment of organic and inorganic pollutants in industrial wastewaters (Rajeshwar and Ibanez, 1997).

Table 1. Current techniques for the treatment of organic and inorganic pollutants

Organics	Inorganics
Incineration	Precipitation/Coagulation
Air stripping	Membrane separation
Carbon adsorption	Distillation
Microbial treatment	Chemical treatment
Chemical processes	Electrochemical treatment

Among different techniques, electrochemical processes play a significant role in the removal of different types of pollutants from industrial wastewaters. Some of their inherent advantages are:

1- Redox reactions involving electron transfer are inherently pollution- free

2- An electrochemical process usually is run at room temperature and atmospheric pressure

3- During electrochemical processes, no sludge is produced

Metal ions and organic compounds are two major types of pollutants, which exist in the wastewater of an electro-coating process. Electrochemical processes have been widely used for metal ion removal and in the lesser extent for destruction of toxic organics from industrial wastewaters. The electrochemical removal of metal ions from wastewaters is often combined with the effort to recycle water for reuse.

2.1.1 Basic principles of electrochemical processes

Electrochemical processes are of a heterogeneous nature in which chemical reactions are taking place at the interface of electrodes and an electrolyte. The main advantage of the electrochemical process is its environmental compatibility, since electrons as main reagents are environmentally clean.

When a metal is immersed in a solution of its ions, the metal sends its ions into the solution or, conversely, the ions deposits on the surface of the metal. This passage of ions creates an electrical double layer at the electrode-electrolyte interface. The potential difference, which exists between metal and solution in the equilibrium state, is called the

Galvanic potential (Raub and Muller, 1967). Since the Galvanic potential is not measurable, a reference electrode is used and all other potentials are expressed relative to this reference electrode. The standard hydrogen electrode is usually used as the reference electrode and its potential is arbitrarily assumed to be zero. The list of the standard electrode potentials of common half reactions in aqueous solution is given in Appendix A. These potentials have been measured relative to the standard hydrogen electrode at $25^{\circ}C$ with all species at unit activity. For example, the standard reduction potentials for zinc and nickel are -0.76 V and -0.23V, respectively.

A typical electrochemical cell consists of electrodes (cathode and anode), electrolyte solution and external wiring. Assuming only one reaction occurs in each of electrodes, the overall cell reaction can be written as:

$$M+N^{z+} \leftrightarrow M^{z+}+N \tag{2.1.1.1}$$
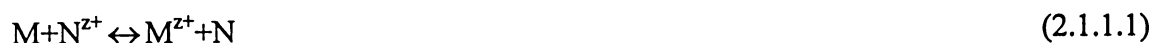
Where M is oxidized at the anode and N is reduced at the cathode surface. Since equilibrium potentials of half-reactions are not usually in their standard states, the Nernst equation gives the electrode potential relative to the standard electrode potential (Brett and Brett, 1996). The Nernst equation is considered to be a fundamental equation in electrochemistry, which is particularly significant for electrode processes. According to the Nernst equation, both anode and cathode potentials have the following form:

$$\text{Potential=standard potential-} \frac{RT}{zF} \ln \{C_{reduced\ species}/ C_{oxidised\ species}\}$$

Thus,

$$E_C^e = E_C^\circ - \frac{RT}{zF} \ln \frac{C_M}{C_{M^{z+}}}$$ (2.1.1.2.a)

$$E_A^e = E_A^\circ - \frac{RT}{zF} \ln \frac{C_N}{C_{N^{z+}}}$$ (2.1.1.2.b)

These oxidation-reduction reactions produce current, which flows through an external circuit. The potential of the electrochemical cell, electromotive force, can be calculated from the reduction electrode potentials of respective half reactions, which are obtained from Nernst equation.

$$E_{cell}^e = E_A - E_C^e = E_{min}$$ (2.1.1.3)

E_{cell}^e is the minimum voltage requirement for the overall cell reaction. A natural process occurs if and only if the associated change in Gibbs free energy, ΔG, for the system is negative. The cell potential is related to ΔG of the overall cell reaction by the following equation:

$$\Delta G = -nFE_{cell}^e$$ (2.1.1.4)

As a result, the value of E_{cell}^e should be positive in order to have spontaneous redox reactions at electrodes. If the value of the cell potential is negative, ΔG will be positive, so that the cell functions spontaneously in the opposite direction. However, when E_{cell}^e is negative, an external source of energy will be required to provide energy for the spontaneous reverse reaction. The applied voltage should be larger than the equilibrium

cell potential to drive a chemical change. In this case, we have an electrolytic cell instead of Galvanic cell and it is widely used in industrial applications.

In an electrolytic cell, the cathode is connected to the negative pole of the direct current source and cations in the electrolyte migrate towards the cathode. The anode is connected to the positive pole of the direct current source and anions migrate towards the anode. The standard electrode potential is applied only to the equilibrium potential of the metal and is the most positive potential at which the metal can be deposited. In actual deposition processes, deposition potentials are usually more negative than standard potentials due to polarization and cell resistance (Brenner, 1963). The variation of the electrode potential from the equilibrium value to the dynamic potential during electrolysis is termed the polarization, η. Sometimes the term overvoltage is used instead of polarization.

$$\eta_A = E_A - E_A^e \qquad\qquad\qquad (2.1.1.5.a)$$

$$\eta_C = E_C - E_C^e \qquad\qquad\qquad (2.1.1.5.b)$$

E_A and E_C are anode and cathode potentials, respectively, during non-equilibrium operation. Practical voltage requirement can be found by:

$$E_{cell} = E_A - E_C + IR_{cell} + IR_{circuit} \qquad\qquad (2.1.1.6.a)$$
or
$$E_{cell} = E_A^e - E_C^e + \eta_A + \eta_C + IR_{cell} + IR_{circuit} \qquad\qquad (2.1.1.6.b)$$

In practice, the overpotential will increase by 30-250 mV, depending on electrolysis conditions and specially the electrode material (Pletcher and Walsh, 1990). The

polarization is produced by various inhibiting factors, which affects reactions at electrodes. The total polarization occurring at an electrode can be divided into different partial polarizations including: activation polarization, concentration polarization and resistance polarization (Raub and Muller, 1967; Pickett, 1979).

One of the main factors in the design of an electrochemical cell is to design the cell with a minimum resistance. The internal cell resistance, R_{cell}, decreases by making the gap between electrodes smaller and using a very conducting electrolyte. Other factors, which cause a potential drop in the electrolyte, are electrodes themselves and the wires, which carry the current. The cell voltage is also influenced by different parameters such as temperature, electrolyte flow rate, electrode material, and electrolyte composition. It is difficult to predict the required cell voltage analytically and it is not usually used as a primary control parameter. Constant cell voltage is used practically for convenient, but constant electrode potential (potentiostatic mode) or constant cell current (galvanostatic mode) are preferable operation modes (Pletcher and Walsh, 1990). Galvanostatic mode was used in the present study for electrochemical removal of metal ions.

One may conclude that, in an aqueous solution, metals with standard electrode potentials more negative than hydrogen can not be deposited since hydrogen deposits at a more positive potential. However, practically, hydrogen deposits at a much more negative potential than its equilibrium value on many types of electrodes; and, consequently, the deposition potential of some of those metals is attained without excessive hydrogen evolution (Brenner, 1963).

2.1.2 Faraday's Law of electrolysis

The current, I, is the rate at which electrons move through the electrolyte and external circuit and is defined as the increment of charge, dQ, flowing across a plane per unit time (Rajeshwar and Ibanez, 1997):

$$I = \frac{dQ}{dt}$$

(2.1.2.1)

It is also a measure of electrode reactions and the overall chemical change in the cell. Another important quantity is the current density, i, which is the current flowing per unit cross sectional area of the electrode. The relationship between the amount of formed products during electrolysis and the quantity of the passed charge was discovered by Faraday (Pletcher and Walsh, 1990). When a single reaction occurs at an electrode with m_j moles of j produced by a current I_j flowing for t seconds, then

$$m_j = \frac{I_j t}{z_j F}$$

(2.1.2.2)

When different reactions occur at the electrode surface:

$$\sum m_j = \frac{t}{F} \sum \frac{I_j}{z_j}$$

(2.1.2.3)

The total current can be calculated using the following equation:

$$I = \sum I_j$$

(2.1.2.4)

The current efficiency for the production of any species at the electrode surface is defined by:

$$\varepsilon_j = \frac{I_j}{I} \qquad (2.1.2.5)$$

and it is usually expressed as percentage.

By eliminating I_j between Equations (2.1.2.2) and (2.1.2.5), another expression for current efficiency in percentage will be obtained:

$$\varepsilon_j = \frac{m_j}{It/z_jF} *100 \qquad (2.1.2.6)$$

In the present study, the total current efficiency for zinc and nickel deposition is calculated by adding the current efficiencies for individual reaction. In an electrolyte containing only single metal ions high current efficiency and consequently low energy consumption can be achieved. However, when different types of metal ions are present, the current efficiency for each cathode reaction decreases due to co-deposition of other metals. Furthermore, in aqueous electrolyte solutions, the main dominant side reaction at the cathode is hydrogen evolution, which lowers the current efficiency of the major electrode reaction. Obviously the sum of all the current efficiencies at an electrode is 100%.

2.1.3 Interactions of electron transfer and mass transfer

Consider the electro-deposition of a metal, R, from its metallic ion, O, at the cathode surface:

$$O + ne^- \leftrightarrow R \qquad (2.1.3.1)$$

For the above simple reduction reaction, the following steps will occur and mass transfer is a part of the overall electrode reaction:

13

$$O_{bulk} \xrightarrow{\text{Mass Transfer}} O_{surface} \xrightarrow{\text{Electron Transfer}} R_{surface} \qquad (2.1.3.2)$$

$$\text{Step 1} \qquad\qquad\qquad \text{Step 2}$$
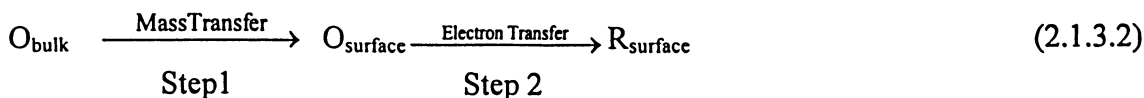
The rate of conversion of reactant to product is determined by the slowest step. A chemical reaction at the electrode surface cannot occur faster than the rate of reactant transfer to the electrode. Consequently, in practical situations, the mass transfer is a predominant consideration, especially when dealing with dilute solutions. At a sufficiently high overpotential, the rate of electron transfer is high; hence, mass transport will become rate-determining step (Genders and Weinburg, 1992).

2.1.4 Mass transfer

In general, there are three modes of mass transport in electrochemical systems: diffusion, migration and convection (Pletcher and Walsh, 1990):

Diffusion: Diffusion is the movement of a species due to concentration gradient. At an electrode surface, compound O is converted to the product R by a chemical reaction and hence, close to the electrode surface a boundary layer is formed. The concentration of O at the surface is lower than in the bulk, hence, O will diffuse toward the electrode.

Migration: The movement of charged species due to a potential gradient is called migration.

Convection: Natural convection is due to density gradients in the solution. Forced convention is defined as the movement of a species due to a mechanical force. Convection is usually induced by stirring, flowing solution through the cell or using rotating electrodes.

For flow systems and dilute solutions, convection will be the predominant mode of operation. Diffusion is more significant when the study involves investigating the role of diffusion or obtaining diffusion coefficient for a particular system. Furthermore, if the electrolysis is carried out in a solution with a high concentration of an inert electrolyte (supporting electrolyte), most of the charge will be carried with those inert ions and migration will not have a significant effect on the transport of electroactive species.

Improving mass transfer by convection cannot entirely eliminate the effect of diffusion on the transfer rate of species to the electrode surface. There is always a stagnant layer close to the electrode surface, in which diffusion is very important. When the solution is vigorously stirred the thickness of this diffusion layer, also known as Nernst diffusion layer, can be reduced but cannot be eliminated completely. Campbell et. al, (1994) used fluidized beads to enhance mixing so that the thickness of the diffusion layer decreased about 90% compared to a simple electro-cell.

Stirring at distances greater than diffusion layer, δ, is efficient for diffusion of the reacting species through the diffusion layer to reach the surface of the electrode. Although there is no sharp distinction between the stagnant and moving regions, an approximation is used to give a definite linear quantity to this layer. This is illustrated in Figure 1.

Concentration gradient of species j at the electrode surface can be expressed by:

$$\left(\frac{\partial C_j}{\partial x}\right)_{x=0} \approx \frac{C_j^b - C_j^s}{\delta} \qquad (2.1.4.1)$$
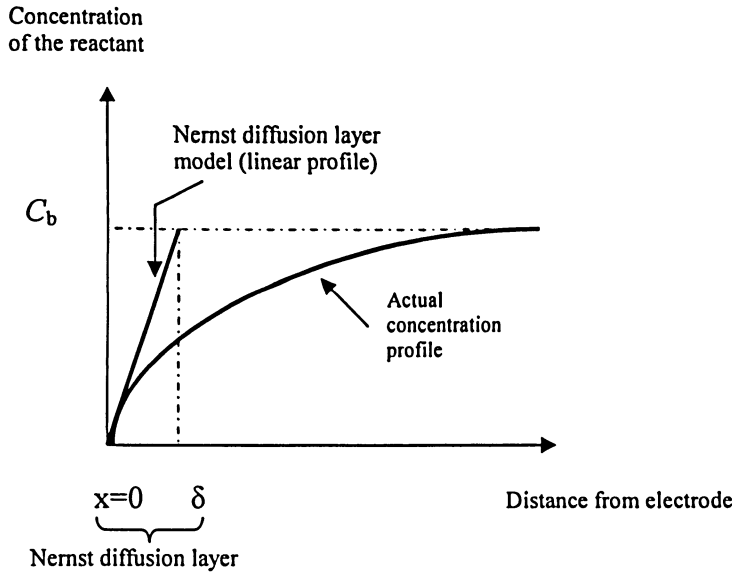
Figure 1. Concentration profile of the reactant during electrolysis, adopted from Paunovic and Schlesinger (1998).

Current density is indicative of the rate of reaction and can be determined by the following:

$$i_j = z_j FD \left(\frac{C_j^b - C_j^s}{\delta} \right) = K_m z_j F \, (C_j^b - C_j^s) \qquad (2.1.4.2)$$

where $K_m = D/\delta$.

As it has been shown in Equation (2.1.4.2), the current density is a function of the concentration gradient. Since mass transfer flux of species j, N_j, is defined as:

$$N_j = K_m (C_j^b - C_j^s) \qquad (2.1.4.3)$$

then

$$i_j = \frac{m_j z_j F}{At} = N_j z_j F \qquad (2.1.4.4)$$

16

The maximum value of i_j can be achieved when the reactant concentration at the electrode surface is zero, i.e. the process is mass transfer limited. This maximum current density corresponding to the maximum concentration gradient is called limiting current density, i_L which is given by Genders and Weinburg (1992):

$$i_L = z_j F K_m C_j^b \qquad (2.1.4.5)$$

where C_j^b and C_j^s are concentration of species j in bulk and at the electrode surface, respectively, and A is the electrode surface area.

Furthermore, the rate of decrease in the reactant concentration, i.e. the reaction rate, can be related to the rate of electron transfer:

$$r = -\frac{I_j}{z_j F} \qquad (2.1.4.6)$$

Under limiting current conditions:

$$r = -\frac{I_L}{z_j F} = -K_m A C_j^b \qquad (2.1.4.7)$$

Therefore, the average mass transfer coefficient, K_m, can be obtained through direct measurement of the limiting current. This procedure is applicable if the bulk concentration of electroactive species does not change during electrolysis. In this case, the graph of current density versus overpotential, also known as a voltamogram, results in a distinct plateau in which the limiting current is reached. An idealized voltamogram is shown in Figure 2.

17
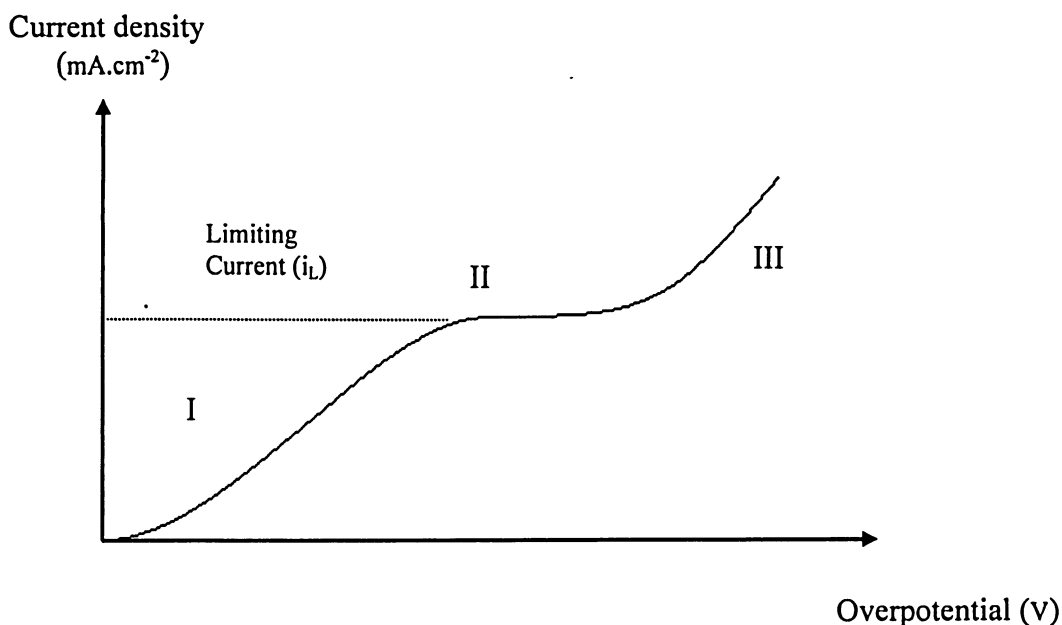
Figure 2. A typical polarization curve (Current versus Overpotential)

Three different regions are shown in Figure 2:

Region (I): In this region, the process is under both mass transfer and charge transfer control. In the case of dilute solutions, for the removal of heavy metal ions, the process would occur in this region since the limiting current would not be reached.

Region (II): The limiting current can be reached if the bulk concentration of the electroactive species can be kept constant. At the limiting current, the process is completely mass transfer controlled, which is not reached in the case of dilute solutions.

Region (III): At current density greater than the limiting current, the double layer becomes further charged and other reactions such as hydrogen evolution can significantly occur.

There are different routes for determination of K_m:

1-via direct measurement of limiting current using Equation (2.1.4.5)

2-manipulation of the converted mass and assumption of a specific reactor model

The first method is the most straightforward route. However, using the limiting current is only applicable for systems with constant bulk concentration of the electroactive species. In wastewater treatment processes, the bulk concentration of the electroactive species is reduced over the treatment time. Consequently, in the present study, the average mass transfer coefficient was determined from the measurement of the change of the electrolyte concentration with time. A model was developed to determine the average mass transfer coefficient in the present system.

2.1.5 Model development for a batch electrochemical reactor with continuous recirculation of the electrolyte

Consider the electrolytic system shown in Figure 3:
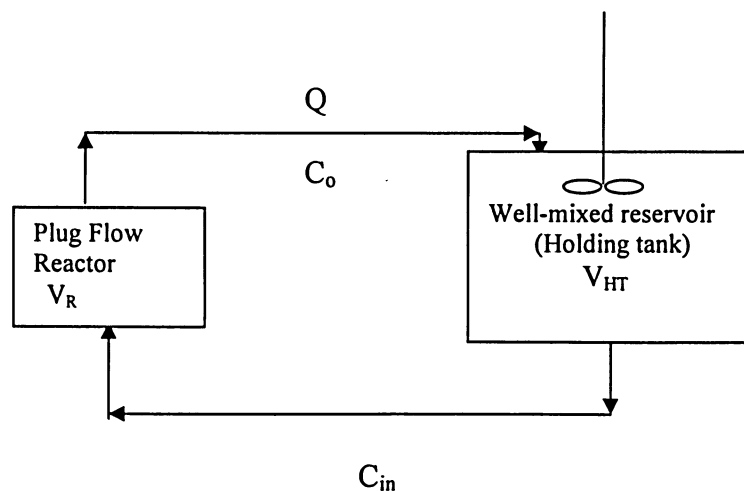
Figure 3. A schematic diagram of a batch system with recirculation

Mass balance over the well-mixed reservoir results:

$$V_{HT} \frac{dC_{in}}{dt} = Q(C_o - C_{in})$$

(2.1.5.1)

or

$$QC_o = QC_{in} + V_{HT} \frac{dC_{in}}{dt}$$

(2.1.5.2)

and mass balance over the electrochemical cell results:

$$V_R \frac{dC_o}{dt} = Q(C_{in} - C_o) + r$$

(2.1.5.3)

Substitution of r from Equation (2.1.4.7) into Equation (2.1.5.3) results in:

$$V_R \frac{dC_o}{dt} = Q(C_{in} - C_o) - K_m A C_o$$

(2.1.5.4)

$$QC_{in} = QC_o + V_R \frac{dC_o}{dt} + K_m A C_o$$

(2.1.5.5)

Substitution of C_{in} from Equation (2.1.5.5) into Equation (2.1.5.2) gives:

$$\tau_R \tau_{HT} \frac{d^2C_o}{dt^2} + \left[\tau_R + \tau_{HT}(1 + \frac{K_m A}{Q}) \right] \frac{dC_o}{dt} + \frac{K_m A C_o}{Q} = 0$$

(2.1.5.6)

where $\tau_R = \dfrac{V_R}{Q}$ and $\tau_{HT} = \dfrac{V_{HT}}{Q}$ are residence times in the electro-cell and reservoir, respectively.

Considering boundary conditions, Pickett (1973) proposed one general solution for the variation of reactant concentration in the whole system with time in terms of flow rate, electrode area and electrolyte volume. This general solution for both the reactor and

reservoir is only true for negligible conversion per pass as typically occurs under most operational conditions.

When the volume of the reservoir is substantially greater than that of electro-cell, the residence time in the electro-cell will be significantly less than that of the reservoir. In this case, as mentioned by Pickett (1973), the cell is so small that it can be regarded as a part of the reservoir. Consequently, the reservoir acts as a cell with a large volume but with very small electrode area. These assumptions will simplify the system under experiment into simple batch reactor without recirculation and the above model can be re-written in terms of C_t, concentration of the reactant in the whole system at time t.

$$\tau_R \tau_{HT} \frac{d^2 C_t}{dt^2} + \left[\tau_R + \tau_{HT}(1 + \frac{K_m A}{Q}) \right] \frac{dC_t}{dt} + \frac{K_m A C_t}{Q} = 0 \qquad (2.1.5.7)$$

when $\tau_R \ll \tau_{HT}$, then

$$\left[\tau_{HT}(1 + \frac{K_m A}{Q}) \right] \frac{dC_t}{dt} + \frac{K_m A C_t}{Q} = 0 \qquad (2.1.5.8)$$

For very small residence time in the reactor $\frac{K_m A}{Q} \ll 1$, and equation (2.1.5.8) can be written as:

$$\tau_{HT} \frac{dC_t}{dt} + \frac{K_m A C_t}{Q} = 0 \qquad (2.1.5.9)$$

$$\frac{dC_t}{dt} = -\frac{K_m A C_t}{Q \tau_{HT}} = -\frac{K_m A C_t}{V} \qquad (2.1.5.10)$$

Where V is the total volume of the electrolyte in the system, which has been used instead of the reservoir volume in the above equation. In a batch reactor, the overall reaction rate

follows first order kinetics with respect to the reactant. The rate of concentration change with time is then expressed by:

$$\frac{dC_t}{dt} = -kC_t \qquad (2.1.5.11)$$

Where k is the apparent rate constant. Considering Equation (2.1.5.10) and Equation (2.1.5.11), the average mass transfer coefficient can be related to the apparent rate constant by the following equation:

$$k = \frac{K_m A}{V} \qquad (2.1.5.12)$$

The product $K_m A$ must be maximized to achieve the highest conversion in the reactor. This quantity can be used as a concise statement of the performance of a given electrochemical reactor (Rajeshwar and Ibanez, 1997).

2.1.6 Anomalous and normal co-deposition

During the normal co-deposition of two metals the more noble metal deposits preferentially. On the other hand, the electrodeposition of Zn-Ni alloy is classified as anomalous co-deposition by Brenner, (1963), where the less noble metal is preferentially deposited. In anomalous co-deposition, the less noble metal deposits preferentially at a higher rate and behaves as the more noble metal. Zinc also has been preferentially deposited from solutions containing Zn-Co and Zn-Fe ions. Analogous anomalies have been encountered frequently in the electroplating of other alloys of the iron-group metals (Dahms and Croll, 1965). Deligianni and Romankiw (1993) reported that in order to

achieve a Ni/Fe ratio of 4:1 in the deposit; it was necessary to have as much as 80:1 molar Ni/Fe ratio in the solution.

Current density is an important parameter, which determines the behavior of the deposition process. Anomalous co-deposition may change to normal co-deposition due to variation in deposition conditions, especially the current density. Fratesi and Roventi (1992) reported that at low current densities, transition from anomalous to normal co-deposition occurred. Fukushima (1988) showed that electrodeposition of Zn-Ni alloy could be either normal or anomalous. At very low current densities, zinc began to deposit at its equilibrium potential, which is more negative than that of nickel, and the more noble nickel deposited preferentially. As a result, normal co-deposition occurred and nickel deposited at a faster rate than zinc. By increasing current density, due to the increased rate of hydrogen evolution, pH in the cathode layer increased and resulted in the formation of zinc hydroxide at the cathode surface. However, nickel remained in its ionic form since the electrolyte was buffered by the hydrolysis of Zn^{+2} ions at a pH much less than that for nickel hydroxide precipitation. Therefore, the deposition sites on the cathode surface for nickel were substantially limited and its deposition was suppressed easily when its deposition sites were occupied by adsorbed zinc hydroxide. The hydroxide suppression mechanism is discussed in section 2.1.7 below.

2.1.7 Proposed mechanisms for the anomalous co-deposition

Although the anomalous co-deposition of Zn-Ni alloys has been known since 1907, the co-deposition mechanisms are not well understood and there is still no universally accepted theory. Several researchers have attempted to interpret the mechanism of the

anomalous co-deposition. Brenner (1963) proposed an "Addition agent theory" to account for anomalous co-deposition of zinc with other iron group metals. He pointed out that the deposition of nickel is very sensitive to the adsorption of addition agents and its discharge can be prevented entirely. He also postulated that the addition agent is produced by the cathode reaction only when the current density is high enough to increase significantly the pH of the cathode diffusion layer. A thin layer of zinc hydroxide at the cathode surface inhibits formation of Ni deposits. This layer is formed due to a rise in pH in the cathode layer, caused by hydrogen evolution during the deposition process.

Dahmas and Croll (1965) conducted a comprehensive investigation on the role of pH at the cathode surface and its effect on anomalous co-deposition of iron-nickel alloys. They demonstrated that when the rate of hydrogen evolution increased at current densities higher than the limiting current, the pH at the cathode surface increased significantly resulting in the formation of ferrous hydroxide. A layer of ferrous hydroxide at the cathode blocked nickel discharge but permitted a high rate of iron discharge. A model was also derived to calculate the surface pH as a function of the bulk pH. The authors showed that the cathode pH could increase to a value about 9 from a bulk pH of 2.5. The hydroxide suppression mechanism, based on the "addition agent theory", in which the formation of the hydroxide film of the less noble metal causes the anomalous co-deposition, has also been proposed and supported by other researchers.

Other mechanisms have also been proposed to describe anomalous co-deposition. Fratesi and Roventi (1992) attributed the anomalous co-deposition of zinc-nickel alloys to the intrinsically slow nickel kinetics. Another proposed mechanism was based on the

adsorbed intermediates that act as catalysts in the deposition of the less noble metal. Chassaing and Wiart (1992) reported that $(NiZn)_{ads}^{+}$ intermediate, which acts as a catalyst has a significant role in the preferential zinc deposition from chloride electrolytes.

Deligianni and Romankiw (1993) experimentally measured the surface pH during Ni-Fe alloy deposition. Starting from a bulk pH value of 2, the surface pH did not increase more than 3 pH units from the bulk value. It was found that the co-deposition was anomalous but the surface pH was much lower than that required for iron hydroxide formation according to the hypothesis proposed by Dahms and Croll (1965). They also showed that metal-ion hydrolyzed species, acting as buffering agents, suppressed the localized pH rise, and played an important role in the anomalous co-deposition of Ni-Fe alloy. In another study conducted by Miranda et al. (1997), it was shown that the surface pH remained close to bulk pH of 3 within a wide range of potentials while anomalous co-deposition was observed.

Since Dahms and Croll calculated the surface pH from other measurable quantities, this value might be greater than the actual surface pH value. However, results from other researchers, who measured experimentally the surface pH, confirmed that an increase did occur. Major differences in views appear to be in the extent of pH rise, permanency of the surface alkalination, and the ability to induce metallic hydroxide film. Since in the present study there was no means of measuring or calculating the cathode pH or confirming the presence of catalytic intermediates at the surface, the proposed theory by Dahms and Croll appeared to provide a reasonable explanation for observed results.

2.2 PHOTOCATALYTIC PROCESS

2.2.1 Advanced oxidation processes (AOPs)

AOPs are oxidative techniques that are applied for water and wastewater treatment. These technologies are fairly new, which have been developed since 1975 (Zhou and Smith, 2001) and have attracted considerable interest in the field of water and wastewater treatment. Two major advantages of these technologies are a high rate of pollution removal and a diverse range of their applicability for wastewater treatment (Stefan et al., 1996).

AOPs include different processes such as UV, UV/H_2O_2, UV/O_3, $UV/H_2O_2/O_3$, H_2O_2/Fe^{+2} (Fenton), $H_2O_2/Fe^{+2}/UV$ (photo-Fenton), and UV/TiO_2 (photocatalysis). O_3, H_2O_2 and/or O_2 are used as oxidants in these processes. These techniques are based on the generation of reactive and oxidizing free radicals, such as $OH^{\bullet}, HO_2^{\bullet}, HO_3^{\bullet}, O_2^{\bullet-}$ and $HO_3^{\bullet}$ radicals, which function as pollutant-killing agents (Rajeshwar and Ibanez, 1997).

A major drawback of AOPs is their high operation and capital costs compared to biological techniques. However, due to their strong oxidation ability, AOPs could be used as a pre- or post-treatment step to improve the biodegradability of refractory or inhibitory organics in wastewaters.

2.2.2 Photocatalysis (TiO_2/UV)

Heterogeneous photolysis or photocatalysis, which is considered one of the AOPs, uses a semiconductor as the catalyst and UV light to induce photoelectrochemical

reactions at the catalyst particle surface (Rajeshwar and Ibanez, 1997). Photocatalysis includes different reactions such as total oxidation of organics, dehydrogenation, metal deposition, water purification and gaseous pollutant removal (Herrmann, 1999). Hydroxyl radicals, $OH^\bullet$, are the main oxidants, which are formed during photocatalysis. Theses strong oxidants can change the organic compound structure by either abstraction of hydrogen atoms or addition to double bonds (Stefan et al., 1996).

Degradation of organics is classified by the extent of their degradation to final products (Bankian, 2004):

1- Primary degradation leads to a structural change in parent compounds.

2- Satisfactory degradation reduces the toxicity of the parent compound or converts a non-biodegradable compound to the biodegradable one.

3- Complete mineralization converts organics to carbon dioxide and water.

4- Improper degradation changes the structure of organic in such a way that the toxicity in water increases.

Since semiconductors have unique electronic properties, they have been generally used as photocatalysts in photocatalysis. The absorption spectrum of metal oxide semiconductors is between 350-400 nm, so they can be activated by absorption of near ultraviolet light. Semiconductor photocatalysts include various metal oxides and sulfides such as: TiO_2, ZnO, WO_3, CeO_2, CdS and ZnS (Herrmann, 1999). The application of CdS and ZnO as photocatalysts has been hampered because of the self-oxidation reactions and production of hazardous metal ions (Peral et al., 1988; Harada, 1985).

It has been proved by different researchers that titanium dioxide has the best photocatalytic performance in water and wastewater treatment. The photocatalytic activity of TiO_2 was first examined by Frank and Bard (1977) for decomposition of cyanide in water. Titania is very cheap, chemically and biologically inert, photo-stable and can be activated by sunlight. Furthermore, photogenerated holes at the surface of TiO_2 are strong enough to oxidize almost all organic pollutants in the wastewater (Fujishima et al., 2000). TiO_2 exists in two main crystalline forms: Anatase and rutile. Anatase is known to be photocatalytically more active than rutile, but thermodynamically less stable. There are various sources of TiO_2, but Degussa P25 TiO_2 has been widely used in different experiments due to its high photoactivity. Since TiO_2 has a very polar surface in aqueous solutions, it is not a good adsorbent for nonpolar organic pollutants (Lepore et al., 1996). At pH below and above the point of zero charge (pH_{zpc}) of TiO_2, the surface of titania becomes positively and negatively charged, respectively. Some techniques, such as immobilization of TiO_2 on the surface of the support materials may provide hydrophobic surface, which adsorbs organics (Takeda et al., 1995). At $pH < pH_{zpc}$ the TiO_2 surface is positively charged and anionic species are adsorbed in a great extent on the surface of TiO_2 (Marchado et al., 2003).

The energy difference between the highest valence band and the lowest conduction band in a photocatalyst semiconductor is called band-gap energy. Photoexcitation occurs when titanium dioxide is illuminated by light of energy equal or greater than its band-gap. In this case, an electron from the valence band is excited into the conduction band and a positive hole remains in the valence band of the semiconductor (Herrmann et al., 1993). The photogenerated electron is negative enough to reduce molecular oxygen and the

photogenerated hole is positive enough to oxidize water molecule to hydroxyl radical (OH·). Hydroxyl radicals react with organic compounds rapidly and non-selectively. They have also been found to be primary oxidants responsible for photocatalytic degradation of organic pollutants in wastewaters.

Another application of the semiconductor photolysis is removal of metal ions in wastewater using photogenerated electrons. Photocatalytic removal or recovery of dissolved metal ions in wastewater is a relatively new technology (Chen et al., 2000). Although photocatalytic oxidation of organics in aqueous solution has been well studied, the range of reducible compounds (especially metal ions) that have been studied by heterogeneous photocatalysis is significantly narrower (Rajeshwar et al., 2002).

The overall photocatalytic process can be carried out in four independent steps:

1. Transfer of reactants from liquid phase to the surface of TiO_2
2. Adsorption of the reactants
3. Reaction at the surface of titania
4. Release of products

2.2.4 Photocatalytic reactors

TiO_2 can be used either in suspension form or immobilized on an appropriate support material within the photoreactor. In most of studies to date, the titanium dioxide has been used in the form of fine particles suspended in the solution. The efficiency of reactors with suspended photocatalysts seems to be higher than those using immobilized TiO_2. Titanium dioxide in suspension form provides a high surface area for reactions. In slurry photoreactors with suspended catalyst particles, the degradation rate is determined by the

UV penetration depth and adsorption properties of all components in the solution. Moreover, the UV penetration depth is limited both by strong adsorption of TiO_2 particles and organic compounds in the solution (Ray and Beenackers, 1997).

In large-scale treatment processes, it would be simpler if the catalyst can be used as a stationary phase attached to a suitable support, where water passes continuously over the catalyst particles. Matthews, (1987) was one of the first researchers who immobilized TiO_2 on the surface of support materials. In this mode, expensive separation processes for removal of the fine catalyst particles from treated water is eliminated. However, coating of TiO_2 on the surface of support material has some problems since all reactions occur at the liquid-solid interface illuminated by UV (Byrne et al., 1998). Hence, the reaction rate is limited by mass transport of pollutants to the catalyst surface. In addition, the depth of penetration of UV light limits the reactor design.

The effective part of all photoreactors, either slurry or static, is the place where TiO_2, organic compound and UV light are present at the same time (Chen et al., 2001). In order to increase the effectiveness of the immobilized photocatalyst and photoreactor, a uniform distribution of UV light, a good anchoring of TiO_2 to the support, a high ratio of catalyst surface area to volume of the solution in the reactor as well as a low mass transfer limitation are required. In order to find out optimal catalyst/support conditions, various parameters such as type of the photocatalyst, support materials, the amount of catalyst coated on the support, deposition technique and calcination temperature should be considered (Zhang et al., 1994).

2.2.5 Photocatalyst supports

The primary role of a catalyst support is to offer a high external surface area to the catalyst and to increase porosity (Bideau et al. 1995). Additionally, since TiO_2 has a very polar surface in an aqueous system, water is more strongly adsorbed to its surface than a typical organic contaminant. Thus, another key property of the support may be providing a hydrophobic surface for organic adsorption (Lepore et al., 1996). Good adherence of the catalyst to the support is one of the most important aspects in TiO_2 immobilization process since if it is not strong enough some of photocatalysts will detach and go to the solution. Photocatalyst particles are usually aggregated during immobilization. This enhances the catalyst thickness layer, but reduces its activity because of void spaces created between the catalyst layers.

There are, generally, two routes for TiO_2 deposition on the surface of the support material (Bideau et al., 1995):

- The use of separately made (SM) Titania, e.g. Degussa P25 TiO_2

- Preparation of catalyst in-situ from a titanium salt, which is known as sol-gel process

Due to its simplicity, the first procedure was used for immobilization technique in the present study. The detailed immobilization technique is explained in Chapter 3. If the catalyst particle diameter is larger than silica gel pore diameter, the TiO_2 will be anchored on the outer surface of the support and will not penetrate within pores. An oxide prepared from a liquid precursor is usually expected to have more adhesion to the support than an oxide prepared separately. However, stronger adhesion of P25 TiO_2 on the silica

gel surface than oxide prepared by sol-gel method was observed by Bideau et al. (1995). Optical transparency of the silica gel under water, its high surface area and its strong adsorptive capacity are some reasons that many researchers have chosen this compound as the support material for photocatalysis. Additionally, transparent supports such as silica gel can assist in the trapping of light by internal reflection.

An overview of some previous studies using immobilized TiO_2 on various solid support materials and different methods for immobilization is brought in Tables 2 and 3.

2.2.6 Mechanism of photocatalysis

Oxidative and reductive characteristics of a semiconductor photocatalyst, such as titanium dioxide, have been explained by band-gap energy theory. The magnitude of band-gap energy (E_{bg}) is defined as the difference between valence band and conduction band energies. The upper of filled bands is called the valence band while the lower of unfilled bands is called the conduction band (Pleskove, 1986). Figure 4 represents that when a semiconductor is illuminated by light with energy equal to or greater than the band-gap energy of the semiconductor, an electron from the valance band is transferred to the conduction band. This results in generation of an electron/hole pair, which can participate in different reactions.

Reaction (2.2.6.1) illustrates the photoexcitation of the TiO_2 photocatalyst by the energy greater than its band gap energy:

$$TiO_2 + h\nu \xrightarrow{\geq E_{bg}} TiO_2 \ (h^+{}_{vb} + e^-{}_{cb}) \hspace{3cm} (2.2.6.1)$$

where $E = h\nu$ is the energy of a photon.

Band-gap energy of anatase TiO_2 is 3.2 eV and energy equal to or greater than this amount is required for photoexcitation of TiO_2 (Dionysiou et al., 2000). Anatase TiO_2 should be irradiated by light with $\lambda < 390$nm in order to generate electron-hole pairs (Marchado et al., 2003). These photogenerated electrons and holes then either migrate to the particle surface participating in redox reactions or they recombine. Electron and hole recombinations are undesired reactions that occur during photocatalysis. These reactions will reduce the photoefficiency since the electric energy is released as heat. In order to overcome this problem, an appropriate reducible species should be added to the solution to consume electrons. Therefore, sufficient amount of holes will be present in the system for oxidation reactions. There are two main pathways for the mineralization of organic compounds after photoexcitation of the titanium dioxide. One of these involves reactions that produce hydroxyl radicals, which are strong oxidants (indirect oxidation). Another alternative is direct hole oxidation (direct oxidation). Although a number of oxidative pathways have been proposed for the photocatalysis, hydroxyl radicals play a critical role in the degradation of the pollutants. The main source of these radicals is water.

Hydroxyl radicals can be produced directly by hole oxidation of surface adsorbed water molecules or adsorbed hydroxide ions at the valence band of TiO_2 (Hidaka and Zhao, 1992):

$$OH^- + h^+ \rightarrow OH^\bullet \qquad \text{(alkaline media)} \qquad (2.2.6.2)$$

$$H_2O + h^+ \rightarrow OH^\bullet + H^+ \qquad \text{(acidic media)} \qquad (2.2.6.3)$$

In the presence of organic compounds, the photogenerated hydroxyl radicals are consumed through reaction (2.2.6.4):

$$OH^{\bullet} + RH \rightarrow R^{\bullet} + H_2O \rightarrow CO_2 + H_2O + mineral\ acids \qquad (2.2.6.4)$$
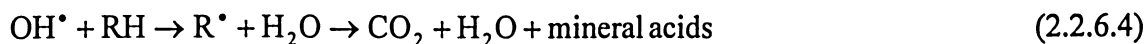
However, if no organic species is present, water will be oxidized by the following reaction (Chen and Ray, 2001):

$$2H_2O + 4h^+ \rightarrow O_2 + 4H^+ \qquad (2.2.6.5)$$

The above reaction is a kinetically slow four-electron process. As water or organic species is oxidized, reduction should also occur at the conduction band in order to maintain electroneutrality (Prairie et al., 1993). Thermodynamically, any dissolved species with a standard reduction potential more positive than the conduction band of the TiO_2 can be reduced by photogenerated electrons (Chen and Ray, 2001).

In photocatalytic systems where the reduction of metal ions is of interest, presence of oxygen molecules would reduce the efficiency of the process since they compete for photogenerated electrons. Oxygen molecules are reduced to produce superoxide radicals, which eventually form $HO_2^{\bullet}$ radicals and enter into oxidation cycle (Somasundaram et al., 2004).

$$O_2 + e^- \rightarrow O_2^{\bullet -} \qquad (2.2.6.6)$$

$$O_2^{\bullet -} + H^+ \rightarrow HO_2^{\bullet} \qquad (2.2.6.7)$$

Table 2. Various types of photoreactors using immobilized photocatalyst.

Photoreactor type	Support for catalyst Type Physical Appearance		Catalyst arrangement	Reference
Batch	Glass	Beads	Fixed bed	(Serpone et al., 1986)
Continuous flow	Glass	Spiral wound around the lamp beads	Wall of the glass spiral	(Mathews, 1987)
Continuous flow	Glass	Beads	Fixed bed in the annular space between the lamp and outer wall	(Al-Ekabi and Serpone, 1988)
Batch	Glass	Hollow beads	Floating bed	(Jackson et al., 1991)
Batch (recirculation)	Sand	Grains	Fixed bed on the reactor bottom	(Matthews, 1991)
Batch (recirculation)	Silica gel	Grains	Fixed bed on the reactor bottom	(Matthews and McEvoy, 1992)
Continuous	Silica based	Sand, glass beads Glass fiber mesh Glass wood fiber	Fixed bed	(Zhang et al., 1994)
Batch (recirculation)	Polymer	Membrane	Disc membrane	(Bellobono et al., 1992)
Batch (recirculation)	Fused silica	Optical fiber	Coating on the surface	(Hofstadler et al., 1994)
Batch	Glass, quartz, stainless steel	Plates	Fixed bed	(Fernandez et al., 1995)
Batch (recirculation)	Anodized iron	Plates	On the reactor bottom	(Muradov, 1994)

35

Table 3. Techniques of immobilization of titanium dioxide on various support substrates

Immobilization methods	Support material	Refrences
Dip coating from suspension	Glass Beads Glass tubing Glass plate Glass fibers Tin oxide coated glass Silica gel Sand	(Bideau et al., 1995; Zhang et al., 1994) (Matthews, 1988; Al-Ekabi and Serpone, 1988) (Chester et al., 1993) (Zhang et al., 1994; Brezova et al., 1995) (Vinodgopal and Kamat, 1995) (Bideau et al., 1995; Zhang et al., 1994) (Zhang et al., 1994)
Sol gel related methods	Quartz Optical fibers Glass beads Silica gel Glass plate	(Fernandez et al., 1995) (Tada and Honda, 1995) (Bideau et al., 1995) (Bideau et al., 1995) (Fernandez et al., 1995)
Thermal	Titanium Titanium alloy	(Camara et al., 1995) (Kudo et al., 1990)
Spray coating	Stainless steel, titanium alloy	(Byrne et al., 1998)
Electrophoretic coating	Stainless steel Titanium, titanium alloy, tin oxide glass	(Byrne et al., 1998) (Byrne et al., 1998)
Liquid phase deposition	Glass plate	(Deki et al., 1996)
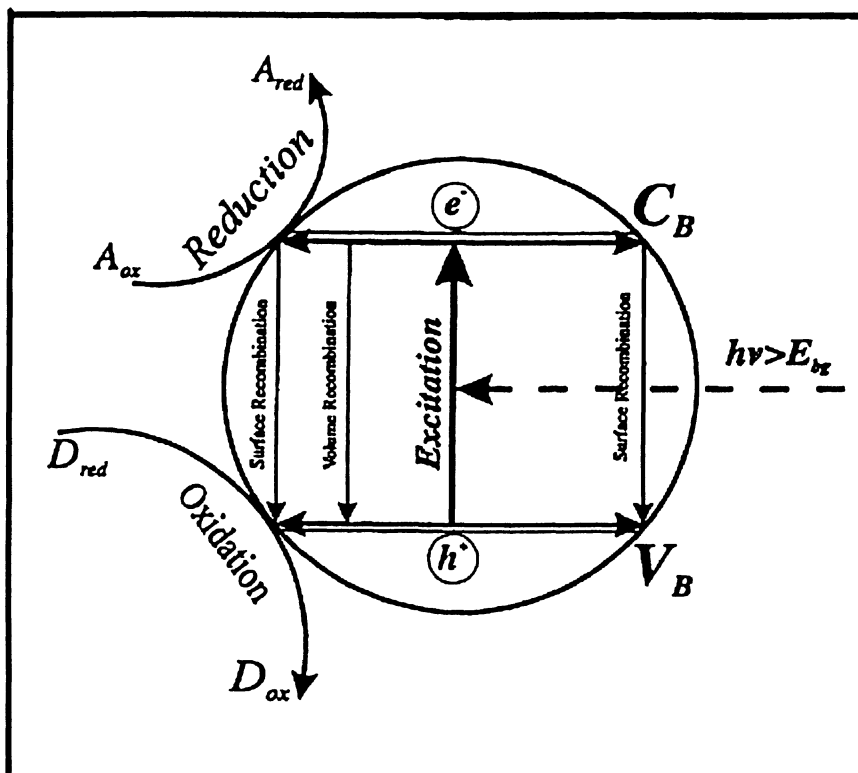
Figure 4. Schematic diagram of photoexcitation of the semiconductor particle with reduction and oxidation reactions, adopted from Mehrvar (1998).

CHAPTER 3
EXPERIMENTAL WORK

3.1 Experimental Set-Up

This section is divided into three parts: electrochemical, photocatalytic and combined processes. Experimental set-up, and equipment required for each process are described separately.

3.1.1 Experimental Set-Up for Sole Electrochemical Experiments

The experiments were performed in a laboratory-scale aluminum tank, which had a height of 5.5 cm, a width of 20 cm and a length of 25 cm. A schematic diagram of the set-up is given in Fig 5. In sole electrochemical experiments, the UV lamp was turned off. The electro-cell used in the current study was a plate-in-tank laboratory-scale cell. This is the simplest cell geometry in which vertical, parallel plate electrodes are hold in a tank. Three 316-stainless steel anodes and two aluminum cathodes, each of 18×5 cm, were used in all experimental runs. The type of the electrical connection is monopolar configuration, in which cathodes and anodes are set in parallel and each electrode is directly connected to the suitable pole of the power supply. Cathodes and anodes were connected to the negative and positive terminals of the power supply, respectively. The gap between anodes and cathodes was fixed at 1.5 cm. The power supply was connected to an adjustable direct current source to provide a constant cell current. An ampmeter was

placed in series in circuit to adjust desired cell current. A voltmeter was used to measure the voltage across cathodes and anodes.

The electrolyte agitation in electro-cell was provided by pumping and the mixture in the feed tank was stirred using two magnetic stirrers. The inlet flow rate was adjusted to a desired value by changing the rate of recycle and feed flows. The feed distribution inside the electro-cell was provided by a liquid distributor, which was set at the bottom of the electro-cell. The electrochemical rector had a flow-by configuration, in which the current flow is perpendicular to that of the solution. This configuration has been chosen to allow the use of flat electrodes, which are thin in the direction of the current and long in the flow direction, so that a high product conversion will be achieved.

The whole experimental set-up was a batch-recycle system in which a gradual reduction in metal ions concentration takes place. Batch recirculation is a convenient and flexible mode of operation. Using a reservoir not only increases the electrolyte inventory, but also it may: (1) help to adjust the pH via addition of reagents, (2) facilitate sampling; and (3) provide a well-mixed zone for the reactant preparation prior to electrolysis.

The electro-cell was maintained in a water bath, which was equipped with a heater and connected to tap water to keep liquid temperature at a constant value. Both initial zinc and nickel ion concentrations were 20 ppm. Also, 250 ppm of potassium sulfate was used in all experimental runs as a supporting electrolyte. The total volume of the simulated wastewater used in sole electrochemical experiments was 15L. Prior to each experiment, the solution was prepared in the holding tank of the apparatus and the content was stirred by two magnetic stirrers inside the reservoir for 1 hour.

3.1.2 Experimental Set-up for Sole Photocatalytic Experiments

The experimental set-up for sole photocatalytic processes was similar to Figure 5. In this set of experiments, the UV lamp (254 nm) was turned on and electrodes were removed from the reactor. In experiments using immobilized TiO_2, a layer of coated silica gel was uniformly put at the bottom of the reactor. The distance between UV lamp and coated silica gel was 10 cm.

Since there was no control on the amount of titanium dioxide coated on the silica gel surface, the effect of different parameters such as pH, flow rate and temperature on photodegradtion of LAS was examined using suspended TiO_2. For all experiments, the solution containing TiO_2 was allowed to equilibrate in the dark for 1 hr. Samples taken at different intervals were centrifuged and then filtered to remove TiO_2 particles.

3.1.3 Experimental Set-up (Combined Electrochemical & Photocatalytic Processes)

In experiments for simultaneous removal of metal ions and photocatalytic degradation of LAS, the experimental set-up was the same as Figure 5. In these experiments, the UV lamp was turned on and electrodes were connected to the power supply. The solution contained metal ions (20 ppm), supporting electrolyte (250ppm), and LAS (100 ppm). The total volume of the solution was 6 L.
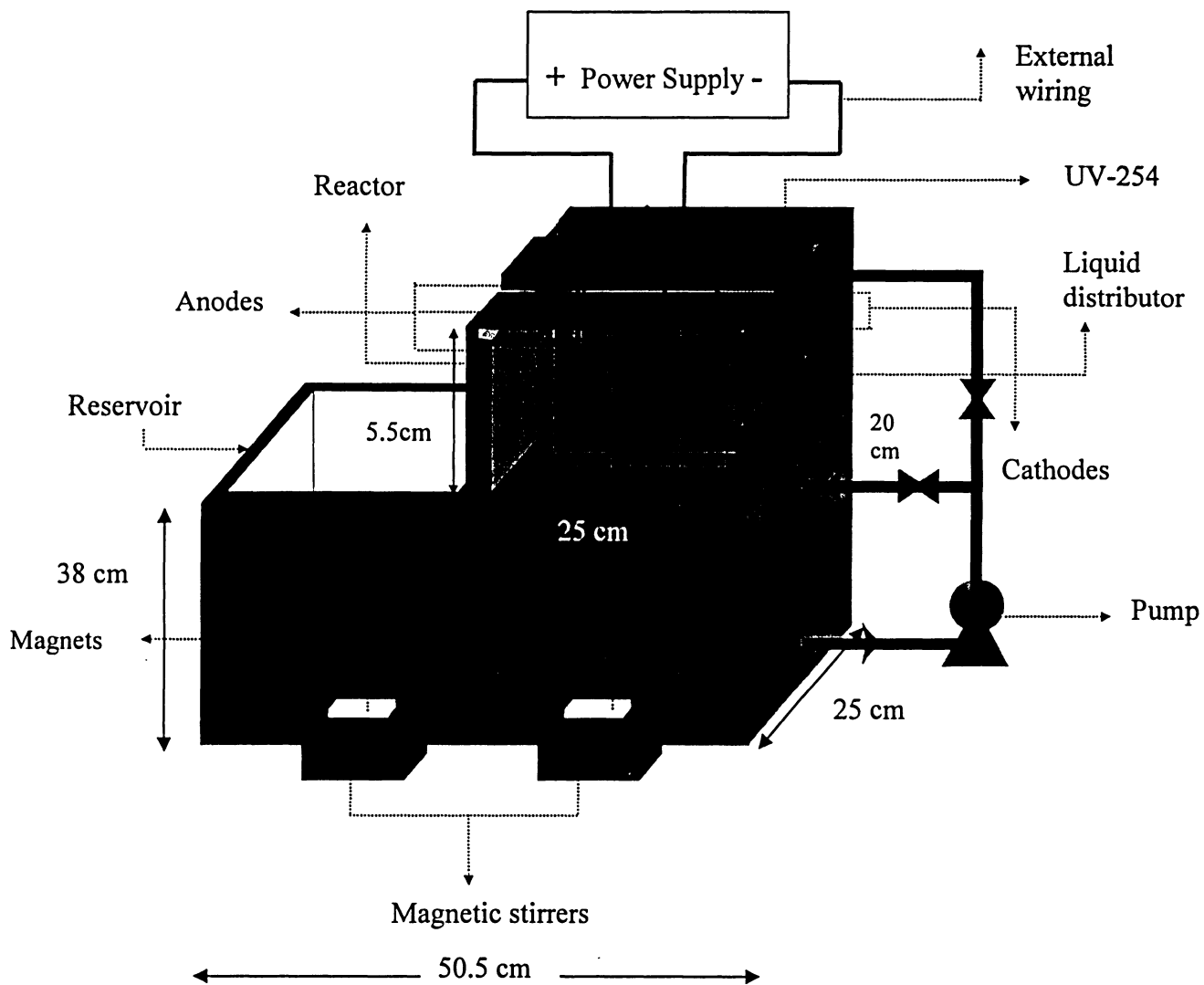
Figure 5. A schematic diagram of the experimental set-up

3.2 Materials

The following materials were used in electrochemical and photocatalytic experiments:

3.2.1 Linear Alkylbenzene Sulfonate (LAS)

The molecular structure of LAS is shown in Figure 6. LAS is the sodium salt of dodecylbenzenesulfonic acid, a mixture of phenyl substituted alkyl chain. LAS used in the present study has 12 carbons in its alkyl chain and was purchased from Aldrich company.
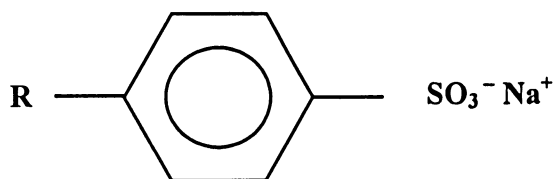
Figure 6. Molecular structure of linear alkylbenzene sulfonate (LAS), where R represent alkyl chain (R=$(CH_2)_{11}CH_3$)

3.2.2 Titanium dioxide (TiO$_2$)

Degussa P25 TiO$_2$ (mainly anatase with surface area 55 m^{2}g^{-1}) used as photocatalyst in this study was donated from Stochem Company, Canada. Concentration of the suspended titanium dioxide in solution was 1.0 g.l^{-1} in all experiments.

3.2.3 Silica gel

Granular silica gel (grade 40, 6-12 mesh) was purchased from Aldrich Company. It was used as supporting material for the TiO$_2$ immobilization.

3.2.4 Chemicals for LAS analysis

Chloroform ($CHCl_3$), methylene blue reagent, phenolphthalein indicator (1% alcoholic), concentrated sulfuric acid (36N), sodium phosphate monobasic monohydrate (Na $H_2PO_4.H_2O$) were all purchased from Aldrich Company.

3.2.5 Chemicals for electrochemical experiments

Nickel sulfate hexahydrate and zinc sulfate heptahydrate (BDH Chemicals and J.T. Baker) were used to prepare the simulated wastewater. Potassium sulfate (J.T. Baker) was also added to the solution as the supporting electrolyte. Test kits for zinc and nickel concentration measurements were bought from VWR Company and used according to manufacturer manual.

3.3 Laboratory Equipment

A list of the instrumentation and laboratory equipment used in the present study is shown in Table 4.

3.4 Analytical Measurements

3.4.1 pH Measurement

The daily calibration was done using buffers of pH=4 and pH=7. In experiments with controlled pH, the pH probe was fixed inside the reactor and the pH of the solution was maintained constant within the desired range by additions of either potassium hydroxide (1N) or sulfuric acid (1N).

3.4.2 Analytical Techniques for Ni^{+2} and Zn^{+2} Measurements

Samples were withdrawn from reservoir inlet at regular intervals and analyzed by spectrophotometer for determination of metal ion concentrations in the solution. According to the manufacturer's manual, the Zincon method was used for measuring zinc ion concentration in the solution with the detection range of 0 to 4 $mg.l^{-1}$ of zinc. For nickel concentration measurements, Dimethylgloxime (Heptoxime) procedure was applied with the detection range of 0 to 0.12 $mg.l^{-1}$.

Table 4. List of instrumentation used

Instrument	Manufacturer & Model	Precision
PH meter	Leici Instrumentation Factory, Shanghai, China: model PHS-3C	± 0.01
Chemical oxygen demand digestor	Bioscience Inc.	± 2°C
Spectrophotometer (For COD and metal ion concentration measurements)	Orbeco Analytical Systems Inc. Farmingdale, New York; model Orbeco-Hellige 975 PM	
UV Spectrophotometer (For LAS measurement)	Perkin Elmer Inc; model Lambda 40	
Balance	Setra Systems Inc.; model EL-200S	± 0.001 g
Power Supply	Electro Product Laboratories Inc.; model D-612 T	

3.4.3 Analytical Technique for LAS Measurement

Analytical measurement of LAS was carried out based on the procedure described in standard methods for determination of anionic surfactants as methylene blue active substances (MBAS) (Standard Methods, 1998). MBAS bring about the transfer of methylene blue, a cationic dye, from an aqueous solution into an immiscible organic liquid through ion pair formation by the MBAS anion and methylene blue cation. The intensity of the formed blue color in the organic solvent (chloroform) is a measure of methylene blue active substances present in the water sample. The blue color in the chloroform was read at 652 nm by UV spectrophotometer.

To prepare methylene blue reagent, 100 mg of methylene blue was dissolved in distilled water and diluted to 100 mL in a volumetric flask. 30 mL of this solution, 500 mL of water, 41 mL of H_2SO_4 6N, and 50 g $NaH_2PO_4.H_2O$ were added to 1000 mL volumetric flask, dissolved thoroughly and diluted to 1000 mL with distilled water. To make wash solution, 41 mL of H_2SO_4 6N was added to 500 mL of distilled water. 50 g of $NaH_2PO_4.H_2O$ was added to the solution, dissolved thoroughly and diluted to 1000 mL by distilled water. Standard LAS solutions were prepared by diluting an appropriate amount of LAS with distilled water. Concentrations were ranging from 0 to 150 mg LAS/L.

The extraction procedure was slightly modified in order to decrease the required chloroform, which is toxic and a suspected carcinogen. Samples of 10 mL volume were periodically taken from reservoir inlet and was centrifuged and further filtered through a 934-AH Whatman glass microfiber filter to remove TiO_2 particles. 2 mL of the centrifuged sample was diluted to 100 mL, so that the measured concentration would be

45

less than 2 mg.l^{-1}. 10 mL of the diluted sample was added to a clean 14 mL centrifuge tube and one drop of phenolphthalein indicator solution was added to the sample and mixed. NaOH 1N was added drop-wise to make solution alkaline (solution became pink) and then, H$_2$SO$_4$ 1N was added drop-wise until the pink color disappeared and solution became slightly acidic. 1 mL of CHCl$_3$ and 2.5 mL of methylene blue reagent was added to the tube and shaken vigorously for 30 seconds. The aqueous solution was removed by a clean pipette and transferred to another tube. The tube containing chloroform was capped to prevent losses and the extraction procedure was repeated two more times. 5 mL of the wash solution was added to all of the combined CHCl$_3$ extracts, shaken vigorously for 30 s, and then allowed to be separated. Finally, the wash solution was extracted two times by chloroform, 1 mL each time, and chloroform extracts were diluted by chloroform to 10 mL. The absorbance at 652 nm was measured against CHCl$_3$ blank by UV spectrophotometer. Standard curve was prepared by measuring the absorbance of the standard solutions in the range of 0 to 150 mg LAS/L. The extraction procedure for standard solution was also the same as described before. Finally, the absorbance of each sample was converted into concentration using standard curve shown in Appendix B.

3.4.4 Measurement of Chemical Oxygen Demand (COD)

COD test was used to determine the amount of oxygen required to oxidize organic compounds. Oxidization is done by a powerful chemical oxidant such as potassium dichromate in acidic solution. Different methods could be used for COD determination, however, the closed refluxed method (colorimetric method) was chosen as it is more economical for the COD values of >50mg/L (Standard Methods, 1998).

10.216 g $K_2Cr_2O_7$, previously dried at 103°C for 2 h, 167 mL concentrated H_2SO_4, and 33.3 g $HgSO_4$ were added to about 500 mL of distilled water, dissolved thoroughly and diluted to 1000 mL (Digestion solution). Sulfuric acid reagent was purchased from VWR Company and used as received.

Samples were periodically taken from the effluent of the reactor and centrifuged to remove suspended solids. 2.5 mL of this sample, 1.5 mL of digestion solution and 3.5 mL of sulfuric acid reagent were added to a clean standard 10-mL vial. A blank was prepared in the same manner but instead of sample solution, 2.5 mL of distilled water was added. Vials were tightly caped, inverted several times to mix completely and were placed in the COD reactor, which was preheated to 150±2°C, for 2 hours. After 2 hours, vials were cooled to room temperature. The absorbance at 608 nm was measured against a blank by spectrophotometer.

3.5 Immobilization procedure

The technique used for the coating of TiO_2 was to thermally bind commercial Degussa TiO_2 P25 onto the surface of silica gel granules. A mixture of 4 g titanium dioxide and 200 ml distilled water was sonicated for 20 min in an ultrasound device. 250 g silica gel was added to the mixture and the entire sample was sonicated for another 20 min. Most of the water was evaporated by heating the sample on a hot plate stirrer. The sample was dried in an oven at 100 °C for 2 hours and then was heated at 500 °C in a furnace for 24 hours. After heating, coated silica gel was washed with distilled water while vigorously shaking. This process removed TiO_2 particles, which were not attached firmly to the support silica gel granules. Washing with distilled water was repeated for several times until the supernatant was free of suspended TiO_2 particles.

3.6 Data Analysis

Uncertainties associated with concentrations of zinc and nickel, and chemical oxygen demand (COD) were calculated from multiple readings (three times). Then, the average of obtained data, $x_{av.}$, was shown in graphs. The value of the standard deviation, SD, was calculated using following formula and used as the value of the error bar or the standard error of the mean in graphs:

$$SD = \sqrt{\frac{\sum(x_i - x_{av.})^2}{n}}$$

(3.6.1)

where n=3 is the number of readings for each sample.

CHAPTER 4

RESULTS AND DISCUSSION

4.1. Electrochemical removal of metal ions

A series of experimental runs were conducted without controlling of bulk electrolyte pH for a 47-hour treatment period. Following section explains the pH change during 47 hours of treatment.

4.1.1 Uncontrolled bulk pH change during electrolysis

In electrochemical cells where anolyte and catholyte compartments are separated, the pH in catholyte part usually increases significantly during electrolysis. Lanza and Bertazzoli (2000) studied the removal of zinc from an aqueous solution using a flow-through cell with separate anolyte and catholyte reservoirs. They observed that the bulk catholyte pH increased from an initial value of 2.5 to a final value of 8, which was believed to be due to hydrogen evolution in the catholyte compartment. Other reactions at the anode did not have any effect on the bulk pH in catholyte compartment. Additionally, in most of alloy deposition processes soluble anode is used to keep the concentration of the depositable ions constant in the bath. However, in alloy deposition systems where insoluble anode is applied, a decrease in electrolyte pH is always observed due to decomposition of water molecules at the anode surface (Brenner, 1963).

In the current study, the electro-cell was not separated into two compartments for the anode and the cathode. In all experiments without pH control, the bulk pH decreased

49

during the first 8 hours, and it then increased slightly at the end of 47 hours of treatment. Furthermore, the magnitude of pH increase was higher for experiments operating under higher current densities. When the current density of 1.11 mA.cm^{-2} was applied, the solution pH decreased from an initial value of 5.6 to 4.6 after 8 hours of treatment and, then, it reached to its final value of about 6.5 at the end of the experiment. However, a final pH value of about 5 was reached using a current density of 0.167 mA cm^{-2}.

Depending on the solution composition, different reactions can occur at cathodes and anodes of an electrochemical cell. In the present study, following reactions were likely to take place within the electro-cell:

(1) Direct electrodeposition of metal cations to the metals at the cathode surface

$$Zn^{++}(aq) + 2e^- \Leftrightarrow Zn(s) \qquad\qquad E^o = -0.76\ V \qquad\qquad (4.1.1.1)$$

$$Ni^{++}(aq) + 2e^- \Leftrightarrow Ni(s) \qquad\qquad E^o = -0.23\ V \qquad\qquad (4.1.1.2)$$

(2) Side reactions such as water decomposition, reduction of oxygen molecules and hydrogen evolution

$$2H_2O + 2e^- \Leftrightarrow H_2 + 2OH^- \qquad\qquad E^o = -0.83\ V \qquad\qquad (4.1.1.3)$$

$$O_2 + 4H^+ + 4e^- \Leftrightarrow 2H_2O \qquad\qquad E^o = +1.23\ V \qquad\qquad (4.1.1.4)$$

$$2H^+ + 2e^- \Leftrightarrow H_2 \qquad\qquad E^o = 0.00\ V \qquad\qquad (4.1.1.5)$$

(3) Anode reaction

$$H_2O \Leftrightarrow \frac{1}{2}O_2 + 2H^+ + 2e^- \qquad\qquad E^o = -1.23\ V \qquad\qquad (4.1.1.6)$$

The rate of pH decrease was fast during the initial 8 hours of experimental runs and it slowed down with the electrolysis time. During initial hours of each experimental run, due to high concentrations of nickel and zinc ions, the main reactions were reduction of these ions at the cathode surface. Furthermore, the only reaction at the anode surface is believed to be water decomposition reaction, which resulted in an increase in the bulk electrolyte acidity. It can be concluded that the rate of side reactions at the cathode surface was slower than that of water decomposition at the anode to counteract the pH decrease in the bulk electrolyte. By increasing electrolysis time, due to depletion of Ni^{+2} and Zn^{+2} ions in the cathode diffusion layer, other side reactions would be occurred in the electro-cell, which increased the pH at the end of experiments.

Hydrogen evolution, oxygen reduction and water decomposition reactions tend to increase pH at the cathode surface by either H^+ consumption through reactions (4.1.1.4) and (4.1.1.5) or OH^- generation through the reaction (4.1.1.3). However, reaction (4.1.1.6) produces H^+ and counteracts the pH increase at the cathode surface.

By comparing the standard reduction potentials of above side reactions with those of zinc and nickel, one can expect that oxygen and hydrogen reduction reactions to occur preferentially. The reduction of dissolved oxygen would be significant at the cathode surface when dealing with low metal ion concentrations (<20 ppm), as the solubility of molecular oxygen is about 8 ppm in aqueous solutions at room temperature (Scott and Paton, 1993). The standard reduction potential for oxygen indicates that oxygen is a strongly oxidizing species. However, since oxygen reduction involves the transfer of four electrons and four hydrogen ions through reaction (4.1.1.4), the overpotential required for

this reaction should be very high. Furthermore, due to presence of the strong oxygen double layer, the reaction kinetics associated with this reaction is very low and an electrode exhibiting catalytic properties, such as platinum, is required to achieve an appropriate rate of reaction (Pletcher and Walsh, 1990). According to above statements, the reduction of oxygen molecules in this study was improbable; therefore, the consumption of hydrogen ions through this reaction may not have occurred.

Another possible side reaction would be that of hydrogen ion reduction. Brenner (1963) suggested that hydrogen ion reduction occurs at more negative potential than its equilibrium potential on many kinds of metal electrodes. The hydrogen overpotential depends on different factors including current density, temperature and the electrode material. In contrast, it is almost independent of the hydrogen ion concentration in solution. For example, metals such as mercury, lead and zinc do not adsorb hydrogen to any great extent and they need a greater overpotential to achieve a significant rate of hydrogen evolution (Pickett, 1979). Aluminium, which was used as the cathode material in all experiments, also has a relatively high hydrogen overvoltage (Pickett, 1979).

In experiments without controlling pH, an increase in pH was observed at the end of experimental runs. As it is illustrated in Figure 8 and Figure 9, graphs of normalized concentrations of both metal ions versus time show an exponential decay behavior. This indicates that the rate of reduction was faster during initial hours of the treatment and slowed down as the electrodeposition proceeded due to the depletion of metal ions in the solution and cathode diffusion layer. Since a constant current was applied through the electro-cell, the cell voltage increased significantly to provide excess electrons.

Consequently, due to the reduction in the concentration of metal ions in the cathode layer, excess electrons were utilized by other reactions such as hydrogen evolution. It is believed that the required cathode potential for reduction of hydrogen ions was reached at the end of experiments and could be a possible explanation for the observed pH raise at the end of experimental runs. Working under high current densities resulted in an increase in solution pH at the end of 24 hours of treatment. This pH rise caused formation of some metal hydroxides within the reactor, which reduced the efficiency of the cell performance.

In experiments conducted by Mitzakov (2004), pH increased significantly in all experimental runs at the end of 48 hours of treatment. A constant cell voltage of 10V was applied which was believed to be high enough for hydrogen evolution reaction at the end of treatment time. Therefore, an increase in acidity of the solution during initial hours of treatment was due to oxidation of water molecules at the anode surface.

It can be concluded that side reactions at the cathode surface were water decomposition and hydrogen evolution through reactions (4.1.1.3) and (4.1.1.5). This reaction would lead to the formation of hydroxide ions in the cathode diffusion layer.

4.1.2 Explanation of anomalous co-deposition in the present study

Standard electrode potentials of zinc and nickel (vs. SHE) are -0.67V and -0.23 V, respectively and one would not expect zinc to co-deposit readily with nickel. Although the standard electrode potential of nickel is more noble than that of zinc and, hence, faster

removal of nickel is expected, it was observed that zinc was removed at faster rate than nickel in all experiments.

In the present study, an anomalous co-deposition was observed in all experimental runs. This can be attributed to the pH rise at the cathode surface. An increase in pH is believed to be due to the decomposition of water molecules at the cathode surface through reaction (4.1.1.3). The formation of hydroxyl ions at the cathode surface causes an increase in the pH value until it is sufficient for the hydrolysis of the metallic ions. According to Richens (1997), the hydrolysis of zinc ions occurs at the lower pH of 8.96 compared with 9.86 for nickel ions. Hydrolysis reactions are followed by the generation of hydrogen ions that suppress the pH rise at the cathode surface (Mitzakov, 2004). It was reported that if hydrolysis reactions were not able to slow down the pH rise, the deposit might include some hydroxides (Pickett, 1979). Since concentrations of zinc and nickel ions in the electrolyte were very low, the concentration of H^+ ions generated from hydrolysis of these ions would not be sufficient to prevent the pH rise at the cathode surface. As a consequence, the formation of zinc hydroxide would occur due to the pH rise at the cathode surface.

According to the theory presented by Dahms and Croll (1965), the hydroxide film of the less noble metal, i.e. iron, would slow down the deposition of the hydrolyzed more noble metal ions, i.e. nickel ions, resulting in the high rate of iron discharge. A similar explanation can be used here for zinc-nickel system in which the deposition of nickel is suppressed by the presence of the zinc hydroxide film at the cathode surface. Nickel deposition mechanism is affected by the formation of the initial layer of zinc hydroxide

since nickel deposit grows according to a nucleation-nucleus growth process (Ohtsuka and Komori, 1998).

4.1.3 Effect of the bulk pH on zinc and nickel ions removal

In all electrochemical experiments without pH control, a gradual reduction in the bulk pH value was observed as the electrolysis proceeded. At the beginning of all experiments, the electrolyte had a typical pH value of about 5.5 and decreased to a lower pH value depending on experimental conditions. One of the main problems related to zinc-nickel deposition is hydrogen evolution, which causes a reduction in current efficiency leading to a higher energy consumption, and local increase in pH that can cause precipitation of metal hydroxides. Thus, it is necessary to select suitable operative conditions, such as the bulk pH, to overcome these problems.

In order to keep the bulk pH constant, an experiment was conducted for 8 hours and pH was monitored every 5 minutes. The pH of solution was maintained in the range of 5.5 to 6 by adding sufficient amount of 1.0 molar KOH.

Figure 7 presents the effect of the bulk pH on the reduction of zinc ions in the electrolyte with time. It is evident from the graph that zinc reduction increases with pH control in the range of 5.5-6. The result for nickel reduction is presented in Figure 8. The graph shows that there appears to be no significant difference for experiments with or without pH control. As it is shown in Figure 9, for both situations, approximately 17 % reduction in nickel ions was obtained while about 64% and 33% reduction in zinc ions occurred with and without pH control, respectively.

Maintaining the bulk pH between 5.5 and 6 during experimental runs would increase the concentration of hydroxyl ions in the cathode layer and would also make conditions favorable for zinc hydroxide film formation. The same result was observed by other researchers (Doan et al., 2003; Simonsson, 1984; Mitzakov, 2004).

Simonsson (1984) reported that electrodeposition of zinc from acidic solution thermodynamically favors the evolution of hydrogen gas. The result show that the higher rate of zinc recovery was achieved at a solution pH of about 6 and increasing pH higher than this value could lead to chemical precipitation of zinc hydroxide.

Effect of acidity on zinc recovery was also examined by Scott et al. (1988). They observed that increasing acidity reduced the rate of zinc deposition due to a higher rate of hydrogen evolution. Since both hydrogen evolution and zinc deposition are reactions competing for the available electrons at the cathode surface, an increase in the rate of one results in a decrease in the rate of other reaction. Lanza and Bertazzoli (2000) found that increasing pH from 2.5 to 4 resulted in shifting zinc deposition potential to a more positive value, which made the zinc reduction much easier. With increasing pH from 2.5 to 4, the time requiring for 90% removal of zinc ions in solution decreased about 30%. They also showed that zinc deposition was relatively pH independent at pH range between 4 and 5.5.

In the case of nickel deposition, Orhan et al. (2002) showed that the highest rate of nickel recovery was achieved at pH about 5.5. In an experiment with no control of pH, the concentration of free acid increased in the cell, which eventually impedes the electrolytic reduction of nickel ions.
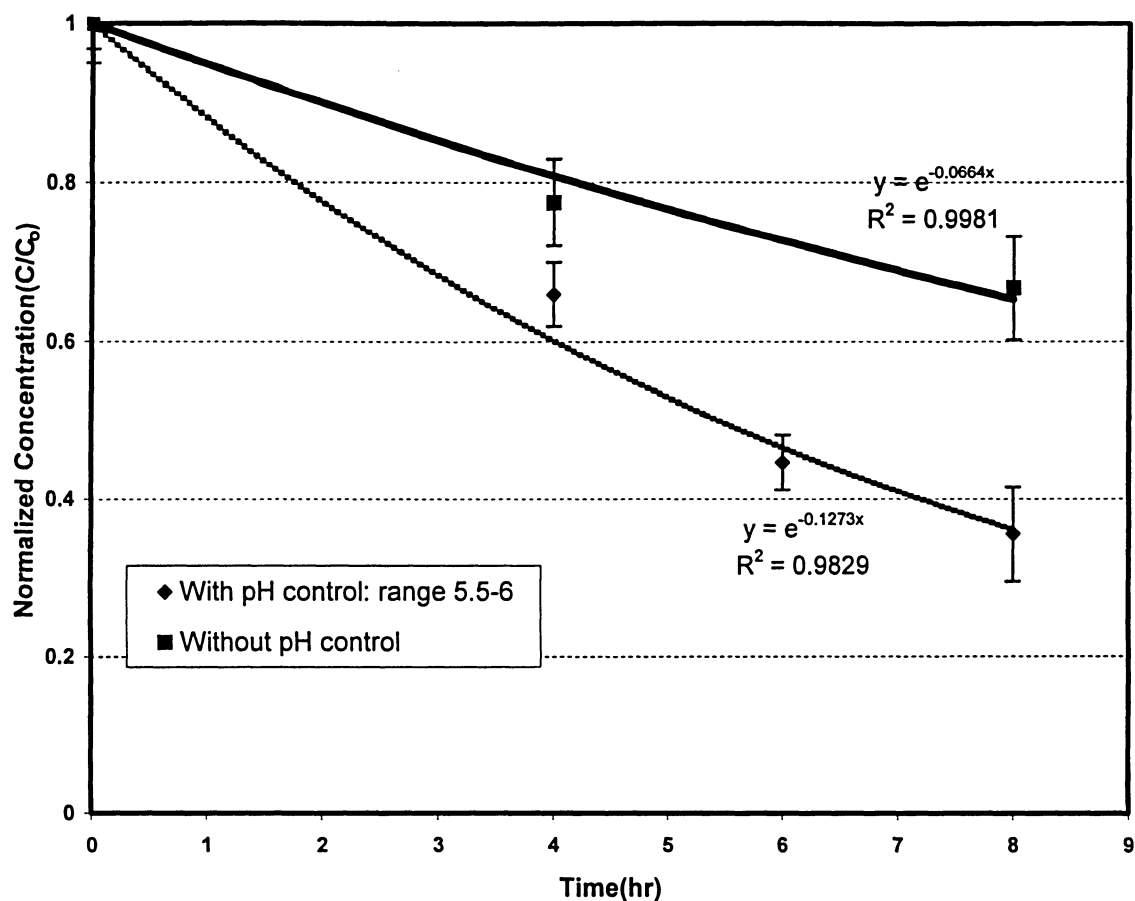
Figure 7. Effect of the bulk liquid pH on Zn^{++} reduction during 8 hours of treatment, Current density=0.167mA.cm^{-2}, $[Ni^{+2}]_o$=$[Zn^{+2}]_o$=20ppm, V=15 L, K_2SO_4=250ppm, T=25°C, Liquid volumetric flux=0.0172 m^3 m^{-2} s^{-1} .
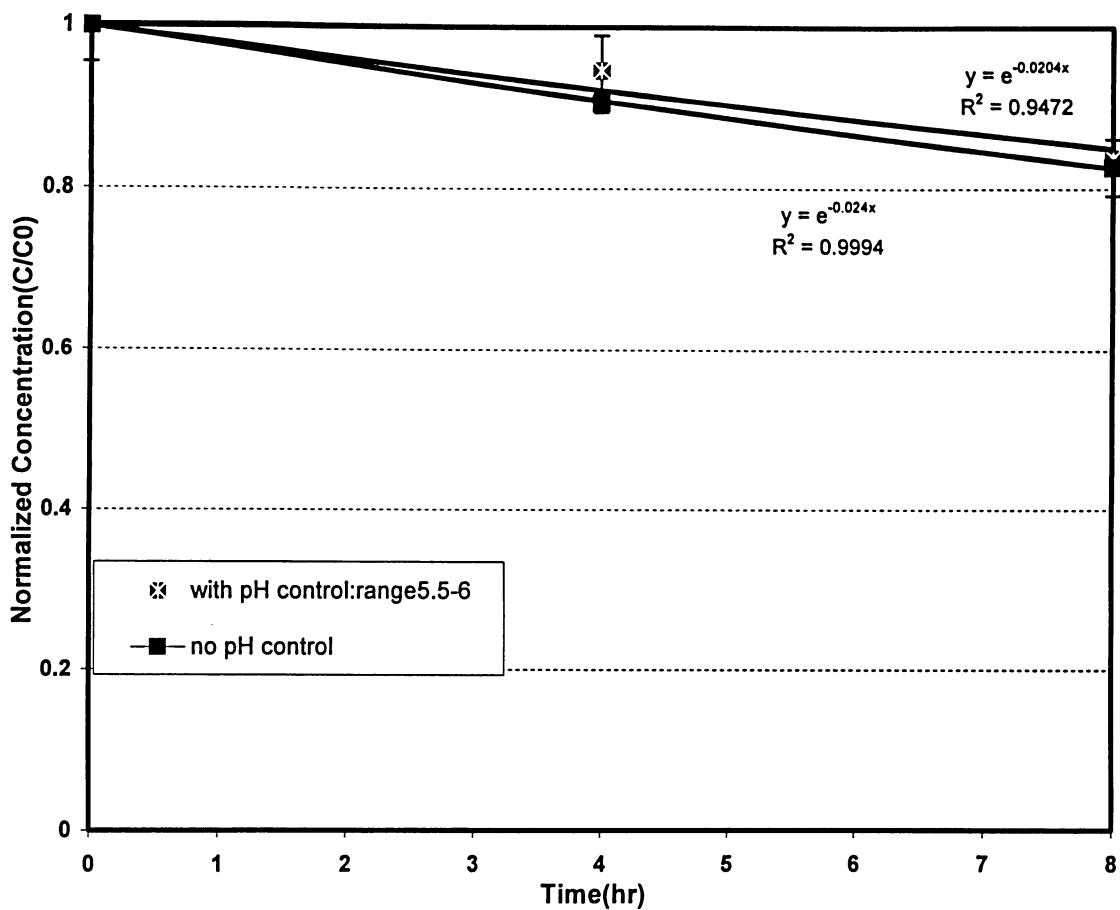
Figure 8. Effect of the bulk liquid pH on Ni^{++} reduction during 8 hours of treatment, Current density=0.166mA cm^{-2}, $[Ni^{+2}]_o=[Zn^{+2}]_o=20$ ppm, V=15 L, K_2SO_4=250 ppm T=25°C, Liquid volumetric flux=0.0172 m^3 m^{-2} s^{-1} .
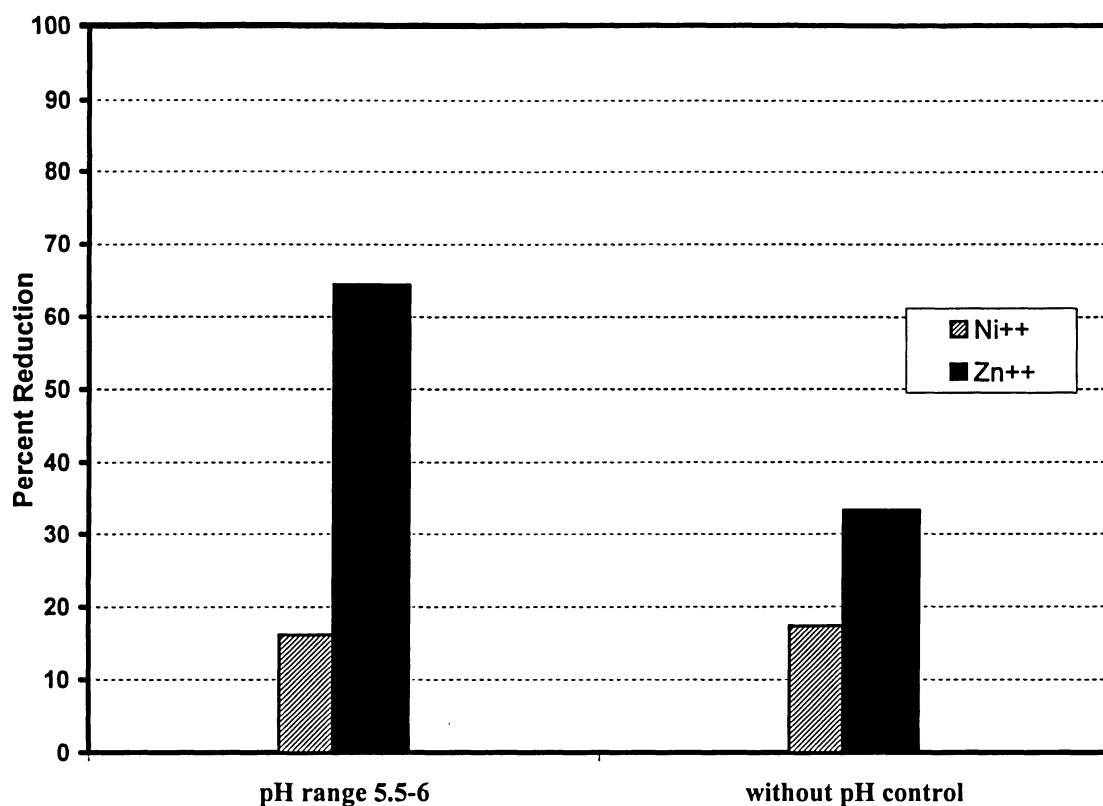
Figure 9. Effect of the bulk liquid pH on percent of Zn^{++} & Ni^{++} reduction after 8 hours of treatment, Current density =0.166 mA cm^{-2}, $[Ni^{+2}]_o=[Zn^{+2}]_o=20$ ppm, V=15 L, $K_2SO_4=250$ ppm T=25°C, Liquid volumetric flux=0.0172 m^3 m^{-2} s^{-1}.

Njau et al. (1998) reported that nickel could be recovered from dilute artificial solutions with the highest current efficiency at pH between 5 and 6. Their results showed that for the bulk electrolyte pH less than 5.5, nickel deposited in metallic form, while it deposited as a mixture of both metallic nickel and nickel hydroxide at pH greater than 5.5, and complete nickel hydroxide deposits could be obtained at pH values higher than 9.

According to different researchers, the cathode pH usually is greater than bulk pH due to hydrogen evolution. Therefore, maintaining the bulk pH in the range of 5.5-6 would result in a sufficient increase in the surface pH for zinc hydroxide film formation. In the current study there was no means of measuring the surface pH, the only way to find out about the nature and the quality of deposits was visual observations. In experiments without pH control, a green deposit, which was spongy and loosely attached to the cathode surface, was formed. This is believed to be nickel hydroxide that was formed due to an increase in pH near the cathode surface. Furthermore, the formation of nickel hydroxide inhibited the reduction of nickel ions to metallic nickel at the cathode surface.

Njau et al. (1998) observed that metallic nickel was formed at the bulk pH less than 5.5 while both metallic nickel and nickel hydroxide were included in deposits at the bulk pH greater than 5.5. For the latter case, the deposit was dark and powdery in nature. In another study conducted by Njau et al. (2000), it was found that at low current densities pure nickel was deposited while at higher current densities two types of deposits were observed: a black powder of nickel oxyhydroxide, and a green powder, which was a mixture of nickel oxide and nickel hydroxide. Similarly, Deligianni and Romankiw (1993) reported that during nickel deposition the surface pH increased from a bulk value

of 2 to 8.5. A black deposit was observed and it was believed that deposits consisted of nickel hydroxide precipitation. During zinc-nickel alloy deposition, Sheela et al. (2002) observed that zinc-rich deposits had a grayish appearance while nickel-rich deposits were semi-bright. The gray deposit is believed to be a mixture of metallic zinc and nickel and the same observation was reported by Abibsi et al. (1991). Zhou and O'Keefe (1997) observed that a smooth silver to gray deposit was formed during alloy deposition. Furthermore, during Zn-Ni alloy deposition, light colored deposits were observed when zinc-rich alloys were formed (Miranda et al., 1997a).

Two different forms of deposits were observed in the current investigation: a layer of gray metallic deposit and a pale green deposit with paste-like texture. Similar observations were reported by Mitzakov (2004) and Doan et al. (2003). The grayish layer appears to resemble those of Sheela et al. (2002), Zhou and O'Keefe (1997) and Abibsi et al. (1991). The observed pale color seems to be similar to that of Njau et al. (2000). When deposits dried in air, they flaked-off and a chalk-like texture appeared.

In the experiment with pH control the rate of nickel deposition did not change significantly while zinc reduction increased significantly. These results are in agreement with hydroxide suppression mechanism in which nickel deposition is inhibited by zinc hydroxide precipitation.

4.1.5 Effect of current density

Figures 10 and 11 show the effect of current density on the rate of removal of metal ion. It is evident that increasing current density improves the rate of Zn^{+2} ion removal while causes a significant reduction in nickel deposition rate. These results are in

agreement with those obtained by Abibsi et al. (1991) for zinc-nickel alloy electrodeposition. Higher percentage of nickel in deposits was obtained in experiments using lower current densities. These results are also in line with the hydroxide suppression mechanism.

Similarly, Roventi et al. (2000) found that the percentage of nickel in Zn-Ni alloy deposits decreased by increasing the cathode potential and the production of nickel rich alloys occurred at very low potentials.

Brenner (1963) reviewed different reports on the zinc-nickel alloy deposition conducted by several researchers. In various studies, it was shown that the zinc content of the deposit increased by increasing current density up to a certain value and then either remained constant or decreased slightly. When the percentage of zinc in the electrolyte bath was high, the content of zinc in deposits was significantly higher than nickel. In one study, the zinc contents of the bath and deposit were 50% and 95%, respectively.

In a study of Zn-Ni deposition by Fabri et al. (1996), the nickel content in deposits was relatively high at low current densities and decreased when the current density increased. However, the zinc content of deposits was always significantly greater than the Ni content of deposits and the maximum Ni content in deposits was 18%. At higher current densities, the reduction of hydrogen ions becomes significant and the current efficiency for metal ion deposition is generally low and falls rapidly with time due to hydrogen generation.

Figure 10. Effect of the current density on Ni^{++} reduction during 47 hours of treatment without pH control, V=15 L, $[Ni^{+2}]_o=[Zn^{+2}]_o=20$ ppm, $K_2SO_4=250$ ppm, T=25°C, Liquid volumetric flux=0.0172 m^3 m^{-2} s^{-1}.
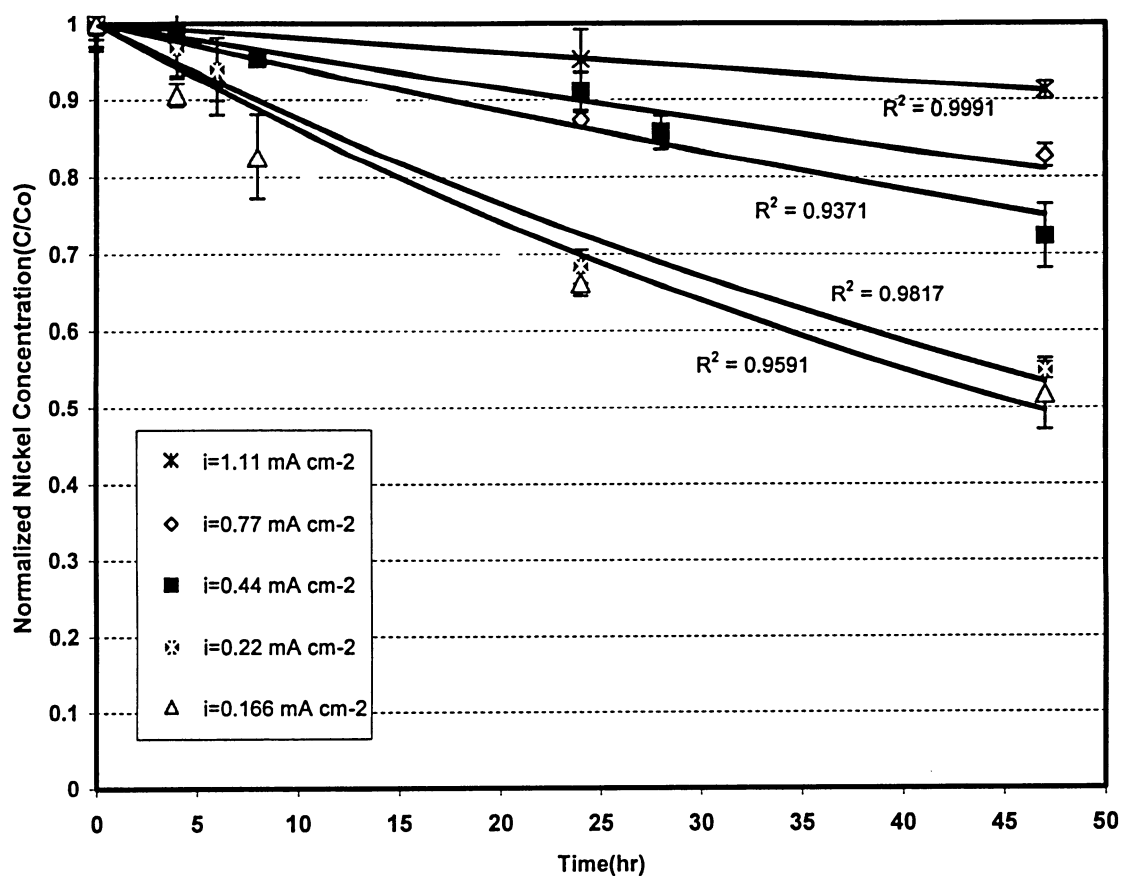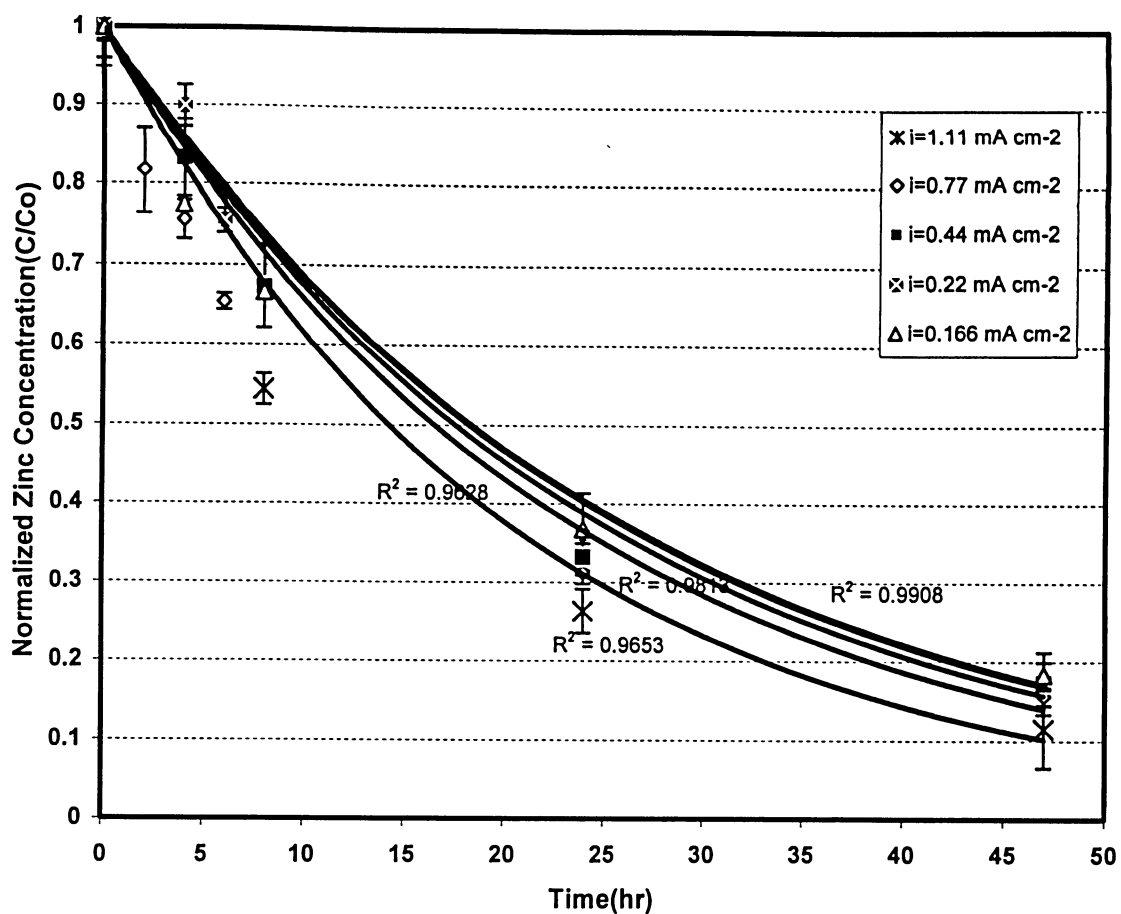
Figure 11. Effect of current density on Zn^{++} reduction during 47 hours of treatment, without pH control, V=15L, $[Ni^{+2}]_o=[Zn^{+2}]_o=20$ ppm, $K_2SO_4=250$ ppm T=25°C, Liquid volumetric flux=0.0172 m^3 m^{-2} s^{-1}.

64

The effect of increasing the current density on the current efficiency of the metal removal is shown in Fig 12. It can be observed that increasing the current density reduces the total current efficiency of metal deposition. Abibsi et al. (1991) reported that a current efficiency around 95% was achieved during zinc-nickel alloy deposition at low current densities. In the current study, the maximum 22% current efficiency was obtained at the current density of 0.166 $mA.cm^{-2}$, which is significantly lower than that obtained by Abibsi et al. (1991). The discrepancy between results could probably be due to low concentration of metal ions in present study so that the rate of hydrogen reduction increased significantly. As the electrolysis proceeded, the cell potential increased due to depletion of metal ions and consequently when the potential for hydrogen evolution was reached, hydrogen evolution and a significant loss in the current efficiency occurred.

4.1.6 Effect of the liquid volumetric flux

Different liquid volumetric fluxes were used to examine their effects on the rate of zinc and nickel removal. There was no attempt for controlling pH in this series of experiments. The maximum liquid volumetric flux provided by the pump was 0.0172 $m^3.m^{-2}.s^{-1}$.

Normalized concentrations of nickel and zinc ions are presented in Figures 13 and 14, respectively. Figure 15 presents data for the percentage of zinc and nickel ion reduction after 47 hours of treatment using different liquid volumetric fluxes. As it is noted, the percentage zinc ion removal increases with increasing liquid volumetric flux. The highest removal of about 81% occurs with the highest flux of 0.0172 $m^3.m^{-2}.s^{-1}$.
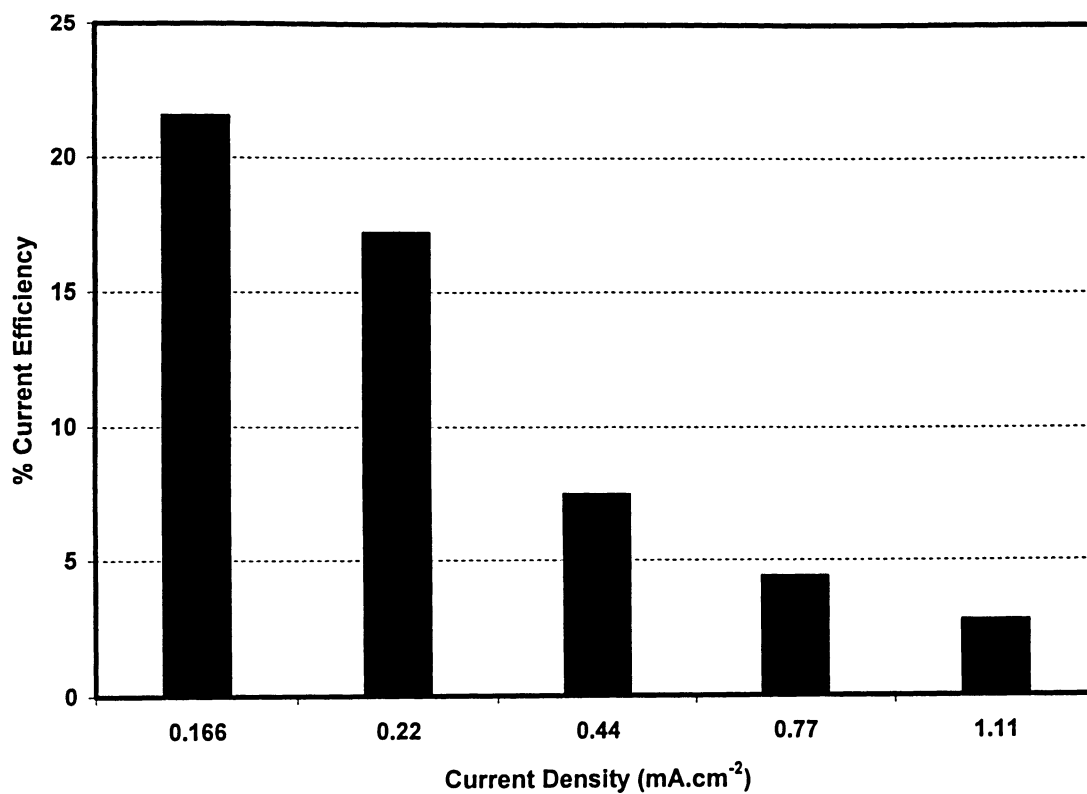
Figure 12. Effect of current density on current efficiency for Zn^{++} & Ni^{++} reduction after 47 hours of treatment without pH control, V=15L, $[Ni^{+2}]_o=[Zn^{+2}]_o=20$ ppm, $K_2SO_4=250$ ppm T=25°C, Liquid volumetric flux=0.0172 m^3 m^{-2} s^{-1}.

However, the percentage nickel reduction does not seem to change significantly when liquid flux changes from 0.00117 to 0.0172 $m^3.m^{-2}.s^{-1}$. A 48% reduction occurs at the highest flux of 0.0172 $m^3.m^{-2}.s^{-1}$. Apparent rate constants, k, and average mass transfer coefficients, K_m, are summarized in Table 5. K_m was calculated using Equation (2.1.5.12) and apparent rate constants were obtained from semi-log plots of the normalized concentration versus time. Results shown in Table 5 indicates that the apparent rate constant for nickel reduction remains relatively constant with a maximum change of only 15% between the minimum and maximum fluxes. However, for the removal of zinc, the rate constant increases significantly with increases in liquid flux. There is a 68% difference in the rate constants at the lowest and highest fluxes. These results are comparable to those obtained by Mitzakov (2004) in laminar flow regime. The apparent rate constants obtained by Mitzakov for zinc and nickel reductions at the flux of 0.00915 $m^3.m^{-2}.s^{-1}$ were 0.0413 h^{-1} and 0.0117 h^{-1}, respectively.

The average mass transfer coefficients for nickel and zinc reduction are less than those obtained by Mitzakov (2004) in laminar flow regime. A supporting electrolyte of 500 ppm was used in his experiments compared with 250 ppm used in the present study. An increase in concentration of supporting electrolyte would increase the metal deposition. In another study conducted by Mitzakov (2004), a decrease in concentration of the supporting electrolyte from 300 ppm to 100 ppm caused a significant reduction in the removal rate of both zinc and nickel ions.

In another study conducted by Doan et al. (2003), potassium chloride of 250 ppm was used as the supporting electrolyte in a simple batch reactor with mild agitation of the electrolyte.
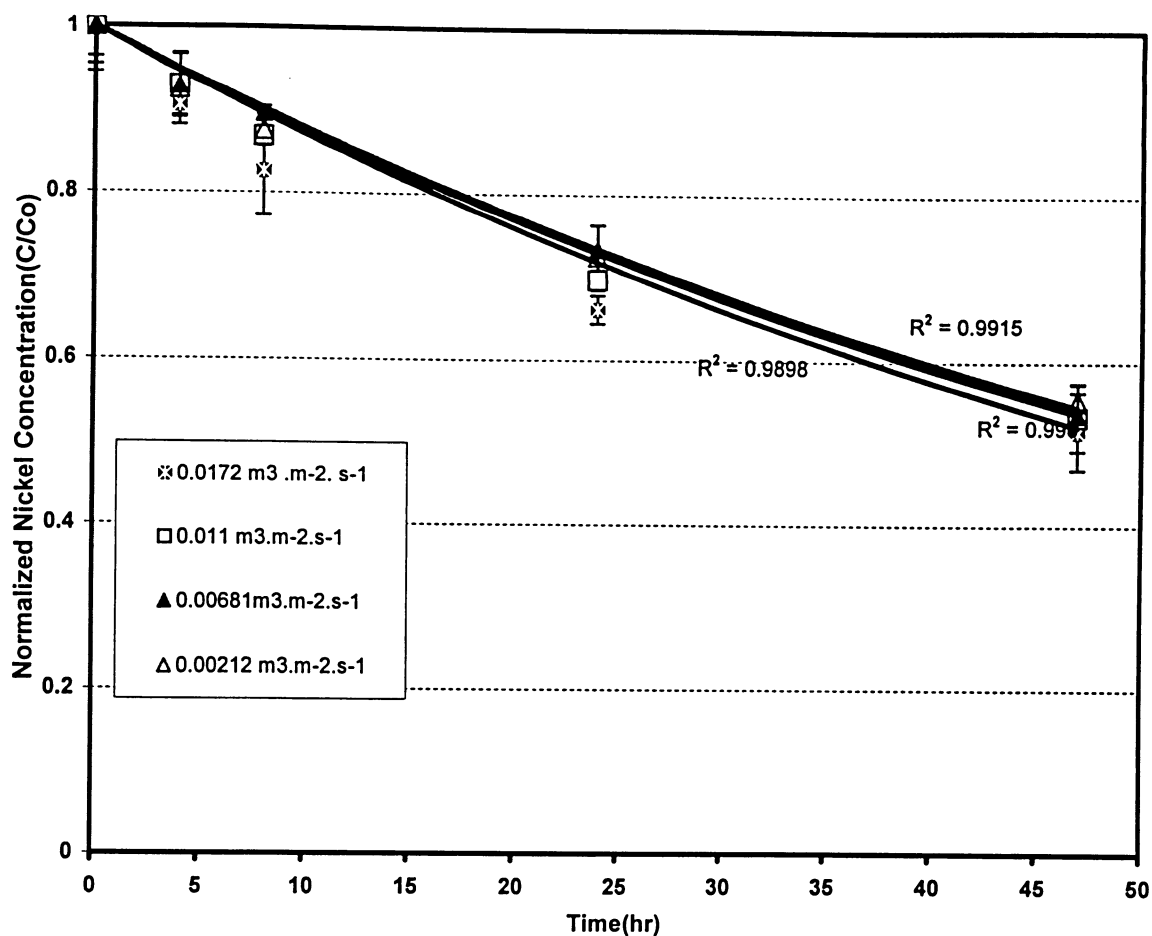
Figure 13. Effect of liquid volumetric flux on Ni^{++} reduction during 47 hours of treatment without pH control, current density=0.166 mA cm^{-2}, V=15L, $[Ni^{+2}]_o=[Zn^{+2}]_o=20$ ppm, $K_2SO_4=250$ ppm, T=25°C.
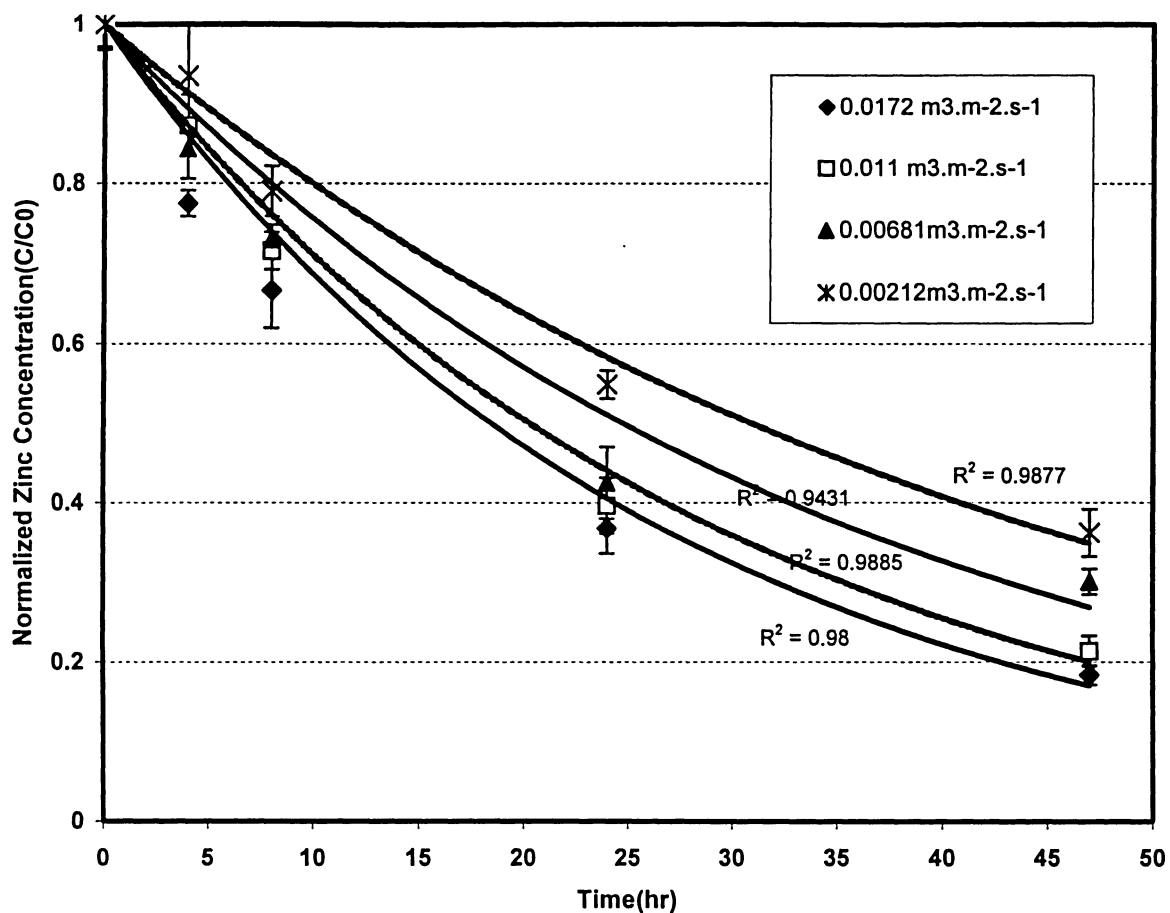
Figure 14. Effect of liquid volumetric flux on Zn^{++} reduction during 47 hours of treatment without pH control, current density=0.166 $mA.cm^{-2}$, V=15L, $[Ni^{+2}]_o=[Zn^{+2}]_o=20$ ppm, $K_2SO_4=250$ ppm, T=25°C.
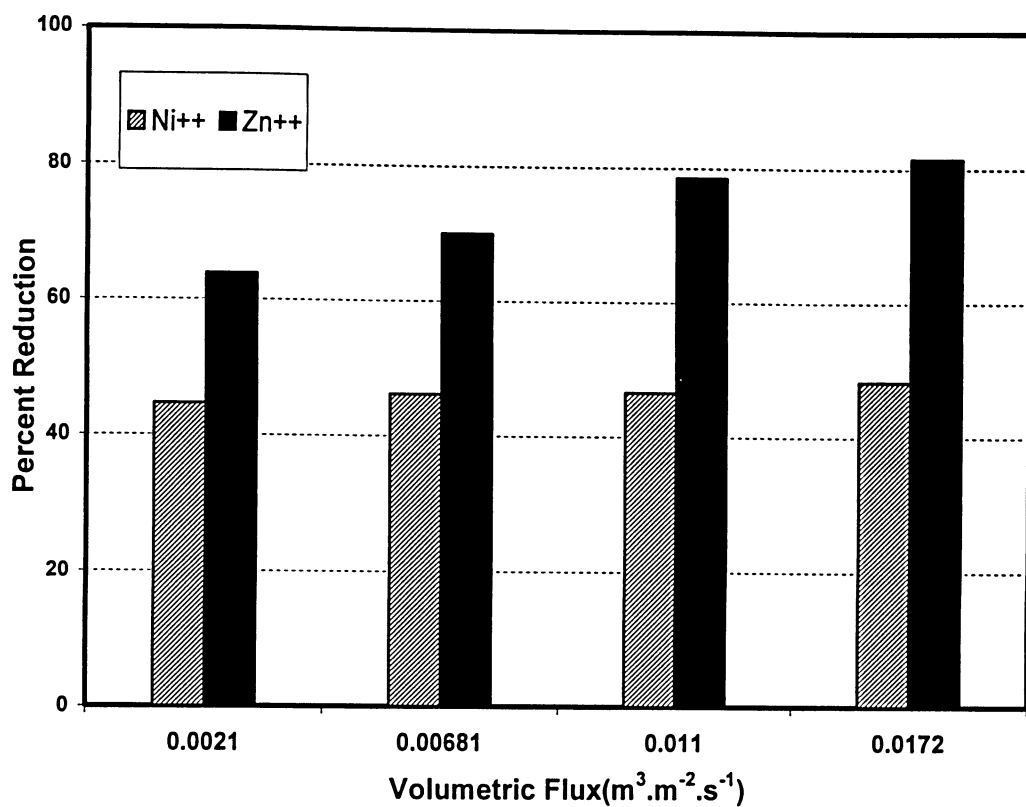
Figure 15. Comparison of percent Zn^{++} & Ni^{++} reduction after 47 hours of treatment at different liquid volumetric fluxes, current density=0.166 $mA.cm^{-2}$, V=15L, $[Ni^{+2}]_o=[Zn^{+2}]_o$=20 ppm, K_2SO_4=250 ppm, T=25°C.

Table 5. Apparent first order rate constants for zinc & nickel ion reduction and average mass transfer coefficients during 47 hours of treatment without pH control.

Ionic Species	Volumetric Flux $(m^3.m^{-2}.s^{-1})$	Apparent rate constant, k (h^{-1})	Average mass transfer coefficient ($\frac{kV}{A}$, cm h^{-1})
Zinc	0.0021	0.0225	0.938
	0.00681	0.0281	1.170
	0.011	0.0342	1.425
	0.0172	0.0377	1.571
Nickel	0.0021	0.0129	0.538
	0.00681	0.0132	0.55
	0.011	0.0138	0.575
	0.0172	0.0149	0.620

For the experiment with pH control about 4.2, which was closer to the lowest pH value encountered in the present study, mass transfer coefficients of 1.64 and 1.90 cm.h^{-1} for nickel and zinc, respectively, were reported. Mass transfer coefficient for nickel obtained in the present study is less than that obtained by Doan et al. (2003) although the concentration of the supporting electrolyte is the same. However, it has been shown by Ji et al., (1995) that the presence of chloride ions in solution can enhance the rate of nickel deposition. Thus, the mass transfer coefficient obtained by Doan et al. (2003) for nickel would be affected by the presence of the chloride ions in the solution.

During electrolysis, due to depletion of metal ions in the cathode diffusion layer, the ratio of metal concentrations in the layer differs from that in the bulk solution. Higher flow rates will increase the transport of the electroactive species, mainly; Ni^{+2} and Zn^{+2} ions, to the cathode diffusion layer and cause the ratio of metal concentrations in diffusion layer to approach that of the bulk solution. This would result in a reduction in the thickness of the cathode diffusion layer. Although the present system was operating in the laminar region, changes in volumetric fluxes corresponding to minimum and maximum Reynolds numbers of 184 and 1485, respectively, would still provide an increase in mass transfer. Assuming that hypothesis proposed by Dahms and Croll (1965) is in affect in the present study, an increase in the concentration of Zn^{+2} ions in the cathode layer increases the rate of $Zn(OH)_2$ formation, which retards the rate of nickel ions discharge to the cathode surface.

4.2 Dark Experiments

4.2.1 Dark adsorption of LAS on the TiO₂ surface

In order to find out if any loss of LAS was due to adsorption on the surface of TiO_2 particles or the experimental set-up, a dark experiment was conducted for a 7-hour period. In the dark experiment, a solution of LAS was recirculated in the system without UV lamp for 7 hours. Samples were taken every hour from the effluent of the reactor and analyzed for LAS concentration. The results obtained are plotted in Figure 16. Figure 16 shows that there was a limited adsorption of LAS on TiO_2 particles over a 7-hour treatment period. A 20% reduction in the concentration of LAS was occurred due to adsorption. Additionally, most reduction in the LAS concentration occurred in the first hour of the experiment from 100 $mg.l^{-1}$ to 81$mg.l^{-1}$. As a result, in order to isolate the reduction in LAS concentration due to physical adsorption, the solution of LAS and TiO_2 was mixed thoroughly for one hour before starting any photo-experiment. Additionally, this stabilizing period allowed the system to reach to the desired temperature by either adjusting the heater input or the cooling water flow rate into the cooling system. Sampling was started right after the stabilizing period and the corresponding concentration was used as the initial concentration of LAS at time zero.

Since substantial amount of foam was generated during the experiments, it was thought that the concentration of LAS in solution might have decreased due to foaming. Thus, a dark experiment without using TiO_2 particles and UV lamp was conducted for a 7-hour period. The results did not show any significant change in the concentrations of LAS over the 7-hour period of the experiment (Figure17). A similar observation was reported by Bankian Tabrizi (2004).

4.2.2 Dark adsorption of metal ions on the TiO₂ surface

Adsorption happens when TiO_2 particles are contacted with dissolved metal ions. The amount of metal ions adsorbed on the TiO_2 surface over a 7-hour period without UV is presented in Figure 18.

Over the dark adsorption period, concentrations of zinc and nickel decreased by 15.5% and 8%, respectively. As it is shown in Figure 18, most reduction of the concentrations of Ni^{+2} and Zn^{+2} ions occurred during first hour of the dark adsorption.

Raheshwar et al. (2002) showed that, in the absence of organic compounds, 16% of Zn^{+2} ions were adsorbed on the TiO_2 surface. It has been also reported that the rate of Zn^{+2} adsorption increased in the presence of organic compounds (Somasundaram et al., 2004).

4.3 Direct photolysis of LAS by UV-254

In order to determine whether photochemical oxidation of LAS could occur in the absence of TiO_2, a blank experiment (TiO_2 free) was carried out. All experimental parameters were kept the same as those of the dark reaction except that a UV-254 lamp was turned on after the stabilizing period. The temperature was kept constant at 25^0C; thus, the effect of increasing temperature due to using UV lamp was eliminated.

The result presented in Figure 19 shows that UV-254 light was capable of direct bond breakage of LAS, and about 20% of LAS was degraded by direct photolysis. Direct photolysis of LAS appears to follow a first order kinetics as shown by a linear relationship of $ln(C/C_o)$ with illumination time in Figure 20. The first order rate constant was found to be 0.0006 min^{-1}.
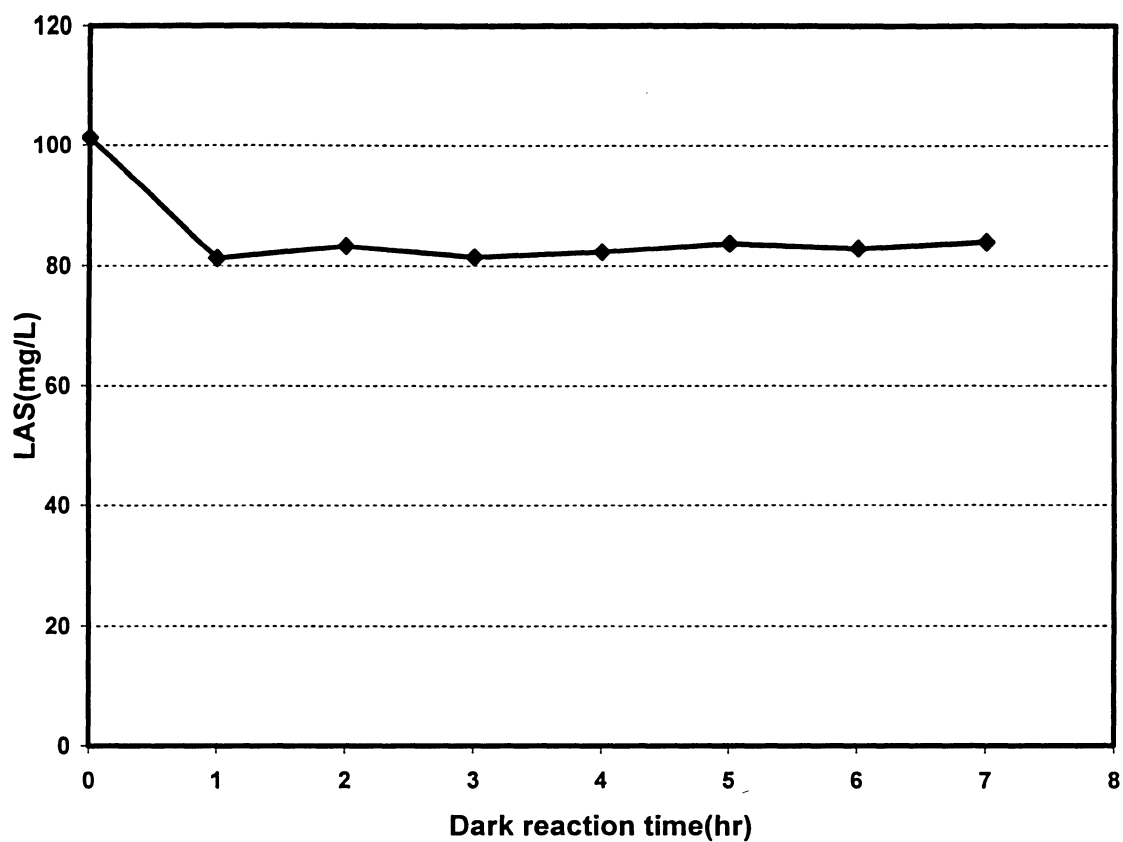
Figure 16. Changes in the LAS concentration during dark adsorption on TiO_2 surface. LAS_o=100 mg.l^{-1}, V=6 L, no UV lamp, T=25°C, volumetric liquid flux=0.0172 m^3 m^{-2} s^{-1}.
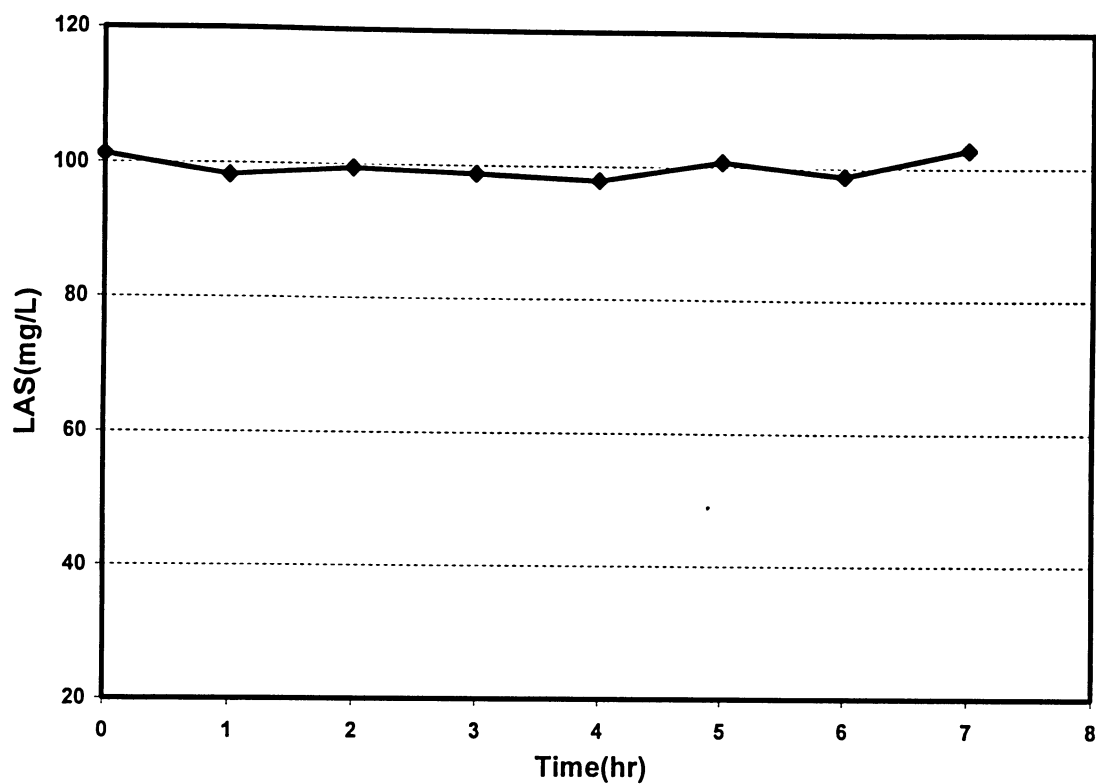
Figure 17. Changes in the concentration of LAS in liquid phase due to foaming, $LAS_0=100$ mg/L, no UV lamp, no TiO_2, V=6L, T=25°C, liquid volumetric flux=0.0172 $m^3m^{-2}s^{-1}$.
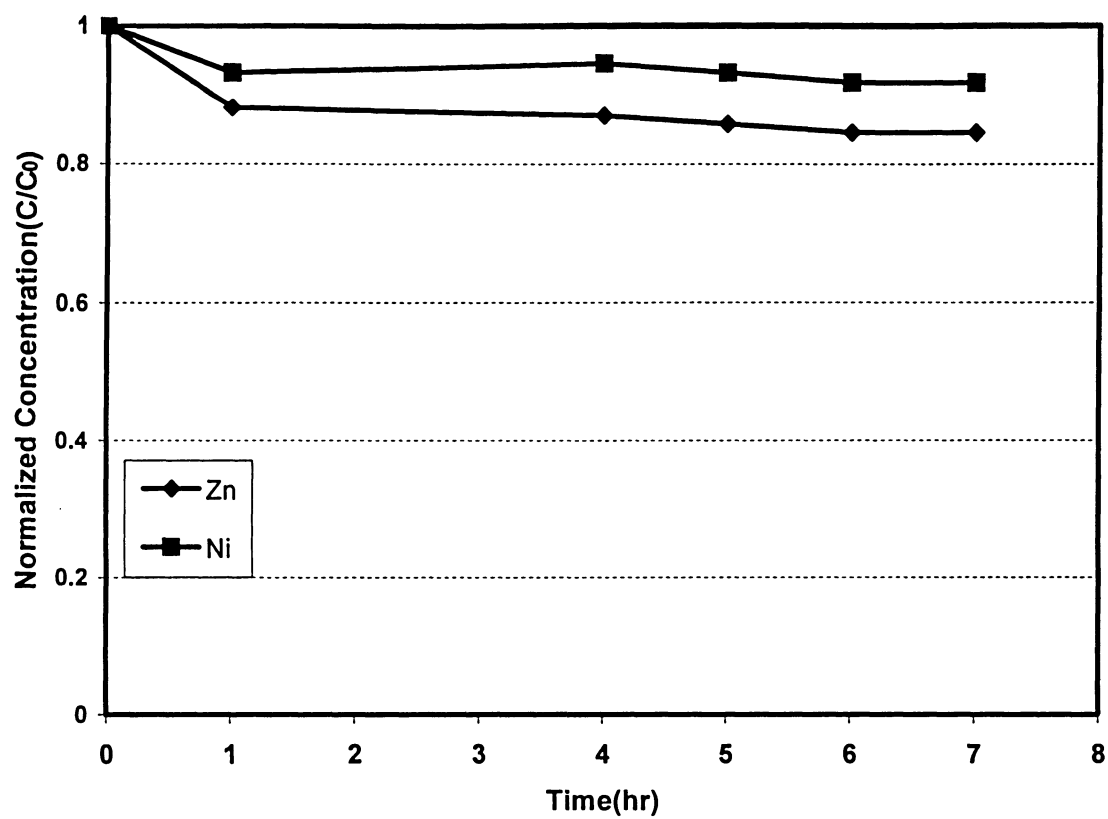
Figure 18. Dark adsorption of metal ions on the TiO_2 surface, $[Ni^{+2}]_o=[Zn^{+2}]_o=20$ ppm, no UV lamp, T=25°C, V=6 L, liquid volumetric flux=0.0172 $m^3 m^{-2} s^{-1}$.

4.4 Photocatalytic reduction of metal ions

Various studies have focused on the photocatalytic reduction of metal ions with positive standard reduction potentials, such as: Cu^{+2}, Ag^{+1}, Cr^{+6}, etc., while only a few reports are available for metal ions, which are more difficult to be reduced, for example Zn^{+2} and Ni^{+2}. Relative position of the potential levels of the conduction and valence bands of TiO_2 at pH 7 and redox potentials of two metals of interest in the present study are shown in Figure 21. According to Chen and Ray (2001), the potential levels of both conduction and valence bands are pH dependent while reduction potentials of metal ions are independent of pH.

Thermodynamically, metal ions with standard reduction potentials more positive than the TiO_2 conduction band can be directly reduced by photogenerated electrons. Metal ions, which either have more negative standard reduction potentials or lie very close to the potential level of the conduction band of TiO_2, cannot be directly photoreduced.

According to Figure 21, direct photoreduction of Zn^{+2} and Ni^{+2} ions is not thermodynamically possible. Somasundaram et al. (2004) and Rajeshwar et al. (2002) also reported that zinc ions could not be reduced to the metallic form in UV-irradiated TiO_2 suspensions. In the case of Ni^{+2} ions, several researchers have shown that UV-irradiated TiO_2 suspensions were not effective for photocatalytically removal of Ni^{+2} ions (Rajeshwar et al., 2002; Chen and Ray, 2001; Prairie et al., 1993).
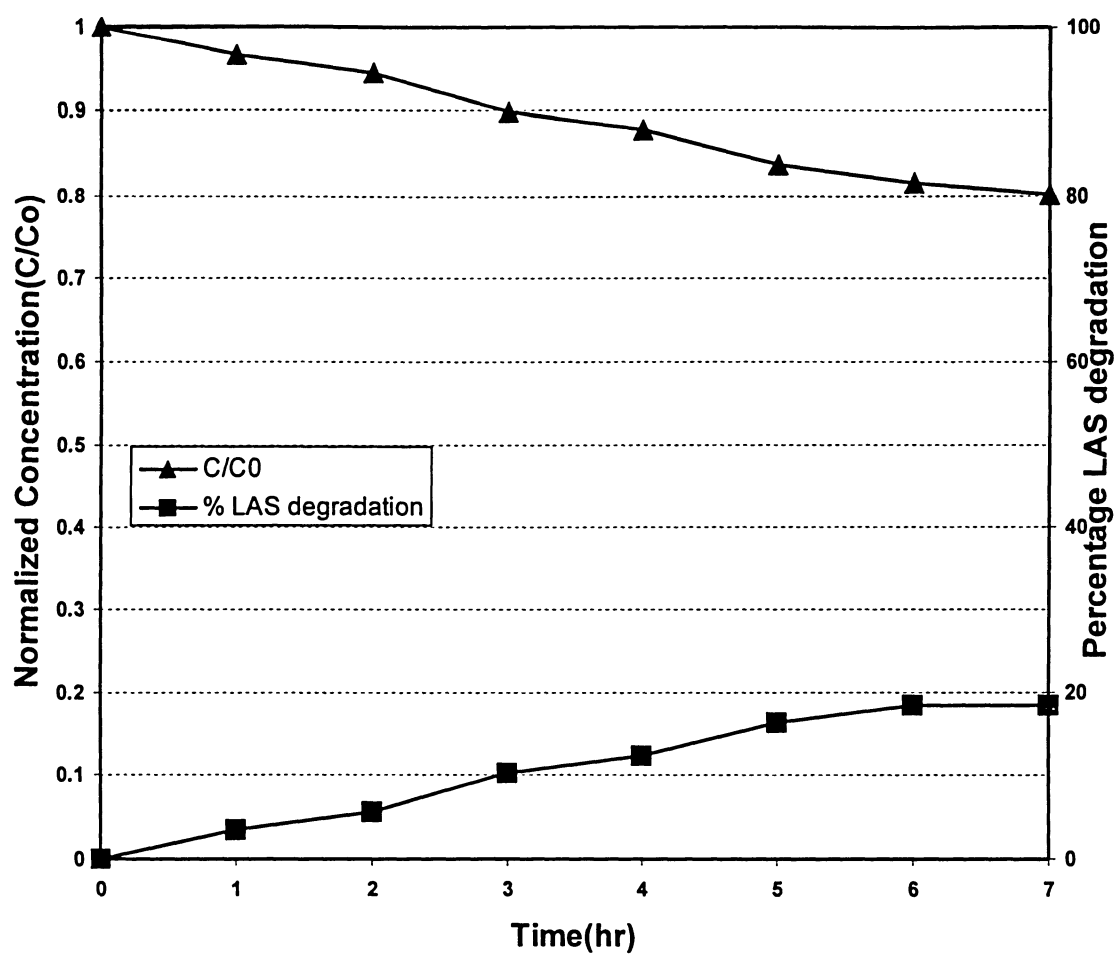
Figure 19. Direct photolysis of LAS using UV-254, no TiO_2, LAS_o=100 mg/L, T=25°C, Volumetric liquid flux=0.0172 m^3 m^{-2} s^{-1}.
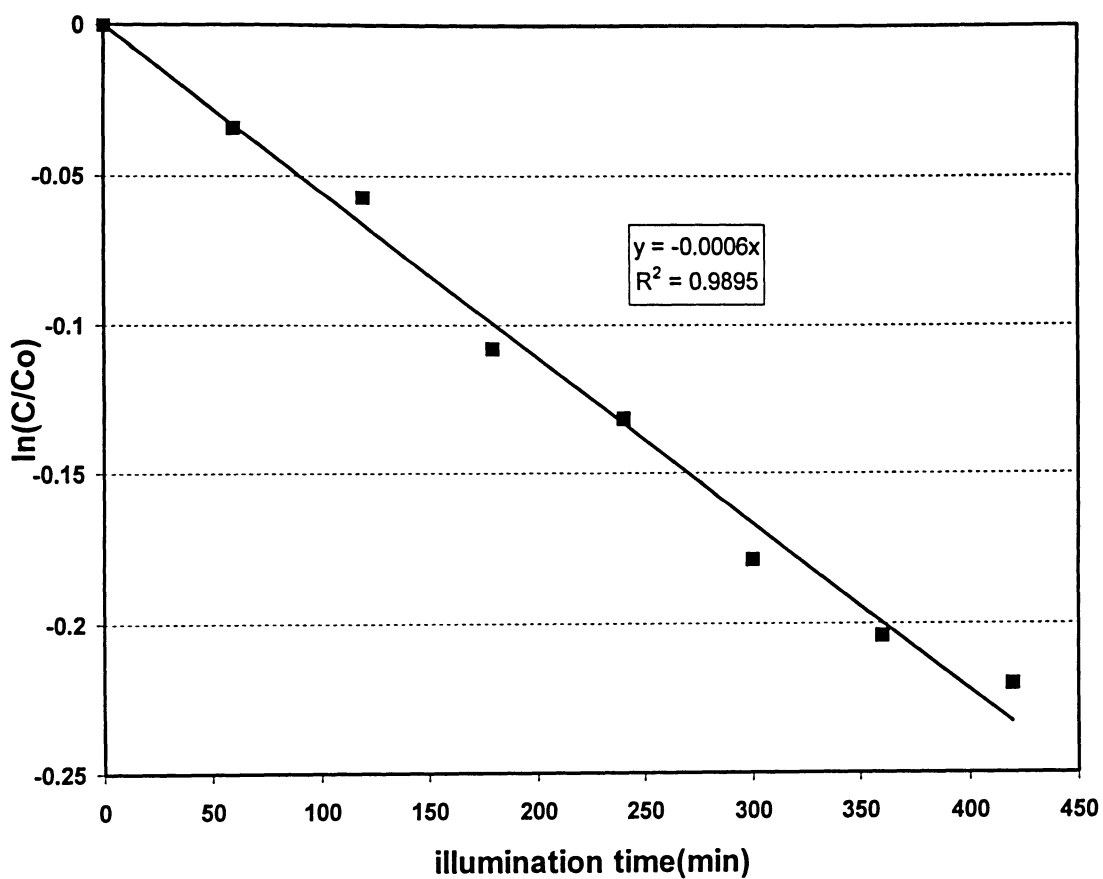
Figure 20. Comparison between the experimental data and first-order model for direct photolysis of LAS, LAS_o=100 mg/L, T=25°C, liquid volumetric flux=0.0172 m^3 m^{-2} s^{-1}.

In order to determine whether any photocatalytic reduction of metal ions could occur, a photocatalytic experiment was conducted using metal ion concentrations of 20 ppm. Before starting of the experiment, the solution of metal ions and TiO_2 suspension was mixed in dark for 1 hour. Sample for time zero was taken at the end of the dark period. Results obtained are presented Figure 22. They are in agreement with those obtained by other researchers. Since Ni^{+2} and Zn^{+2} ions could not be reduced photocatalytically and no organic species was present in the solution, it is expected that oxygen molecules were reduced by photogenerated electrons while water molecules were oxidized by photogenerated holes.

$E_{CB}(-0.5 \text{ V})$

-0.8

-Zn^{+2}/Zn (-0.7618)

-Ni^{+2}/Ni (-0.251)

0.0

0.4

$E_{VB}(2.7V)$

3.0

PH 7
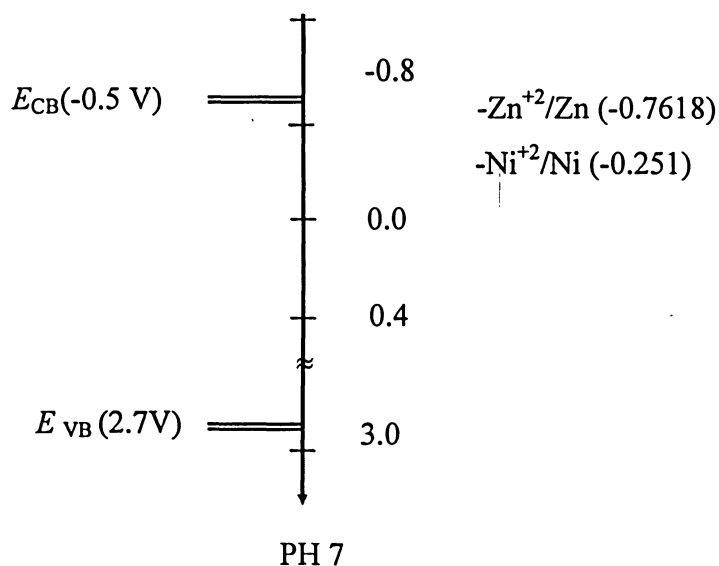
Figure 21. Relative position of the energy levels in TiO_2 and solution species, adopted from Rajeshwar et al. (2002).

81

4.5 Photocatalytic oxidation of LAS

There are a number of variables that are expected to affect the rate of the photocatalytic degradation of LAS. Thus, several experiments were performed to assess the influence of different process variables on the rate of reaction. Among those considered in the present study are pH, temperature, and the fluid volumetric flux.

4.5.1 Effect of pH

A series of experiments was conducted to examine the effect of pH on the rate of LAS degradation. The pH was varied between 2 and 12. The solution pH was adjusted to a desired value by adding appropriate amounts of NaOH(1N) or H_2SO_4(1N) to the solution during a 7-hour treatment period. Additionally, for very acidic solutions (initial pH=2 and 3), the pH did not change significantly during experimental runs; thus, there was no need for controlling pH over the duration of the runs.

In experiments without pH control, the solution pH decreased from a typical value of 6.4 to a final value of 4.5 after 7 hours of treatment. Figure 23 shows the normalized concentration of LAS as a function of illumination time at different pH values. As it is shown, the normalized concentration of LAS versus time exhibits an exponential decay in all plots. This implies that the removal of LAS by UV/TiO_2 followed a first-order model. Generally, the kinetics of heterogeneous photocatalytic reactions is expressed by the Langmuir-Hinshelwood mechanism (Hermann, 1999):

$$-\frac{dC}{dt} = \frac{kKC}{1+KC} \qquad (4.5.1.1)$$

where k is the reaction rate constant and K is the equilibrium constant of adsorption. In solutions with low concentration C, KC<<1 and the reaction becomes the first-order. This is consistent with the obtained results and suggested model.

It was observed that the highest rate of LAS degradation was obtained at pH value of about 5 compared with the LAS degradation rates at very acidic, neutral or basic conditions. Figure 24 presents data for percentage of LAS degradation at different solution pH. The greatest LAS degradation of 60% was achieved by controlling pH between 5 and 5.5, and the lowest LAS decomposition of 40% was obtained at solution pH about 12.

TiO$_2$ P25 has the zero point of charge (pH$_{zpc}$) of 6.25 and it is known to have an amphoteric character when it is contacted with aqueous media (Kormann et al., 1991). Its principal amphoteric surface functionality is denoted as >TiOH. The surface hydroxyl groups, >TiOH, undergo different acid-base reactions and depending on the pH value in the medium, it will be either positively or negatively charged. At pH above the pH$_{zpc}$, the surface has a net negative charge while at pH below pH$_{zpc}$, the TiO$_2$ surface accumulates a net positive charge. In general, the net charge on the TiO$_2$ surface indicates what type of organic species can be absorbed at a given pH. Anionic surfactants, which have an electron-attracting group such as sulfonate or sulfate, are easily photodegradable (Hidaka et al., 1990). The pH will influence not only the adsorption quantity of organics but also the way adsorbates are coordinated to the titanium dioxide surface. As a result, the pH would significantly influence the photocatalytic oxidation kinetics of adsorbates.
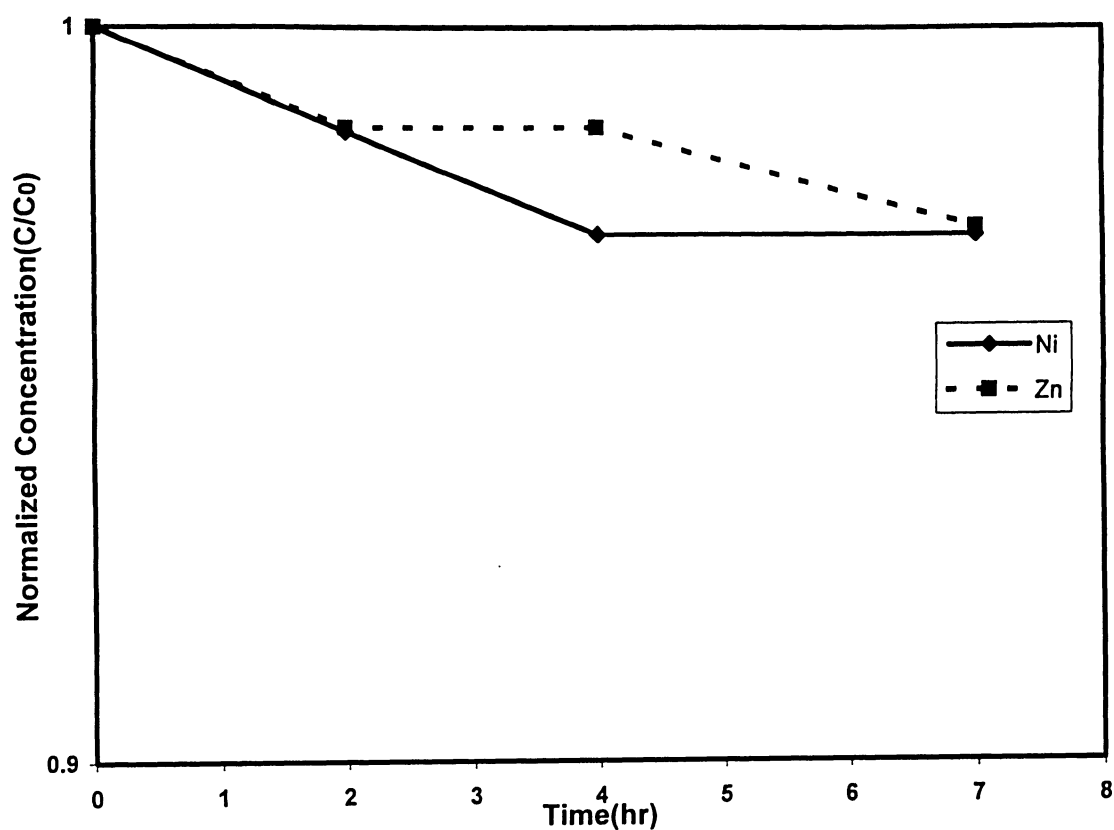
Figure 22. Photocatalytic reduction of Zn^{+2} and Ni^{+2} ions using UV-254 nm, $[Ni^{+2}]_o=[Zn^{+2}]_o=20$ ppm , T=25°C, no LAS, liquid volumetric flux=0.0172 m^3 m^{-2} s^{-1}.

84
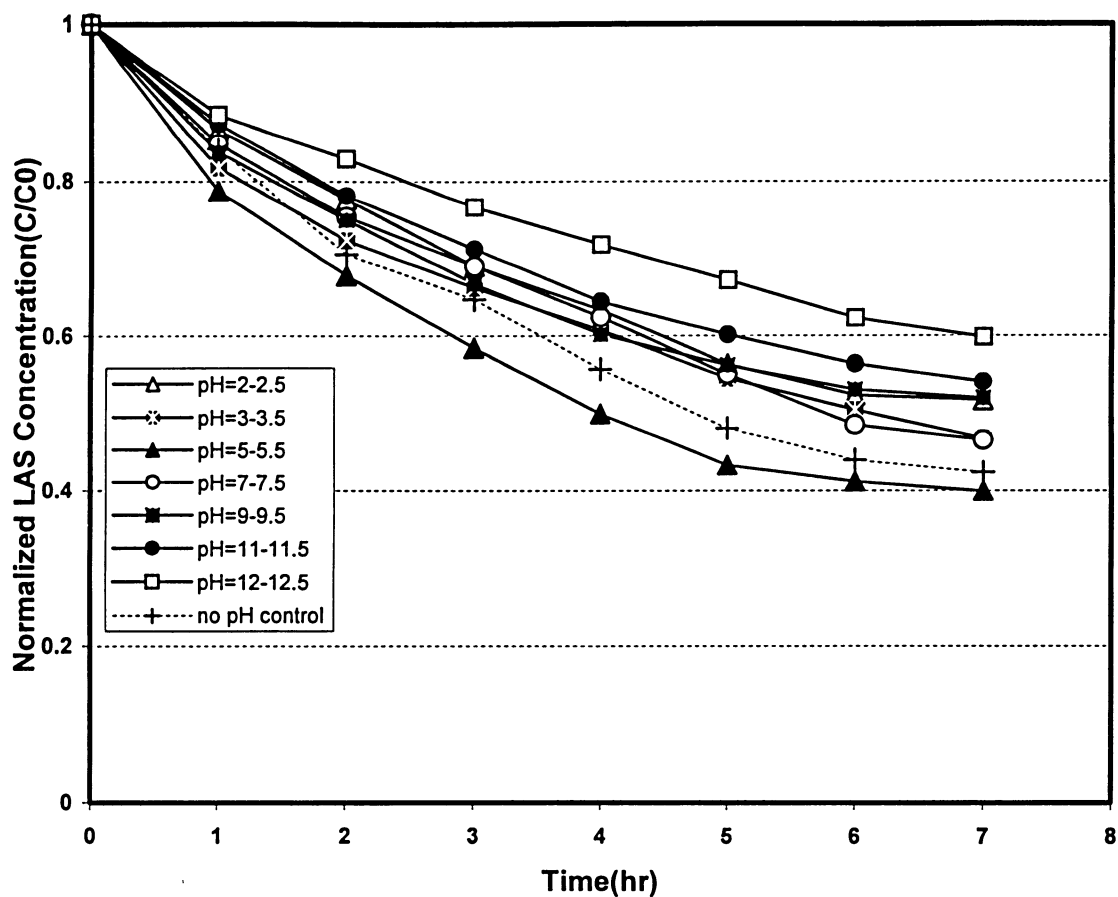
Figure 23. Effect of pH on LAS degradation during 7 hours of the photocatalytic treatment, LAS_o=100 mg/L, T=25°C, V=15 L, Liquid volumetric flux=0.0172 m^3 m^{-2} s^{-1}.

Results from Figure 24 indicates that at $pH > pH_{zpc}$, electrostatic repulsion makes the formation of the complex between TiO_2 particles and LAS, an anionic surfactant, more difficult; thus, the rate of LAS decomposition is reduced. Since the lifetime of hydroxyl radicals is very short, reactions between these radicals and LAS molecules existing far from the catalyst surface could not complete effectively.

As it is shown in Figure 24, the highest rate of LAS degradation is obtained at pH around 5, which is less than pH_{zpc}. However, at pH<5, the presence of other anions from the dissociation of added acids and their adsorption to the TiO_2 surface would probably decrease the chance of LAS adsorption on the catalyst surface and, consequently, the rate of LAS decreased.

Furthermore, the plot of normalized COD versus illumination time is presented in Figure 25. It can be observed that only 44% COD removal was obtained within 7 hours at pH about 5 compared to 60% LAS decomposition at the same time. It can be concluded that only 44% of LAS was completely degraded to CO_2 and the rest was converted to other intermediates.

Hidaka and Kubota (1986) showed that the aromatic group in sodium dodecylbenzene sulphonate was easily decomposed, while the long aliphatic chain was slowly and partially oxidized.

Although the complete mineralization of LAS did not occur over a 7-hour treatment period, the suppression of its surface activity might have occurred via either desulphonation or decomposition of the aromatic part since foaming decreased significantly by irradiation time (Hidaka and Kubota, 1986).
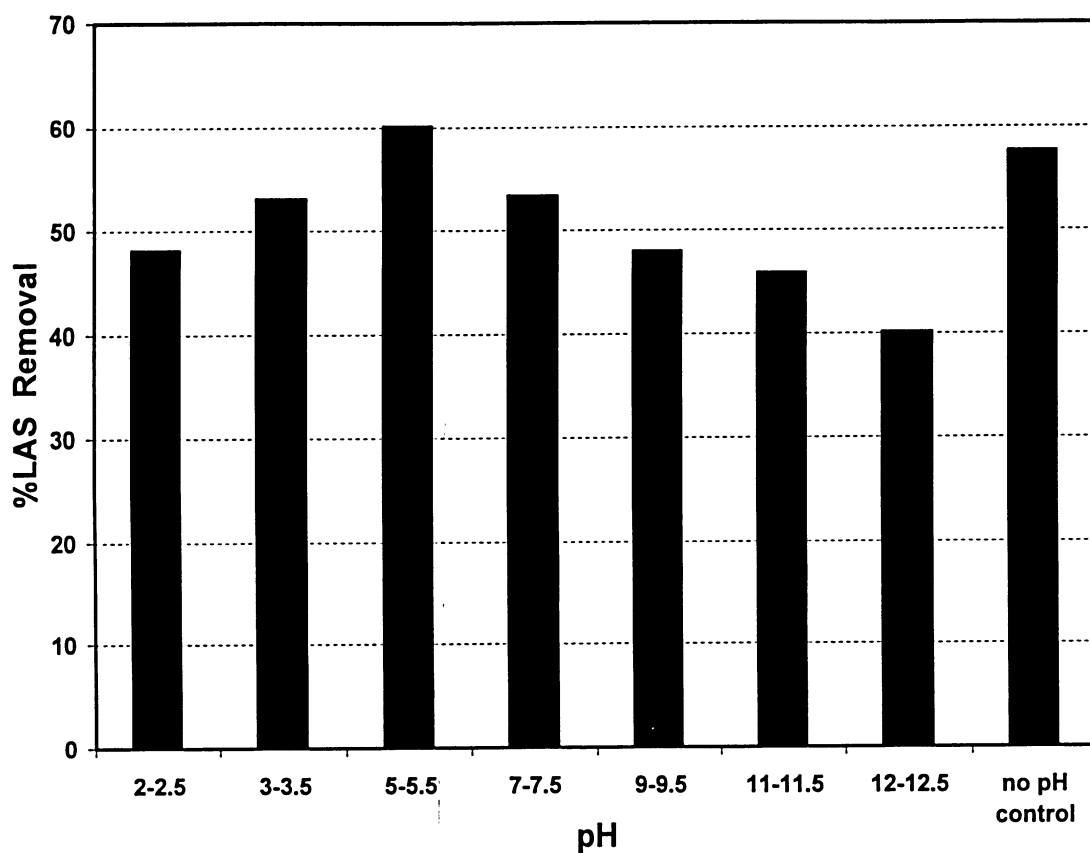
Figure 24. Effect of pH on the percentage of LAS degradation during 7 hours of treatment. LAS_o=100 mg/L, T=25°C, Volumetric flux=0.0172 m^3 m^{-2} s^{-1}. In experiment without pH control, the solution pH decreased from a typical value of 6.4 to a final value of 4.5 after 7 hours of treatment

If LAS can be cleaved partially at a certain position, e.g. $C-SO_3Na$, the remaining compound from surfactant decomposition would be hydrophobic and exhibit no surface activity (Hidaka and Kubota, 1986). They also reported that sodium benzene sulphonate, which has no alkyl chain, was photodegraded easily and completely to carbon dioxide and water.

A reduction in pH during experiments without pH control could be due to the generation of different acidic intermediates in solution. Hidaka and Kubota (1986) identified some intermediates, such as: peroxides, alcohols, aldehydes and carboxylic acid, during the photodegrdation of DBS using IR and NMR spectroscopy.

Although a detailed mechanism for photodegradation of LAS was not determined in the present study, the photodegradation of LAS was likely to follow the pathway of photooxidation proposed by other researchers. The complete mineralization pathway for DBS has been shown elsewhere (Hidaka and Zhao, 1992).

4.5.2 Effect of Temperature

The effect of temperature on the rate of LAS decomposition is shown in Figure 26. Since UV lamp generated heat inside the photoreactor, the necessity of the cooling system was indicated by the following experiment. An experiment was conducted without temperature control in which temperature increased from an initial value of $22^{o}C$ to about $40^{o}C$ at the end of 7 hours of irradiation. In experiments with controlled temperature, the reactor temperature was varied from 20 to $35^{o}C$ with 5-dgree increments while other parameters were kept constant. Results from Figure 26 indicate that the rate of LAS decomposition does not change significantly with the temperature variation.
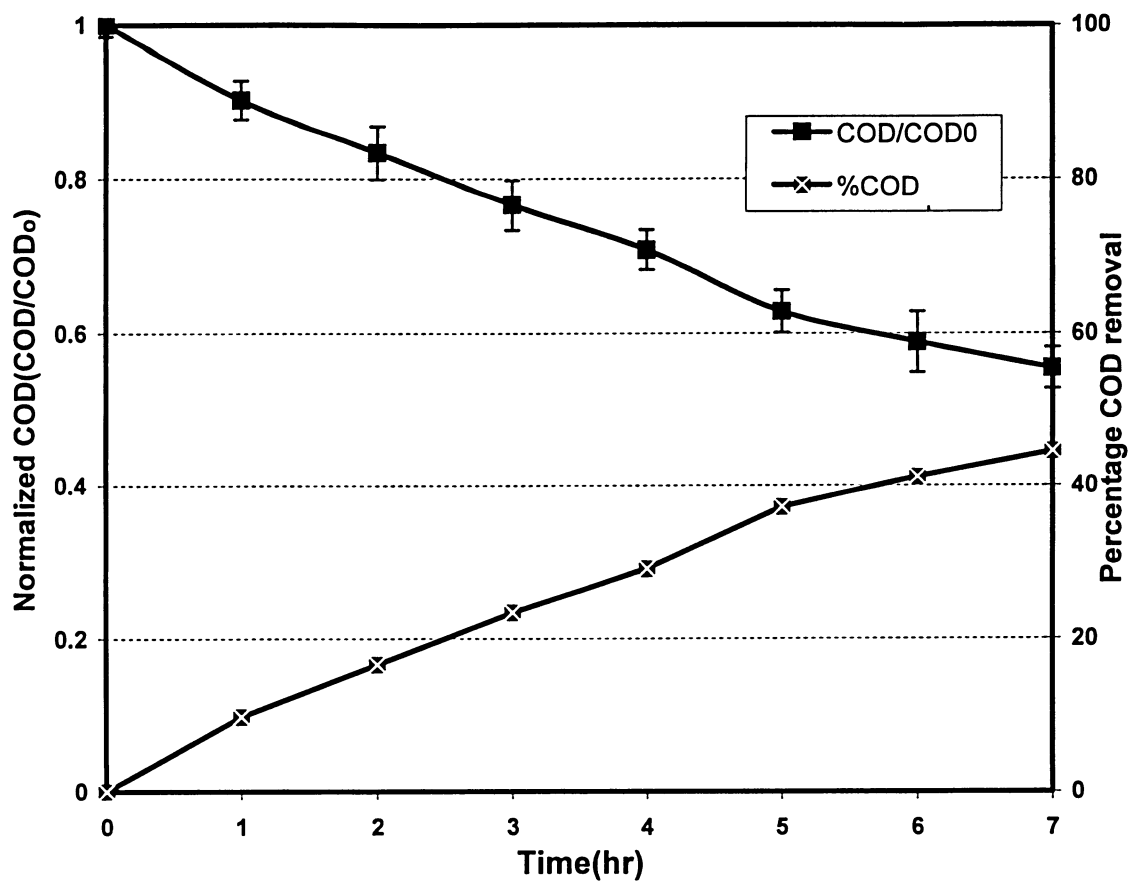
Figure 25. COD removal during photocatalytic degradation of LAS at pH=5-5.5, LAS_o=100 mg.l^{-1}, V=6 L, T=25°C, volumetric flux=0.0172 m^3 m^{-2} s^{-1}.

Although adsorption, desorption and surface migration are potentially temperature dependent steps, they do not seem to be the rate determining steps in the present study. This is an advantageous feature for the practical scale-up since the need for temperature control is eliminated.

4.5.3 Effect of liquid volumetric flux

The effect of liquid volumetric flux on the degradation of LAS was studied over 24 hours of treatment. Liquid volumetric fluxes used in these experiments were 0.00212, 0.00681, 0.011, and 0.0172 $m^3.m^{-2}.s^{-1}$ corresponding to the Reynolds numbers of 182, 586, 1016, and 1485, respectively. All the Reynolds numbers, which were calculated based on the hydraulic diameter of the reactor, fall in the laminar region. Figure 27 illustrates that the rate of LAS decomposition does not vary significantly with the liquid flux. The residence time was not an important factor in the present study since the whole system was operated in a batch mode. The results obtained also indicate that mass transfer of LAS molecules to the surface of TiO_2 particles was not a limiting step of the photocatalytic treatment of LAS.

4.6 Direct electrochemical oxidation of LAS

In recent years, electrochemical techniques have been used widely to treat toxic organics in wastewaters. The mechanism of electrochemical oxidation of organic compounds in aqueous solution is very complicated (Pletcher and Walsh, 1990). It is known that electrochemical reactions can follow two different pathways: the direct oxidation at the anode surface and indirect electrochemical oxidation by anodically

formed oxidants. With sufficient power supply, organic molecules are decomposed into smaller molecules.

In electrochemical processes, the organic substrates are oxidized by hydroxyl radicals, which are formed on the anode surface by decomposition of water and/or by direct oxidation of hydroxide ions according to following reactions:

$$2H_2O \rightarrow 2OH^{\bullet} + 2H^{+} + 2e^{-} \qquad (4.6.1)$$

$$OH^{-} \rightarrow OH^{\bullet} + e^{-} \qquad (4.6.2)$$

Hydroxyl radicals have a very short lifetime and either oxidize organics directly or form other oxidants, such as: O_2, H_2O_2 or O_3. These oxidants, which have reasonably long lifetime, diffuse into the bulk of the solution and oxidize organic compounds. However, the direct electrochemical oxidation of the organic substrate by hydroxyl radicals at the anode surface is more effective since the secondary oxidants are not able to completely degrade organics to carbon dioxide and water.

It is believed that two oxidation pathways are involved in direct electrochemical oxidation of organics by hydroxyl radicals: chemisorption of hydroxyl radicals at active electrodes and physisorption of hydroxyl radicals at non-active electrodes. One electrode is considered to be active when the active sites M on its surface can undergo the following chemisorption reaction (Canizares et al., 1999):

$$M + OH^{\bullet} \rightarrow MO + H^{+} + e^{-} \qquad (4.6.3)$$

$$MO + R \rightarrow RO + M \qquad (4.6.4)$$
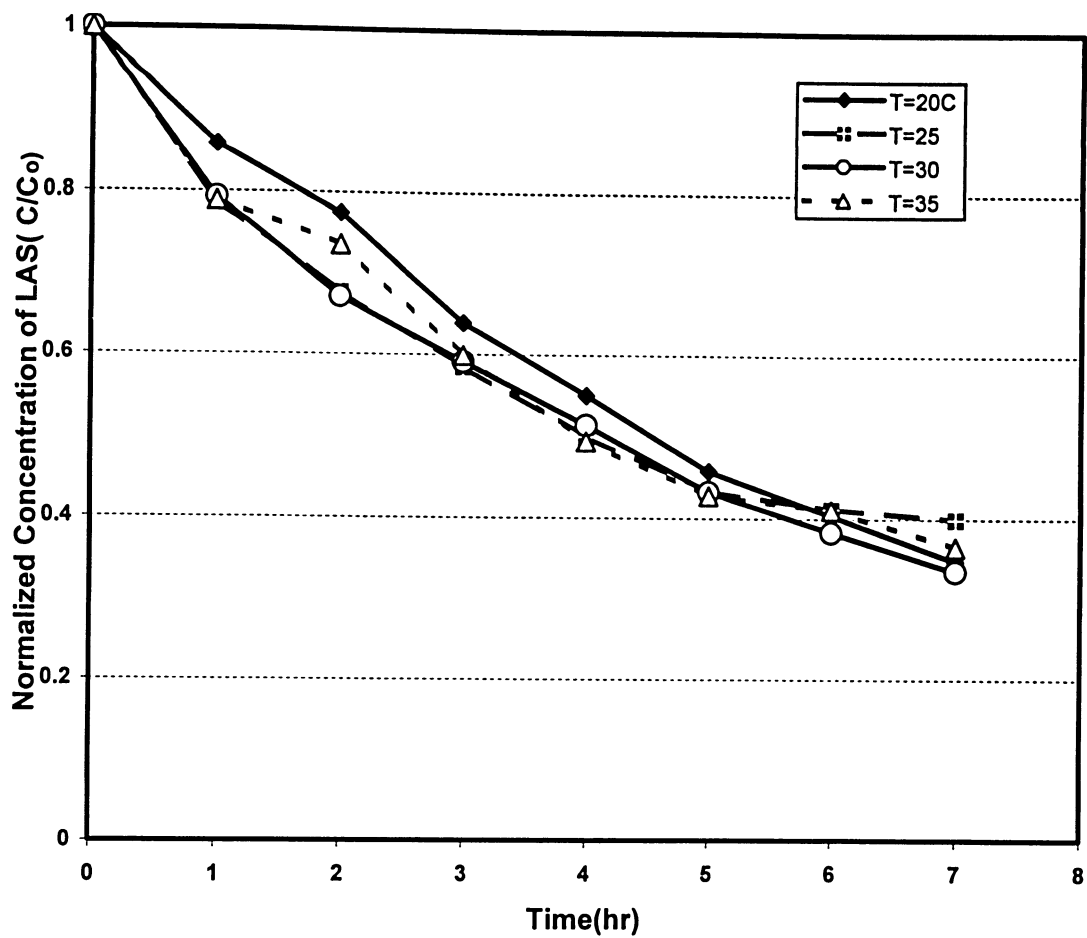
Figure 26. Effect of temperature on the rate of LAS degradation, pH=5-5.5, $[LAS]_o$=100 mg/L, V=6L, volumetric flux=0.0172 m^3 m^{-2} s^{-1}.

Consequently, in the presence of oxidizable organic compounds (R), chemiosorbed hydroxyl radicals react with organic compounds, being reduced to the original state. In this case, the chemiosorbed hydroxyl radicals participate in the formation of selective oxidation products according to reaction (4.6.4). The oxidation products then can be transformed to carbon dioxide and water. The chemical oxidation pathway usually does not lead to direct mineralization of organics to carbon dioxide. Some intermediates are produced and then they are converted to CO_2 (Indirect oxidation pathway).

However, active sites on non-active electrodes do not react chemically with hydroxyl radicals. The physisorbed $OH^{\bullet}$ radicals oxidize organic compounds completely and directly to carbon dioxide (direct oxidation pathway) as followings:

$$M + OH^{\bullet} \rightarrow M(OH^{\bullet}) \tag{4.6.5}$$

$$M(OH^{\bullet}) + R \rightarrow mCO_2 + nH_2O + M \tag{4.6.6}$$

According to Foti et al. (1999), a steel anode is considered as an active electrode. So during the electrochemical oxidation of LAS, LAS might be oxidized to other intermediates. The intermediates were then converted into carbon dioxide and water.

In order to determine if LAS was degraded by the electrochemical oxidation, an experiment was performed using the electrochemical cell shown in Figure 6. The cathode current density was 0.167 mA.cm^{-2}. Anodes and cathodes were stainless steel and aluminum plates, respectively
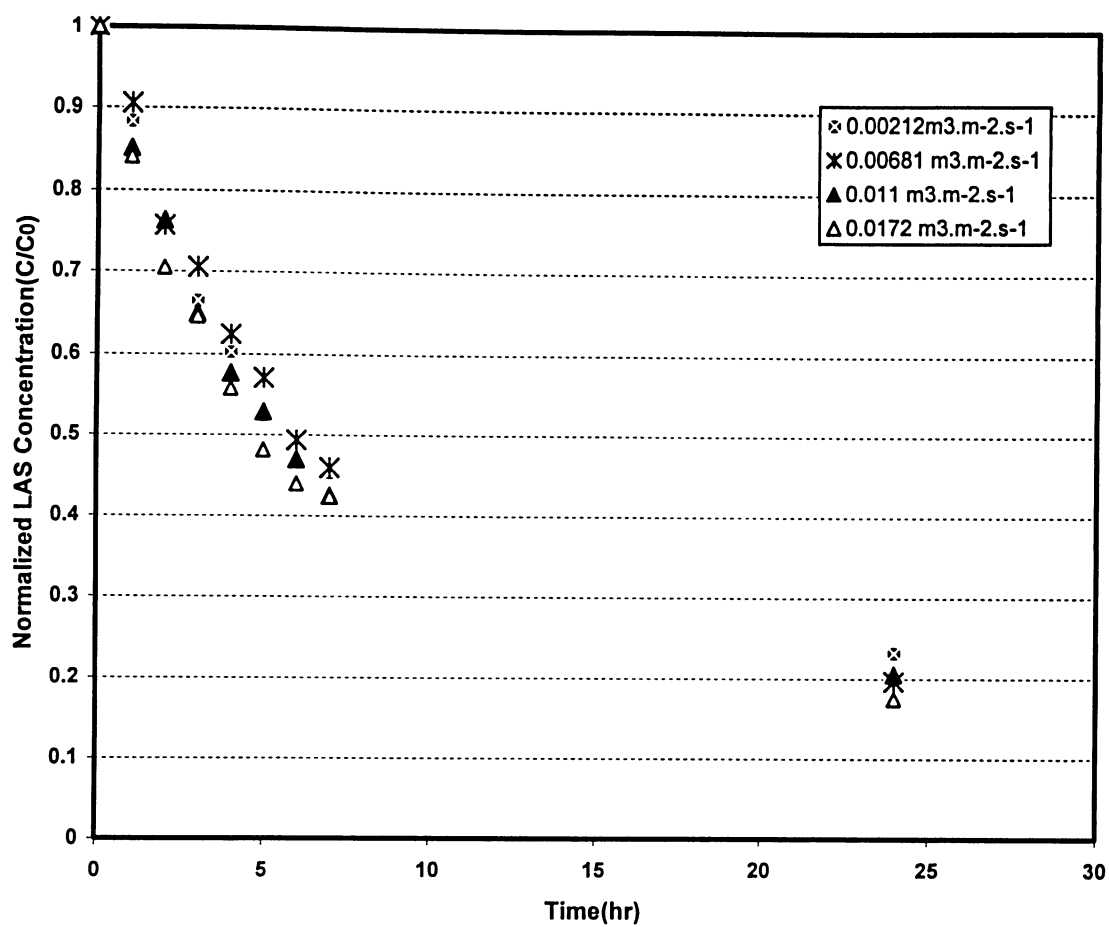
Figure 27. Effect of the liquid volumetric flux on the rate of LAS degradation, without pH control, V=6 L, [LAS]$_o$=100 mg/L, T=25°C.

The pH was monitored during the experiment and it increased from an initial value of 5.8 to a final value of 7.38 at the end of a 7-hour period. H^+ ions were produced from the dissociation of acidic intermediates in solution. Since the only reducible compounds were hydrogen ions in the solution, the hydrogen evolution at the cathodes also occurred leading to a rise in the solution pH. It appeared that the rate of hydrogen evolution was higher than the rate of H^+ ion generation, which resulted in a net rise in the pH of the solution.

Results from Figure 28 show that 24% of LAS was decomposed by direct electrochemical oxidation. COD removal was only 17% indicating that some intermediates were produced during the electrochemical oxidation of LAS. The low rate of LAS degradation could be due to the low current density used in the present study.

4.7 Combined photocatalytic and electrochemical techniques

A series of experiments were performed to examine the effectiveness of the combined electrochemical and photocatalytic system for the treatment of the wastewater containing both metal ions and LAS. The influence of the pH and the volumetric flux at constant current density on the rate of metal ion removal and LAS destruction was investigated. Some experiments were also performed to determine whether the presence of metal ions had any effect on the rate of LAS degradation and vise versa. The initial concentration of metal ions and LAS were 20 ppm and 100 ppm, respectively.

4.7.1 Comparison of LAS degradation in different systems

Figure 29 illustrates the normalized LAS degradation versus time for different systems. The rate of LAS removal by photocatalytic and electrochemical system is higher than those obtained in photocatalytic and electrochemical systems alone.

The combined effect of photocatalytic and anodic oxidations leads to an improvement in the rate of LAS destruction. The greatest LAS degradation of 71% was achieved in the combined system after 7 hours compared to 58% and 24% degradation in photocatalytic and electrochemical systems, respectively.

4.7.2 Effect of metal ions on the rate of LAS degradation using the combined system

Figure 30 shows a comparison of the rate of LAS degradation in a solution containing only LAS with that containing LAS and metal ions, by the combined system. The presence of metal ions did not have any significant effect on the rate of LAS degradation in the combined system. There was no attempt for pH control in these series of experiments. In the solution containing only LAS (no metal ions), the pH increased from 5.5 to about 7 during the 7-hour treatment period.

Although during both electrochemical and photocatalytic oxidation of LAS some acidic intermediates were produced, the rate of hydrogen evolution at cathodes seemed to be higher than the rate of H^+ ion generation at the anodes, which resulted in a net increase in the solution pH. However, when both metal ions and LAS were present, the solution pH decreased in the combined photocatalytic and electrochemical system. The reduction of metal ions hindered the hydrogen evolution at the cathodes.
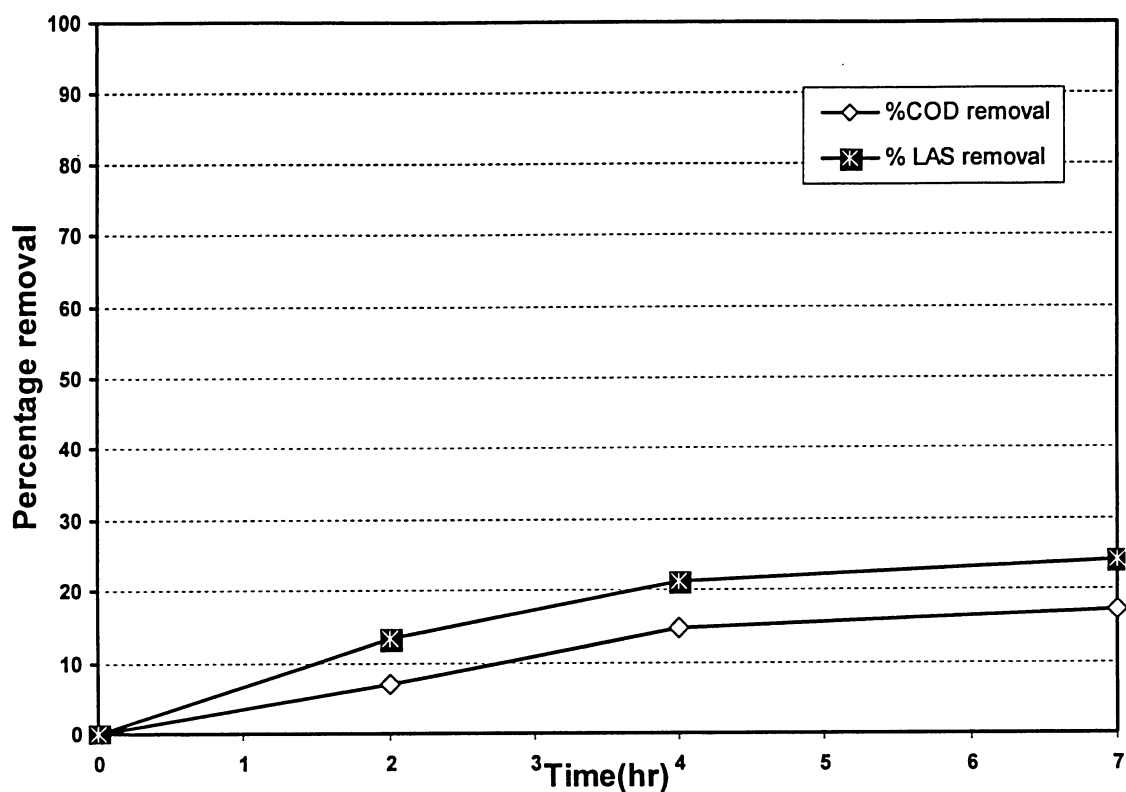
Figure 28. Direct electrochemical oxidation of LAS, without Zn^{+2} & Ni^{+2} ions in solution, no UV lamp, no pH control, current density=0.166 mA cm^{-2}, V=6 L, $[LAS]_o$=100 mg/L, liquid volumetric flux=0.0172 m^3 m^{-2} s^{-1}.
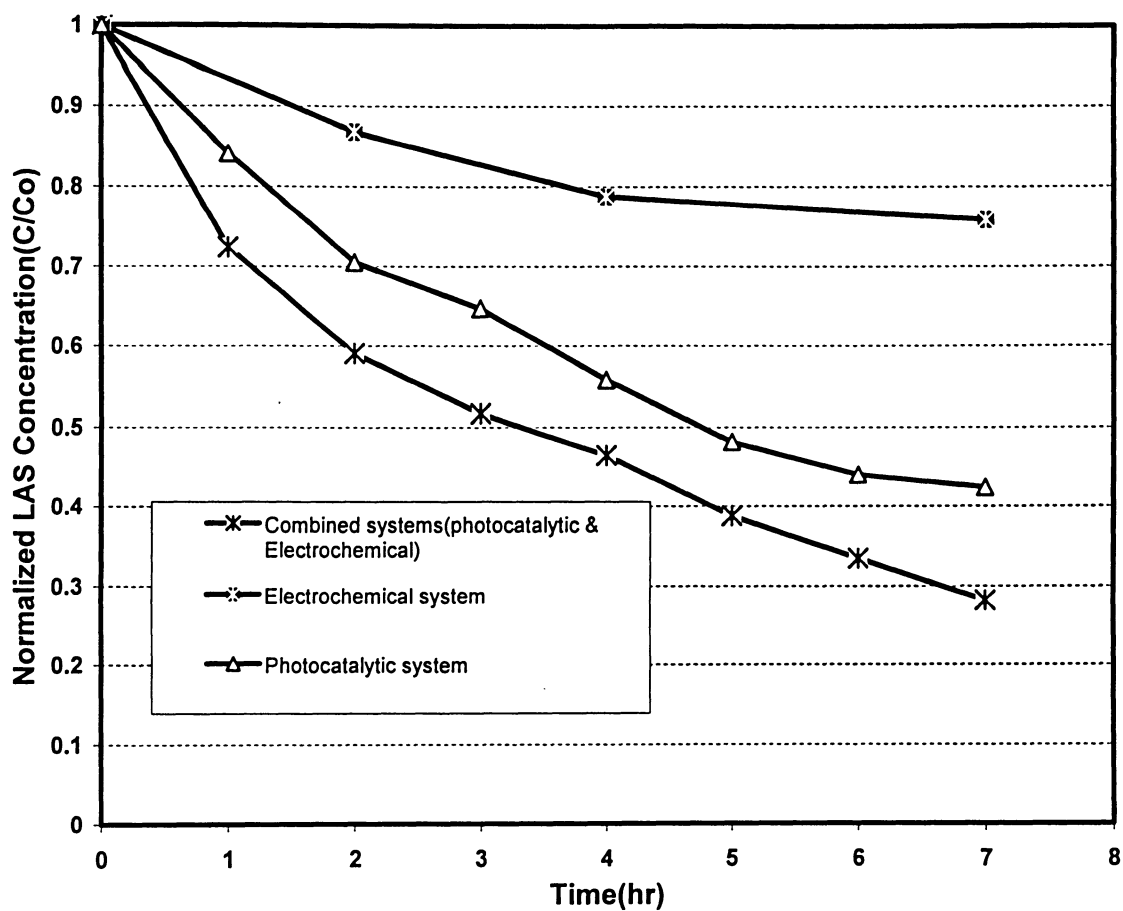
Figure 29. Comparison of LAS degradation in different systems. In all systems: volumetric flux=0.0172 m^3 m^{-2} s^{-1}, $[LAS]_o$=100 mg/L, no metal ions and no pH control.

In the electrochemical system: current density=0.166 mA cm^{-2}.
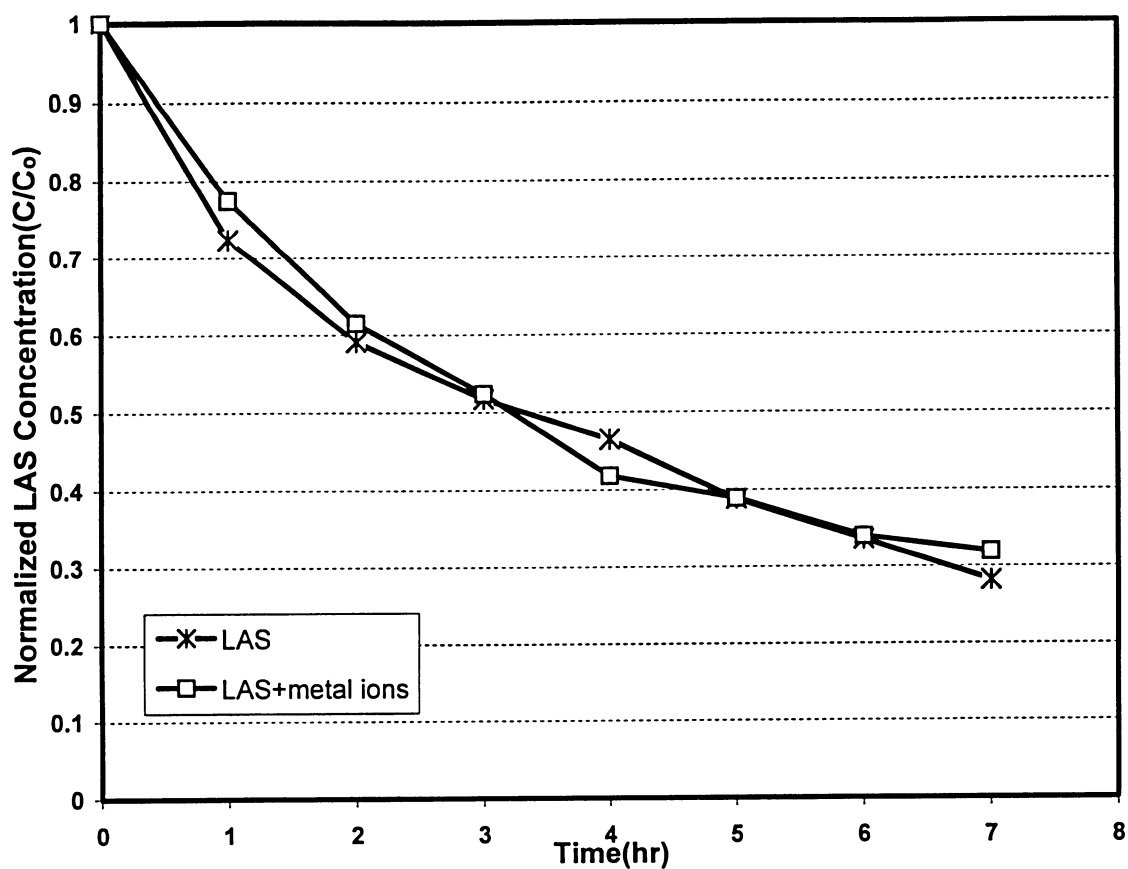
Figure 30. Effect of metal ions on the rate of LAS degradation using the combined system. Volumetric flux=$0.0172m^3m^{-2}s^{-1}$, $[LAS]_o$=100 mg/L, no pH control, $[Ni^{+2}]_o=[Zn^{+2}]_o$=20 ppm, current density=0.166 mA cm^{-2}

Consequently, the generation of acidic intermediates during both photocatalytic and electrochemical oxidation of LAS caused a reduction in the pH of the solution. The pH decreased from an initial value of 5.6 to a final value of 4.7 after a 7-hour period.

4.7.3 Effect of pH on the rate of LAS degradation using the combined system

Figure 31 presents the effect of pH on the rate of LAS degradation in the combined system. As it is shown, the higher rate of LAS removal was achieved in the experiment with controlling pH in the range of 5-5.5 compared to that without pH control.The percentage of LAS removal in experiments with pH control and without pH control was 76% and 68%, respectively.

Figure 32 presents the percentage of COD removal in both experiments. The COD was removed by 55% and 48% in experiments with and without pH control, respectively. The difference between the percentage of LAS degradation and COD removal was attributed to the generation of some intermediates in solution.

As explained before, the photocatalytic degradation of LAS is strongly pH dependent. At a pH of about 5, the surface of TiO_2 particles is positively charged and can easily adsorb the negatively charged anionic surfactant (LAS). As a result, the rate of LAS decomposition increased compared to the experiment without pH control in which the solution pH decreased over the treatment time.
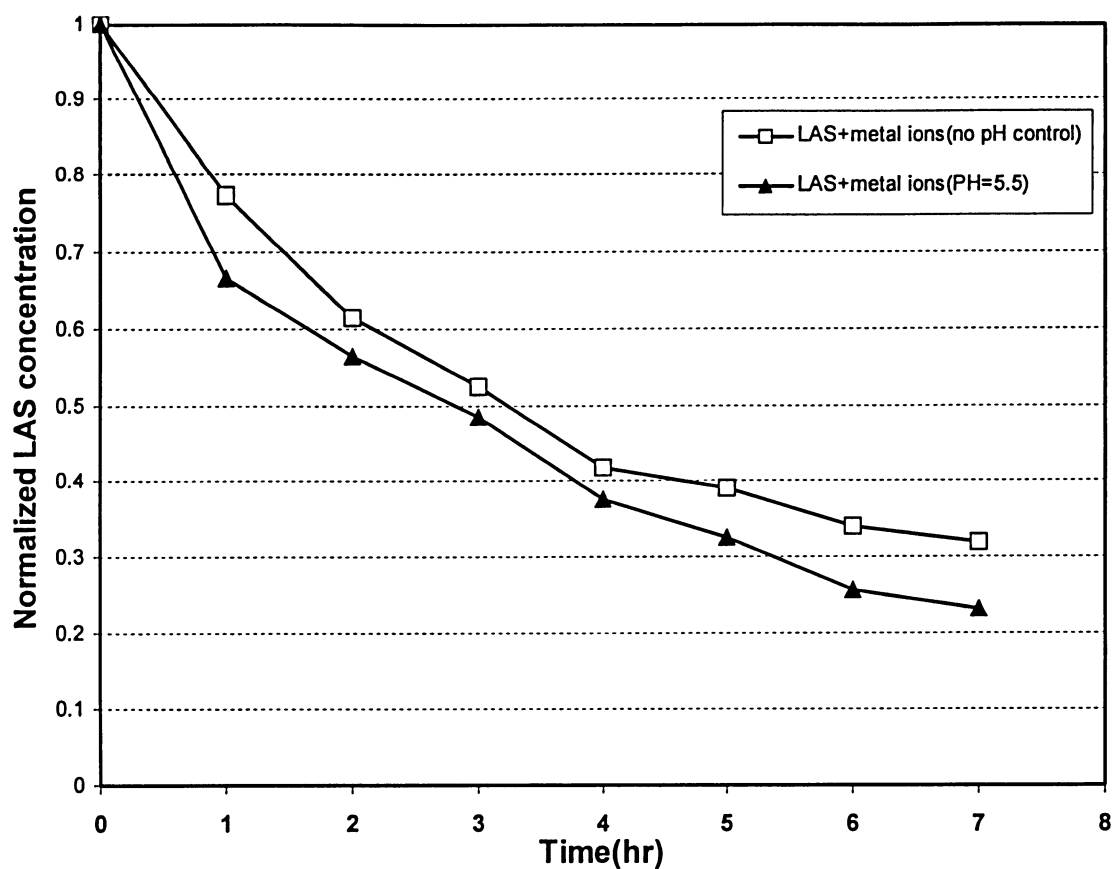
Figure 31. Effect of pH on the rate of LAS degradation using the combined system. Volumetric liquid flux=0.0172 m^3 m^{-2} s^{-1}, $[LAS]_o$=100 mg/L, $[Ni^{+2}]_o$=$[Zn^{+2}]_o$=20ppm, current density=0.166 mA cm^{-2}.
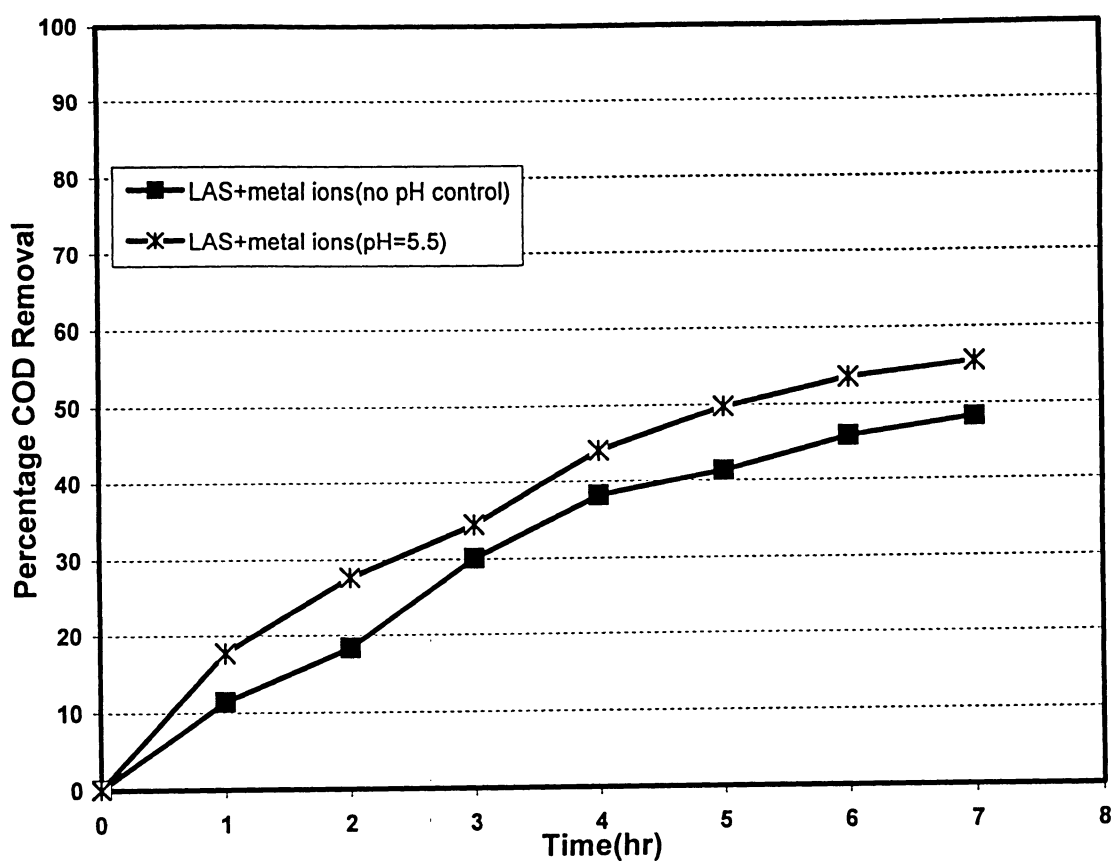
Figure 32. Effect of pH on COD removal using combined system. Volumetric liquid flux=0.0172m^3 m^{-2} s^{-1}, [LAS]$_o$=100 mg/L, [Ni^{+2}]$_o$=[Zn^{+2}]$_o$=20 ppm, K$_2$SO$_4$=250 ppm, current density=0.166 mA cm^{-2}.

102

4.7.4 Comparison of metal ion removal in different systems

As explained before, the photocatalytic reduction of Ni^{+2} and Zn^{+2} ions is not thermodynamically possible. Figure 33 compares the rate of metal ion reduction in the electrochemical system with that in the combined system. Results indicate that, in the presence of LAS and TiO_2 particles, the rate of metal ion removal decreases in the combined system.

Figure 34 illustrates the effect of pH on the percentage of metal ion removal in different systems. As it is shown, the highest percentage of removal for both metal ions was obtained in the electrochemical system with controlling pH in the range of 5-5.5.

The above results are in agreement with those obtained by other researchers. Surfactants can be adsorbed at the cathode surface and decrease the effective cathode surface area (Huang, 1995). Ahmed and Sedahmed (1989) showed that the rate of mass transfer of metal ions to the cathode decreased in the presence of surfactants. Since surfactants have a longer molecular length than water, they cause a decrease in the mass transfer coefficient of the electrolyte at the cathode-solution interface and prevent free migration of metal ions into the cathode surface (Huang, 1995).

As different surfactants have different surface activities and molecular chain lengths, the electrowining efficiency depends to a great extent upon the nature of surfactants. Therefore, the presence of surfactants in the electrolyte solution causes a reduction in cathode current efficiency (Huang, 1995). Chaudhary et al. (2001) also showed that the presence of TiO_2 and organic compounds reduced the efficiency of the metal recovery in an electro-cell. They suggested that the formation of a complex between the metal and the organic was a clear indication of the reduced efficiency of the metal recovery.
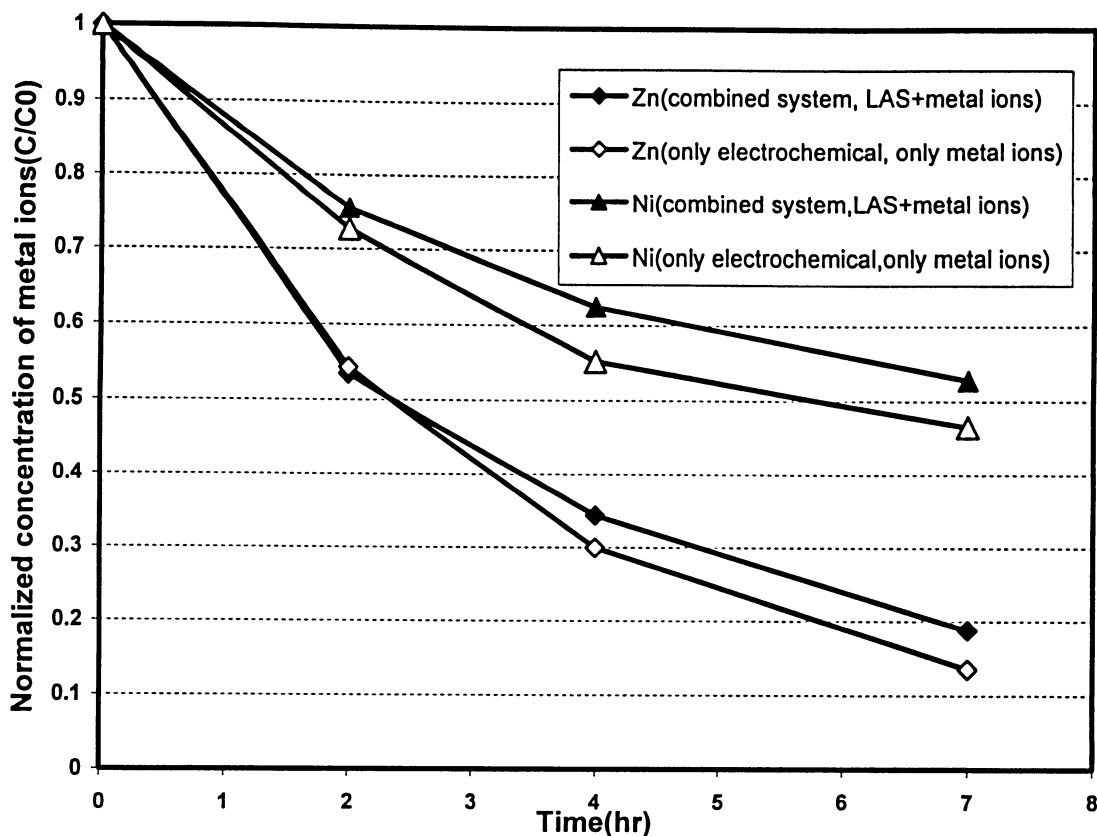
Figure 33. Comparison of metal ion reduction in different systems. Volumetric liquid flux=0.0172 m^3 m^{-2} s^{-1}, $[LAS]_o$=100 mg/L, $[Ni^{+2}]_o$=$[Zn^{+2}]_o$=20ppm, current density=0.166 mA cm^{-2}, pH=5-5.5, total volume of the solution=6L.

104
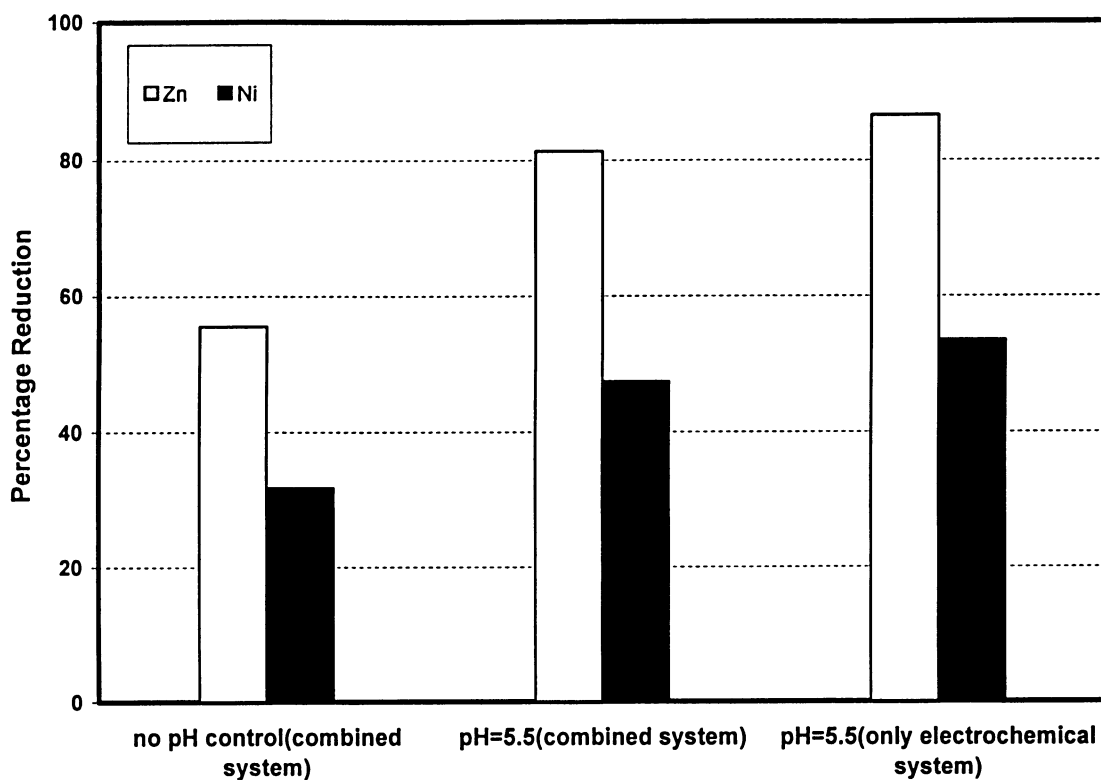
Figure 34. Effect of pH on the percentage removal of metal ions in different systems over a 7-hour period. Volumetric liquid flux=0.0172 m^3 m^{-2} $s^{-1,}$ $[LAS]_o$=100 mg/L, $[Ni^{+2}]_o$=$[Zn^{+2}]_o$=20ppm, current density=0.166 mA cm^{-2}, total volume of the solution=6L.

4.8 Photocatalytic degradation of LAS using immobilized TiO_2

An experiment was conducted to determine the effectiveness of immobilized TiO_2 particles on the surface of the silica gel support on LAS degradation. A complete procedure of immobilization was presented in chapter 3.

In order to determine if physical adsorption causes a reduction in LAS concentration, a dark experiment was conducted. 260 g silica gel granules coated with TiO_2 particles were uniformly placed at the bottom of the reactor with a thickness around 2 mm. Experimental parameters are shown in Figure 35. A 29 % reduction in the concentration of LAS was observed. This was due to physical adsorption of LAS on the surface of silica gel particles. As a result, prior to any photocatalytic experiment, the solution of LAS was recirculated through the reactor in the dark (without UV light) for 1 hour, and the sample of time zero was taken after this equilibrium period. The result showed in Figure 36 indicates that 31 % of LAS was degraded using supported TiO_2 on silica gel particles. The low rate of degradation might be due to small ratio of A/V, where A is the area of the reactor bottom and V is the total volume of the solution in reactor.

Matthews (1991) showed that increasing A/V ratio had a significant effect on the rate of organic removal using immobilized TiO_2.

In order to examine the photoactivity of the supported TiO_2, the above experiment was repeated three times. All experimental parameters were kept constant in all three experiments. After each experiment, coated silica gel particles were washed thoroughly with distilled water and dried in air. Dried silica gel granules were placed at the bottom of the reactor for a new photocatalytic experiment. As shown in Figure 36 there was a small

decrease in the rate of LAS degradation in repeated experiments. This might be due to a loss of some TiO_2 particles during first and second experiments. Washing silica gel particles after each experiment might also result in detachment of some TiO_2 particles from the surface. Brezova et al. (1995) supported TiO_2 particles on the surface of fiberglass by thermal binding.

They reported that after photocatalytic experiments the release of TiO_2 particles from the support was not observed. However, during the repeated degradation experiments, the degradation rate of phenol decreased significantly. It was suggested that this could be due to saturation of TiO_2 surface by adsorbed intermediates during experiments.
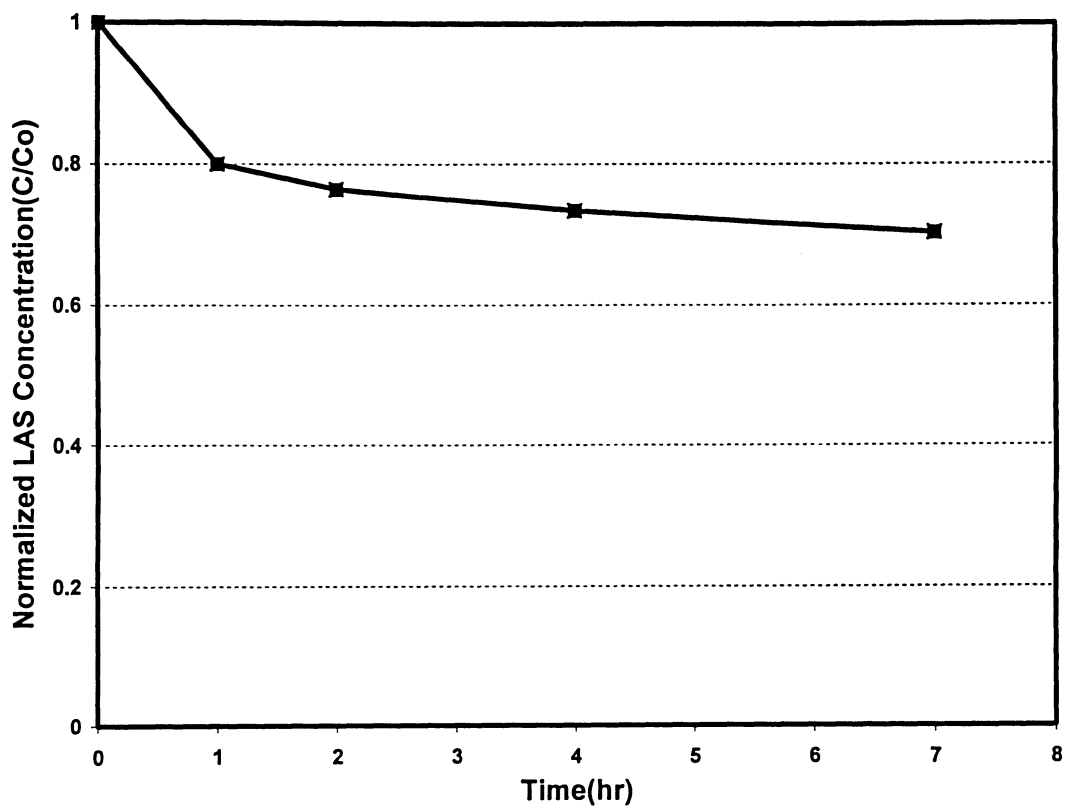
Figure 35. Dark adsorption of LAS on the surface of coated silica gel particles. Volumetric liquid flux=0.0172 m^3 m^{-2} $s^{-1,}$ [LAS]$_o$=100 mg/L, , total volume of the solution=6L, pH=5.5-5, no UV lamp.
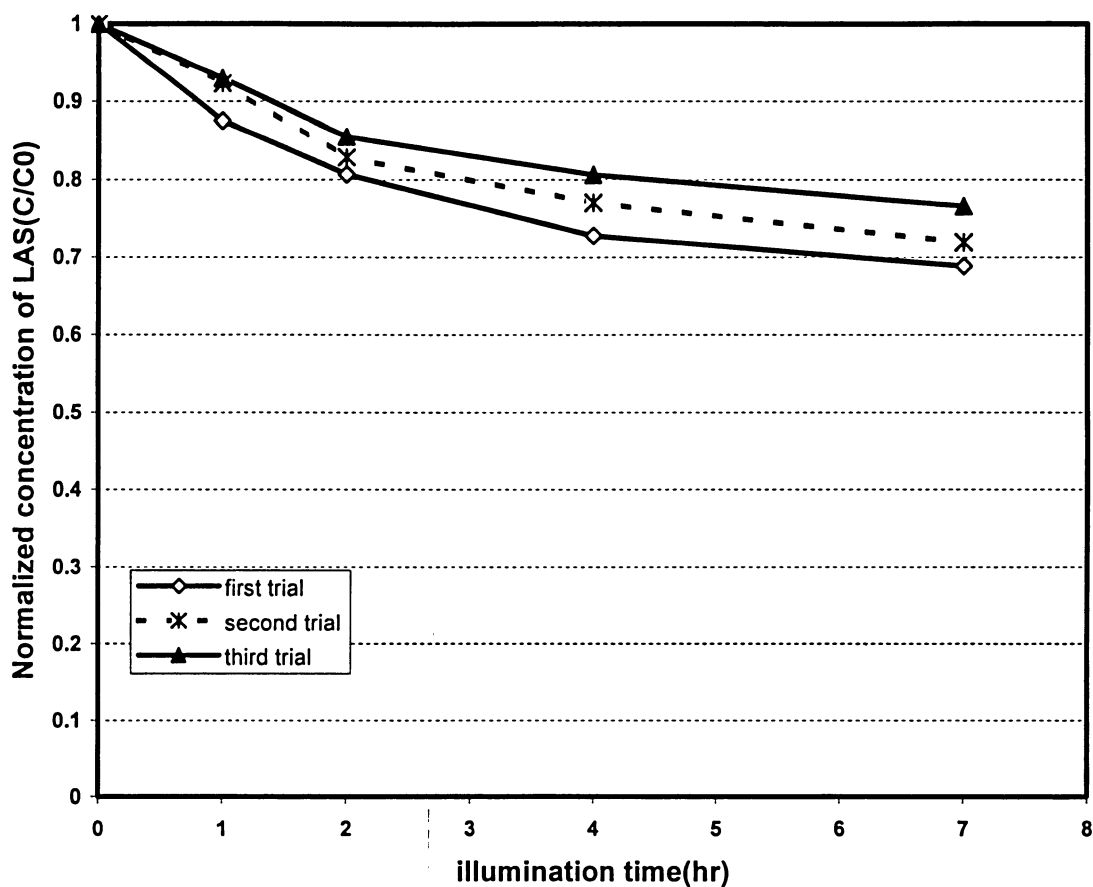
Figure 36. Photocatalytic degradation of LAS using supported TiO_2 on the surface of silica gel particles. Volumetric liquid flux=0.0172 m^3 m^{-2} s^{-1}, [LAS]$_o$=100 mg/L, , total volume of the solution=6L, pH=5.5-5.

CHAPTER 5

CONCLUSIONS AND RECOMMENDATIONS

5.1 Conclusions

In the present study, the electrochemical removal of zinc and nickel ions and photocatalytic decomposition of linear alkylbenzene sulfonate (LAS) was investigated. Simultaneous removal of those metal ions and degradation of LAS in aqueous systems by a combination of electrolytic and photolytic processes was the objective of the present study. From the analysis of the results, the following conclusions were drawn:

Using the sole electrochemical technique for metal ion reduction,

- Zinc and nickel were removed by 33% and 17%, respectively, in experiments without controlling the bulk electrolyte pH and a total electrolyte volume of 15L. Controlling the bulk electrolyte pH in the range of 5.5-6 enhanced the rate of zinc reduction but it did not have any significant effect on the rate of nickel removal. In these experiments, zinc and nickel were reduced by 64% and 16%, respectively, during 8 hours of treatment.

- The highest current efficiency of 22% was obtained using the lowest current density of 0.166 $mA.cm^{-2}$.

- Increasing volumetric flux from 0.00212 to 0.0172 $m^3.m^{-2}.s^{-1}$ enhanced the rate of zinc reduction. The highest zinc reduction of about 81% was obtained at the highest liquid flux of 0.0172 $m^3.m^{-2}.s^{-1}$ after 47 hours of treatment. However, the

percentage of nickel reduction did not change significantly with liquid fluxes from 0.00212 to 0.0172 $m^3.m^{-2}.s^{-1}$. A 48% reduction in nickel ions was obtained at the highest flux of 0.0172 $m^3.m^{-2}.s^{-1}$.

Using sole photocatalytic method for LAS degradation,

- Controlling the bulk pH in the range of 5-5.5 resulted in the highest rate of LAS degradation compared to very acidic and basic conditions. With controlling pH, LAS was degraded by 60% while COD was removed only by 44% over a 7-hour period.

- Both variation in the volumetric liquid flux and temperature did not seem to have any significant effect on the rate of LAS degradation.

- Using TiO_2 supported on silica gel particles, LAS was degraded by only 31% during 7 hours. Repeating experiments resulted in a reduction in the rate of LAS decomposition.

Using a combined photolytic-electrolytic system (with suspended TiO_2 particles),

- In an experiment without controlling pH, LAS was degraded by 68% in the combined system compared to 57% in the photolytic system alone.

- Controlling pH in the range of 5-5.5 enhanced the rate of LAS degradation in the combined system. LAS was degraded by 76% and 68% in experiments with and without controlling pH, respectively, over a-7 hour treatment period.

- The rate of metal ion reduction decreased slightly in the combined system compared to the electrochemical system alone. After 7 hours of treatment, zinc and nickel were reduced by 81% and 47% in the combined system, respectively,

111

while they were removed by 86% and 53% in the sole electrochemical system, respectively, using total electrolyte volume of 6 L.

In conclusion, the combined system can be used for the treatment of mixed effluent streams containing heavy metal ions and organic compounds.

5.2 Recommendations

- In order to obtain a higher rate of metal removal, the ratio of cathode surface area per volume of the reactor should be increased. Three-dimensional electrodes such as porous electrodes offer a high surface area compared to flat electrodes.

- The effect of higher volumetric fluxes on the rate of metal ion removal should be investigated.

- Studies should be performed to identify and quantify the intermediates generated during the photocatalytic degradation of LAS.

- A new reactor configuration, which is long in length, shallow in depth, and equipped with multi UV lamps, can increase the efficiency of the process. Long parallel plate 3-D electrodes can provide a higher surface area for reactions.

REFFERENCES

Abibsi, A.; Dennis, J. K.; Short, N. R., The effect of plating variables on zinc-nickel alloy electrodeposition. *Trans. Inst. Metall. Finish.*, **69**, 145-148, 1991.

Ahmed A. M. and Sedahmed G. H., Effect of surfactants on the rate of mass transfer at gas-evolving electrodes. *J. Appl. Electrochem.* **19**, 219-224, 1989.

Al-Ekabi, H. and Serpone, N. Kinetics studies in heterogeneous photocatalysis. I. Photocatalytic degradation of chlorinated phenols in aerated aqueous solutions over titania supported on a glass matrix. *J. Phys. Chem.* **92**, 5726-5731, 1988.

Bankian Tabrizi, G., Pilot plant study of aqueous linear alkylbenzene sulfonate degradation by combined advanced oxidation and biological processes. M. A. Sc. thesis, Ryerson University, Toronto, Ontario, Canada, 2004.

Bellobono, I. R.; Bonardi, M.; Castellano, L.; Selli, E.; Righetto, L., Degradation of some chloro-aliphatic water contaminants by photocatalytic membranes immobilizing titanium dioxide. *J. Photochem. Photobiol. A: Chem.*, **67**,109-115,1992.

Bideau, M.; Claudel, B.; Dubien, C.; Faure, L.; Kazouan, H. On the "immobilization" of titanium dioxide in the photocatalytic oxidation of spent waters. *J. Photochem. Photobiol. A: Chem.*, **91**,137-144, 1995.

Brenner, A., Electrodeposition of Alloys. Principles and Practice Vol.1&2. Academic Press, New York, 1963.

Brett, M.A. and Brett A.M.O., Electrochemistry principles, methods, and applications, Oxford University Press, Oxford New York , Tokyo, 1996.

Brezova, V.; Blazkova, A.; Breznan, M.; Kottas, P., Phenol degradation on glass fibers with immobilized titanium dioxide particles. *Collect. Czech. Chem. Commun.* **60**, 788-794, 1995.

Byrne, J. A.; Eggins, B. R; Brown, N.M.D.; Mckinney, B.; Rouse, M., Immobilization of TiO_2 powder for the treatment of polluted water. *Appl. Catal. B: Chem.* **17**, 25-36, 1998.

Camara, O. R.; De Pauli, C. P.; Vaschetto, M. E.; Retamal, B.; Aquuirre, M.J.; Zagal, J. H., Biaggio, S. R., Semiconducting properties of TiO_2 films thermally formed at 400°C. *J. Appl. Electrochem.* **25**, 247-251, 1995.

Campbell, D.A.; Dalrymple, I.M.; Sunderland, J.G.; Tilston., D., *Resour., Conserv. Recycling,* **10**, 25-33, 1994.

Canizares, P.; Dominguez, J. A.; Rodrigo, M. A.; Villasenor, J.; Rodriguez, J., Effect of current intensity in the electrochemical oxidation of aqueous phenol wastes at an activated carbon and steel anode. *Ind. Eng. Chem. Res.,* **38**, 3779-3785, 1999.

Chassaing, E.; Wiart, R., Electrocrystallization mechanism of Zn-Ni alloys in chloride electrolytes, *Electrochimica Acta.* **37**, 545-553, 1992.

Chaudhary, A. J.; Grimes, S. M.; Hassan, M., Simultaneous recovery of copper and degradation of 2,4-dichlorophenoxyacetic acid in aqueous systems by a combination of electrolytic and photolytic processes. *Chemosphere,* **44**, 1223-1230, 2001.

Chen, A.; Lu, G. T.; Dal, Z.; Gu, H., Novel photocatalytic immobilized on springs and packed photoreactor. *Mater. Phys. Mech.* **4**, 121-124, 2001.

Chen, D; Ray, A.K., Removal of toxic metal ions from wastewater by semiconductor photocatalysis. *Chem. Eng. Sci.* **56**, 1561-1570, 2001.

Chen, D. W.; Sivakumar, M.; Ray, A. K., Heterogeneous photocatalysis in environmental remediation, *Develop. Chem. Eng. Min. Proc. J.,* **8**, 505-550, 2000.

Chester, G.; Anderson, M.; Read H., A jacketed annular membrane photocatalytic reactor for wastewater treatment: degradation of formic acid and atrazine. *J. Photochem. Photobiol A: Chem.* **71**, 291-297, 1993.

Dahms, H. and Croll, I. M., The anomalous co-deposition of iron-nickel alloys. *J. Electrochem. Soc.* **112**(8), 771-775, 1965.

De Almedia, J.L. G.; Dufaux, M.; Taarit, Y.B.; Naccache, C., *J. Am. Oil Chem. Soc.,* **71**, 675-694, 1994.

Deki, S.; Aoi, Y.; Hiroi, O.; Kahinami, A., Titanium (IV) oxide thin films prepared from aqueous solution. *Chem. Lett.,* **25** ,433-434,1996.

Deligianni, H.; Romankiw, L. T., In situ surface pH measurement during electrolysis using a rotating electrode. *IBM J. Res. Develop.***37**, 85-95, 1993.

Dionysiou, D. D.; Khodadoust, A. P.; Kern, A. M.; Suidan, M. T., Baudin, I.; Lain, J. M., Continuous- mode photocatalytic degradation of chlorinated phenols and pestisides in water using a batch-scale $TriO_2$ rotating disk reactor. *Appl. Catal. B: Environ.,* **24**, 139-155, 2000.

Doan, H. D. and Wu, J., Biological treatment of wastewater from a polymer coating process. *J. Chem. Tech. And BioTech.* **77**, 1076-1083, 2002.

Doan, H.D.; Wu, J.; Boithi, E.; Storrar, M., Treatment of wastewater using a combined biological and electrochemical technique, *J. Chem. Technol. Biotechnol,* **78**, 632-641, 2003.

Fabri Miranda, F. J.; Barcia, O.E; Diaz, S.L; Mattos, O. R.; Wiart, R., Electrodeposition of Zn-Ni alloys in sulfate electrolysis. *Electrochimica Acta*, **41**, 1041-1049, 1996.

Fernandez, A.; Lassaletta, G.; Jimenez, V. M.; Justo, A.; Gonzalez-Elipe, A. R.; Herrmann, J.-M.; Tahiri, H.; Ait-Ichou, Y., Preparation and characterization of TiO_2 photocatalysts supported on various rigid supports (glass, quartz and stainless steel). Comparative studies of photocatalytic activity in water purification., *Appl. Catal. B: Environ.*, **7**, 49-63, 1995.

Foti, G.; Gandini, D.; Comninellis, C.; Perret, A.; Haenni, W. Oxidation of organics by intermediates of water discharge on IrO2 and synthetic diamond anodes. *Electrochem. Solid-State Lett.*, **2**, 228, 1999.

Frank, S. N. and Bard, A. J., Heterogeneous photocatalytic oxidation of cyanide ion in aqueous solutions at semiconductor powders. *J. Am. Chem. Soc.***99**, 303-304, 1977.

Fratesi, R. and Roventi, G., Electrodeposition of zinc-nickel alloy coatings from a chloride bath containing NH_4Cl. *J. Appl. Electrochem.* **22**, 657-662, 1992.

Fujishima, A.; Rao, T. N.; Tryk, D. A., Titanium dioxide photocatalysis. *J. Photochem. Photobiol. C: Photochem. Reviews*, **1**, 1-21, 2000.

Fukushima, H., Electrodeposition behavior of Zn-Ni alloys from sulfate baths over a wide range of current density, *Metall*, **42**, 242-247, 1988.

Genders, D.J. and Weinburg, N., Electrochemistry for a Cleaner Environment. The Electrosynthesis Company, East Amherst, New York, 1992.

Harada, H.; Sakata, T.; Ueda, T.; Effect of semiconductor in photocatalytic decomposition of lactic acid. *J. Am. Chem. Soc.*, **107**, 1773, 1985.

Herrmann, J. M.; Guillard, C.; Pichat, P., Heterogeneous photocatalysis: an emerging technology for water treatment. *Catal. Today*, **17**, 7-20, 1993.

Herrmann, J. M., Heterogeneous photocatalysis: fundamentals and applications to the removal of various types of aqueous pollutants. *Catal. Today*, **53**, 115-129, 1999.

Hidaka, H. and Kubota, H., Photodegrdation of surfactantsII: Degradation of sodium dodecylbenzene sulfonate catalysed by titanium dioxide particles., *J. Photochem,* **35**, 219-230, 1986.

Hidaka, H. and Zhao, J., Photodegrdation of surfactantsVIII. Comparision of photocatalytic processes between anionic sodium dodecylbenzenesulfonate and cationic benzyldodecyldimethylammonium chloride on the TiO2 surface. *J. Phys. Chem.,* **96**, 2226-2230, 1992.

Hidaka, H.; Yamada, S.; Suenaga, S.; Zhao, J., Photodegrdation of surfactants Part VI: Complete photocatalytic degradation of anionic, cationic and nonionic surfactants in aqueous semiconductor dispersions. *J. Mol. Catal.,* 59, 270-290, 1990.

Hoffmann, M. R.; Martin, S. T; Choi, W.; Bahnemann, D. W., Environmental applications of semiconductor photocatalysis. *Chem. Rev.,* **95**, 69-96, 1995.

Hofstadler, K.; Bauer, R.; Novalic, S.; Heisler, G., New reactor design for photocatalytic wastewater treatment with TiO_2 immobilized on fused-silica glass fibers: Photomineralization of 4-Chlorophenol. *Environ. Sci. Technol.,* **28**, 670-674, 1994.

Huang, C. H.; Effect of surfactants on recovery of nickel from nickel plating wastewater by electrowinning. *Wat. Res.,* **29**, 1821-1826, 1995

Huang, X.; Ellis, T.; Kaiser, S., Extent biodegradation testing with linear alkylbenzene sulfonate in laboratory and field activated sludge systems, *Water Environmental Federation,* 2000.

Jackson, N.B.; Wang, C. M.; Luo, Z.; Schwitzgebel, J.; Ekerdt, J. G.; Brock, J. R.; Heller A., Attachment of TiO_2 powders to hollow glass microbeads: Activity of the TiO_2-coated beads in the photoassisted oxidation of ethanol to acetaldehyde. *J. Electrochem. Soc.,* **138,** 3660-3664, 1991.

Ji, J.; Cooper, W. C.; Dreisinger, D. B.; and Peters, E., Surface pH measurements during nickel electrodeposition. *J. Appl. Electrochem.* **25,** 642-650, 1995.

Juttner, K.; Galla, U.; and Schmieder, H., Electrochemical approaches to environmental problems in the process industry. *Electrochimica Acta,* **45,** 2575-2594, 2000.

Kormann, C.; Behnemann, W.; Hoffmann, M. R., Photolysis of chloroform and other organic molecules in aqueous TiO_2 suspensions. *Environ. Sci. Technol.* **25,** 494-500, 1991.

Kudo, A.; Steinberg, M.; Bard, A. J.; Campion, A.; Fox, M. A.; Mallouk, T. E.; Webber, S. E.; White, J. M., Photoelectrochemical properties of titanium dioxide electrode prepared from titanium alloy. *J. Electrochem. Soc.,* **137,** 3846-3849, 1990.

Lanza, M.R.V. and Bertazzoli, R., Removal of Zn(II) from chloride medium using a porous electrode: current potential within the cathode. *J. Appl. Electrochem.,* **30,** 61-70, 2000.

Lepore, G.P.; Persaud, L.; Langford, C.H., Supporting titanium dioxide photocatalysts on silica gel and hydrophobically modified silica gel. *J. Photochem. Photobiol. A: Chem.***98,** 103-111, 1996.

Leu, H. G.; Lin, S. H.; Lin, T. M., Enhanced electrochemical oxidation of anionic surfactants. *J. Environ. Sci. Health A*, **33**, 681-699, 1998.

Marchado, A.E.H.; Miranda, J.A; Freitas, R.F.; Duarte, E.T.F.M; Ferreira, L.F.; Albuquerque, Y.D.T.; Ruggiero, R.; Sattler, C.; Oliveira, L., Destruction of the organic matter present in effluent from a cellulose and paper industry using photocatalysis. *J. Photochem. Photobiol. A: Chem.* **155**, 231-241, 2003.

Matthews, R. W., Photooxidation of organic impurities in water using thin films of titanium dioxide, *J. Phys. Chem.* **91**, 3328-3333, 1987.

Matthews, R.W. Kinetics of photocatalytic oxidation of organic solutes over titanium dioxide. *J. Catal.* **111**, 264-272, 1988.

Matthews, R. W. Photooxidative degradation of coloured organics in water using supported catalysts TiO$_2$ on sand. *Wat. Res.* **25**, 1169-1176, 1991.

Matthews, R. W.; and McEvoy, S. R. Destruction of phenol in water with sun, sand, and photocatalysis. *Sol. Energy,* **49**, 507-513, 1992.

Mehrvar, M., Kinetic modeling and novel packed bed photocatalytic reactor. PhD thesis, University of Waterloo, Waterloo, Ontario, Canada, 1998.

Miranda, F.; Barcia, F.J.O.E.; Mattos, O. R.; and Wiart, R., Electrodeposition of Zn-Ni alloys in sulfate electrolytes 1. Experimental approach, *J. Electrochem. Soc.,* **144**, 3441-3448, 1997(a).

Miranda, F.; Barcia, F. J. O.E.; Mattos, O. R.; Wiart, R., Electrodeposition of Zn-Ni alloys in sulfate electrolytes 2. Reaction modeling. *J. Electrochem. Soc.,* **144**, 3449-3457, 1997(b).

Mitzakov, R., Combined electrochemical and biological treatment of industrial wastewater using porous electrodes and a packed bed reactor, M. A. Sc Thesis, Ryerson University, 2004.

Muradov, N. Z., Solar detoxification of nitroglycerine-contaminated water using immobilized titania . *Sol. Energy*, **52**, 283-288, 1994.

Njau, K. N.; Hosseini, Y. M.; Janssen, L. J. J., Electrochemical reduction of nickel ions from dilute artificial solutions in a GBC reactor, *J. Appl. Electrochem*, **28**, 689-696, 1998.

Njau, K. N.; Woude, M.; Visser, G. J.; Janssen, L.J.J., Electrochemical removal of nickel ions from industrial wastewater, *Chem. Eng. Journal.*, **79**, 187-195, 2000.

Ohtsuka, T. and Komori, A., Study of initial layer formation of Zn-Ni alloy electrodeposition by in situ ellipsometry, *Electrochimica Acta,* **43**, 3269-3276, 1998.

Orhan, G.; Arslan, C.; Bombach, H.; Stelter, M., Nickel recovery from the rinse waters of plating baths, *Hydrometallurgy*, **65**, 1-8, 2002.

Patterson, D.; Metcalfe, I.; Xiong, F.; Livingston, A., Biodegradability of linear alkylbenzene sulfonates subjected to wet air oxidation, *J. Chem. Technol Biotechnol.,* **77**, 1039-1049, 2002.

Paunovic, M. and Schlesinger, M., Fundamentals of electrochemical deposition, New York, 1998.

Peral, J.; Casado, J.; Domenech, J., Light induced oxidation of phenol over ZnO powder. *J.Photochem. Photobiol. A; Chem.*, **44**, 209-217, 1988.

Pickett, D.J., The analysis of a batch electrochemical reactor with continuously recirculating electrolyte. *Electrochimica Acta.*, **18**, 835-837, 1973.

Pickett, D. J., Electrochemical Reactor Design, 2nd ed., Elsevier Scientific Publishing Company, Amsterdam-Oxford-New York, 1979.

Pletcher, D. and Walsh, F. C., Industrial Electrochemistry, 2nd ed. Chapman-Hall, London, 1990.

Pleskov Y. V. and Gurevich Y.Y., Semiconductor photoelectrochemistry, Consultants Bureau, New York, 1986.

PPG Industrial Electrocoat Training. Module 1. PPG industries, Inc. Springdale, Pennsylvania, 2001.

Prairie, M.R.; Evans, L.R.; Stange, B.M.; Martinez, S.L., An investigation of TiO_2 photocatalysis for the treatment of water contaminated with metals and organic chemicals. *Environ. Sci. Technol.* **27**, 1776-1782, 1993.

Rajeshwar, K. and Ibanez, J. G., Environmental electrochemistry, fundamentals and applications in pollution abatement, Academic Press 1997.

Rajeshwar, K.; Chenthamarakshan, C. R.; Ming Y.; Sun, W., Cathodic photoprocesses on titania films and in aqueous suspensions. *J. Electroanal. Chem.*, **538-539**, 173-182, 2002.

Ray, A. K. and Beenackers, A. A. C. M., Novel swirl-flow reactor for kinetic studies of semiconductor phototcatalysis. *A.I.Ch.E. J.* **43**, 2571-2578, 1997.

Raub, E. and Muller, K., Fundamentals of metal deposition, Elsvier publishing company, Amsterdam, London, New York, 1967

Richens, D. T., The chemistry of aqueous ions. John Wiley&Sons, Chichester, England, 1997.

Roventi, G.; Fratesi, R.; Della Guardia R. A.; Barucca. G., Normal and anomalous co-deposition of Zn-Ni alloys from chloride bath. *J. Appl. Electrochem.*, **30**, 173-179, 2000.

Scott, A. C.; Pitblado, R. M.; Barton, G.W., Experimental determination of the factors affecting zinc electrowinning efficiency. *J. Appl. Electrochem.*, **18**, 120-127, 1988.

Scott, K. and E.M. Patton, An analysis of metal recovery by electrodeposition from mixed metal ion solution-part I. Theoretical behavior of batch recycle operation, *Electrochimica Acta*, **38**, 2181-2189, 1993.

Serpone, N.; Borgarello, E.; Cahill, P.; Harris, R.; Borgarello, M.; Pelizzetti, E. Photocatalysis over TiO_2 supported on a glass substrate. *Sol. Energy. Mater.* **14**, 121-127, 1986.

Simonsson, D., A., Flow-by packed bed electrode for removal of metal ions from wastewaters, *J. Appl. Electrochem*, **14**, 595-604, 1984.

Sheela, G.; Pushpavanam, M.; Pushpavanam, S., Zinc-nickel alloy electrodeposits for water electrolysis, *Int. J. Hydrogen. Energ.*, **27**, 627-633, 2002.

Somasundaram, S.; Ming, Y.; Chenthamarakshan, C.R.; Schelly, Z.A.; Rajeshwar, K., Free radical-mediated heterogeneous photocatalytic reduction of metal ions in UV-irradiated titanium dioxide suspensions. *J. Phys. Chem. B*, **108**, 4784-4788, 2004.

Standards Methods for the Examination of Water and Wastewater/prepared and published jointly by American Public Health Association, Water Pollution Control Federation, 1998.

Stefan, M. I.; Hoy, A. R.; Bolton, J. R., Kinetics and mechanism of the degradation and mineralization of acetone in dilute aqueous solution sensitized by UV photolysis of hydrogen peroxide. *Environ. Sci. Technol.* **30**, 2382-2390, 1996.

Tada, H. and Honda, H., Photocatalytic activity of TiO_2 film coated on internal lightguide. *J. Electrochem. Soc.,* **142**, 3438-3443, 1995.

Takeda, N.; Torimoto, T.; Sampath, S.; Kuwabata, S.; Yoneyama, H.; Sampath, S.; Effect of inert supports for titanium dioxide loading on enhancement of photodecomposition rate of gaseous propionaldehyde. *J. Phys. Chem.* **99**, 9986-9991, 1995.

Vinodgopal, K.; Kamat, P. V. Enhanced rates of photocatalytic degradation of an azo Dye using SnO_2/TiO_2 coupled semiconductor thin films. *Environ. Sci. Technol.* **29**, 841-845, 1995.

Waldron, H. A, Ed., Metals in the Environment, Academic Press, London, 1980.

Walker, A. T. S. and Wragg, A. A., The modeling of concentration-time relationship in recirculating electrochemical reactor systems, *Electrochimica Acta.,* **22**, 1129-1234, 1977.

Zhang, C.; Valsaraj, K. T.; Constant, W. D.; and Roy, D., Aerobic biodegradation kinetics of four anionic and nonanionic surfactants at sub-and supra-critical micelle concnetratints (CMCs), *Wat. Res.,* **33**(1), 115-124, 1999.

Zhang, Y.; Crittenden, J.C.; Hand, D.W.; Perram, D.L., Fixed-bed photocatalysts for solar decontamination of water. *Environ. Sci. Technol.* **28**, 435-442,1994.

Zhou, H. and Smith, D. W., Advanced technologies in water and wastewater treatment. *Can. J. Civil Eng.,* **28**, 49-66, 2001.

Zhou, Z. and O'Keefe, T. J., Modification of anomalous deposition of Zn-Ni alloy by using tin additions. *Sur. Coat. Tech.,* **96**, 191-197, 1997.

APPENDIX

A: Selected standard reduction potentials in aqueous media at 25°C

Table 6. Standard reduction potentials

Cathode (Reduction)	Half-Reaction Standard Potential E° (V)
$Li^+(aq) + e^- \rightarrow Li(s)$	-3.04
$Rb^+ + e^- \rightarrow Rb\ (s)$	-2.98
$K^+(aq) + e^- \rightarrow K(s)$	-2.93
$Cs^+(aq) + e^- \rightarrow Cs(s)$	-2.92
$Ba^{2+}(aq) + 2e^- \rightarrow Ba(s)$	-2.91
$Sr^{2+}(aq) + 2e^- \rightarrow Sr(s)$	-2.89
$Ca^{2+}(aq) + 2e^- \rightarrow Ca(s)$	-2.76
$Na^+(aq) + e^- \rightarrow Na(s)$	-2.71
$Mg^{2+}(aq) + 2e^- \rightarrow Mg(s)$	-2.38
$Al^{3+}(aq) + 3e^- \rightarrow Al(s)$	-1.66
$Zn(OH)_4^{2-} + 2e^- \rightarrow Zn + 4OH^-$	-1.29
$Mn^{2+}(aq) + 2e^- \rightarrow Mg(s)$	-1.19
$2H_2O(l) + 2e^- \rightarrow H_2(g) + 2OH^-(aq)$	-0.83
$Zn^{2+}(aq) + 2e^- \rightarrow Zn(s)$	-0.76
$Cr^{3+}(aq) + 3e^- \rightarrow Cr(s)$	-0.74
$Fe^{2+}(aq) + 2e^- \rightarrow Fe(s)$	-0.41
$Cd^{2+}(aq) + 2e^- \rightarrow Cd(s)$	-0.40
$Co^{2+}(aq) + 2e^- \rightarrow Co(s)$	-0.28
$Ni^{2+}(aq) + 2e^- \rightarrow Ni(s)$	-0.23
$Fe^{3+}(aq) + 3e^- \rightarrow Fe(s)$	-0.04
$2H^+(aq) + 2e^- \rightarrow H_2(g)$	0.00
$Cu^{2+}(aq) + e^- \rightarrow Cu^+(aq)$	0.16
$Cu^{2+}(aq) + 2e^- \rightarrow Cu(s)$	0.34
$O_2 + 4H^+ + 4e^- \rightarrow 2H_2O$	1.23

http://hyperphysics.phy-astr.gsu.edu/hbase/tables/electpot.html#c1

B: Calibration curve for LAS measurement
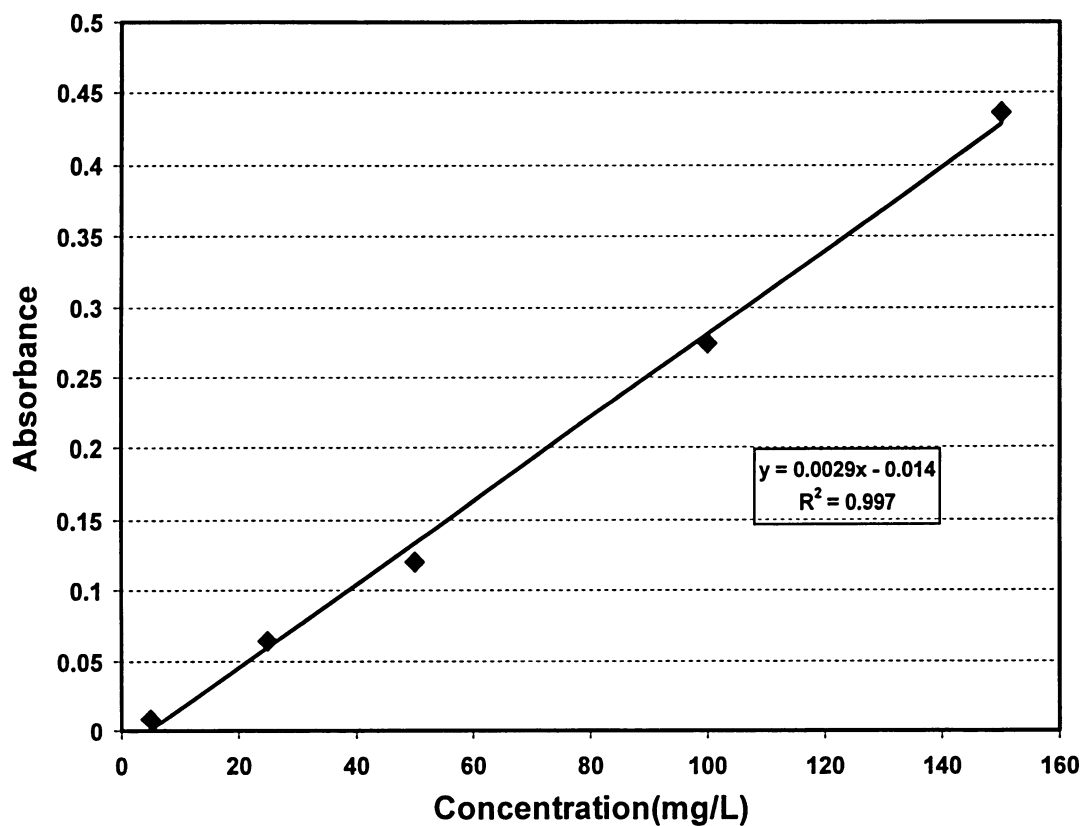

Figure 37. The calibration curve for LAS using MBAS method

C: Determination of removal efficiency

In the current study, the percentage of metal ion removal or LAS degradation was considered as the performance of the system that can be expressed as removal efficiency (RE):

$$RE = \frac{C_o - C_t}{C_o} \times 100$$

(C.1)

where C_o and C_t are the initial and residual concentration of metal ions or LAS, respectively, in solution.

D: Current efficiency calculation

The total current efficiency for zinc and nickel deposition was calculated by adding the current efficiencies for individual reaction. The current efficiency for deposition of each metal was found using Equation (2.1.2.6):

$$\varepsilon_j = \frac{m_j}{It/z_jF} *100$$

(D.1)

ε total metal deposition $= \varepsilon$ zinc deposition $+\varepsilon$ nickel deposition

For example with the following experimental conditions:

Current density=0.166mA.cm^{-2}, Cathode surface area=360cm^2 and t=47h, the following results was obtained:

Amount of zinc was reduced=36.74 mg
Amount of nickel was reduced=11.263 mg

Therefore;

126

$$\varepsilon_{\text{zinc deposition}} = \frac{(2 \times 96500 \times 36.74 \times 0.001 \times 100}{0.166 \times 360 \times 0.001 \times 47 \times 3600 \times 65.39} = 16.087$$

$$\varepsilon_{\text{nicke deposition}} = \frac{(2 \times 96500 \times 11.263 \times 0.001 \times 100}{0.166 \times 360 \times 0.001 \times 47 \times 3600 \times 58.69} = 5.49$$

$\varepsilon_{\text{total metal deposition}} = 16.087 + 5.49 = 21.577$

E: The Reynolds Number Calculation

Reynolds numbers were calculated using following formula:

$$Re = \frac{\rho v D}{\mu} \tag{E.1}$$

where $\mu = 0.001$ kg.m^{-1}.s^{-1} , $\rho = 1000$ kg.m^{-3}@ 25°C , v is liquid volumetric flux, D is hydraulic diameter of the reactor, which can be calculated from following equation:

$$D = \frac{4xy}{2(x+y)} \tag{E.2}$$

where:

x=0.055 m and y=0.2 m are the height and width of the reactor, respectively.

For example, Reynolds number corresponding to liquid volumetric flux of 0.0172m^3.m^{-2}.s-^{1} can be calculated according to the following:

$$Re = \cfrac{1000 \times \cfrac{4 \times 0.055 \times 0.2}{2(0.055 + 0.2)} \times 0.0172}{0.001} = 1485.455$$

F: Determination of reaction rate constant

Since both electrochemical reduction of metal ions and LAS degradation followed the first order reaction in a batch reactor, the reaction rate can be expressed as the following:

$$\frac{dC}{dt} = -kC \tag{F.1}$$

$$\int_{C_0}^{C_t} \frac{dC}{dt} = -k \int_0^t dt \tag{F.2}$$

$$\frac{C_t}{C_0} = e^{-kt} \tag{F.3}$$

or

$$-\ln \frac{C_t}{C_0} = kt \tag{F.4}$$

where

C_0 = initial concentration of reactive species, $mg.l^{-1}$

C_t = concentration of reactive species, $mg.l^{-1}$

t = reaction time, Time

k = first order rate constant, $time^{-1}$

By linear regression on natural logarithm of C_t/C_0 versus time, the first-order rate constant can be determined from the slope of the line.

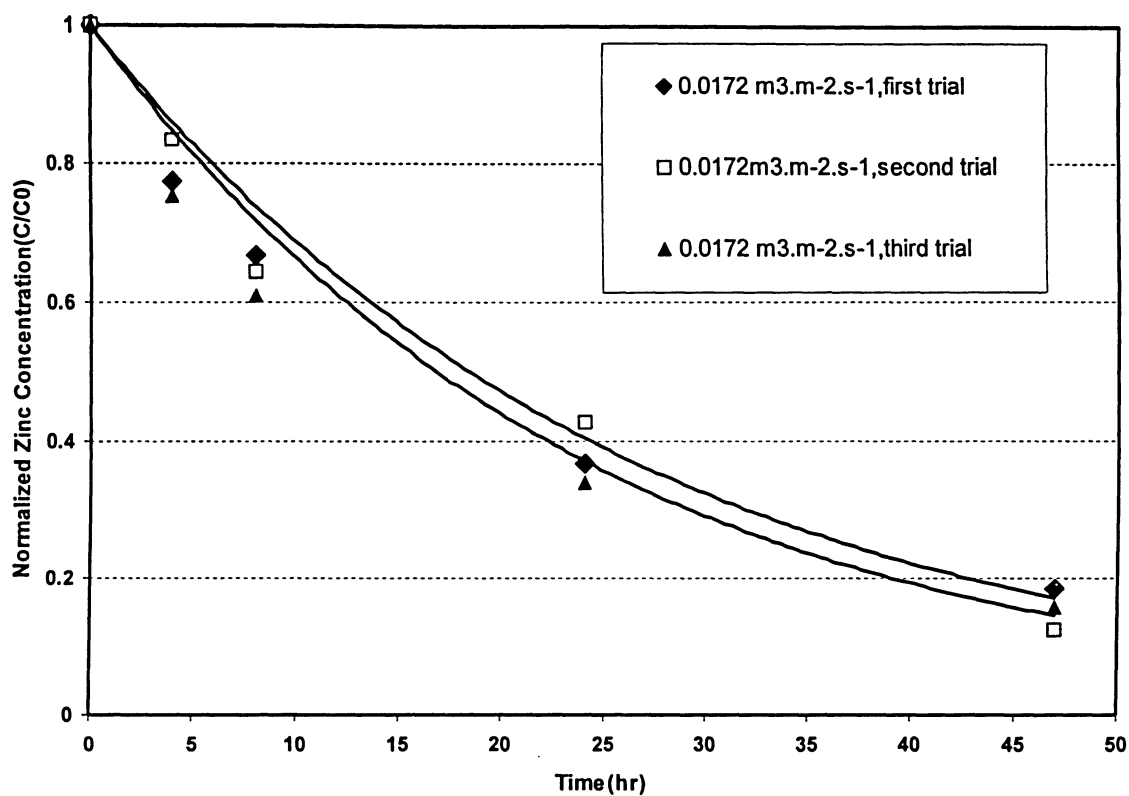## G. Repeated experiments to show reproducibility of the results

Figure 38. Effect of liquid volumetric flux on Zn^{++} reduction during 47 hours of treatment without pH control, current density=0.166 $mA.cm^{-2}$, $[Ni^{+2}]_o=[Zn^{+2}]_o=20$ ppm, $K_2SO_4=250$ ppm, T=25°C.(3 repeated experiments to show the reproducibility of the results)